

https://dspace.org/

A traveller's guide to the geology of Everest (a traverse from Lukla to Everest)

Hochreiter, Rene Carlo

2016

http://hdl.handle.net/10539/21688

Hochreiter, Rene Carlo (2016) A traveller's guide to the geology of Everest (a traverse from Lukla to Everest), University of Witwatersrand, Johannesburg, <http://wiredspace.wits.ac.za/handle/10539/21688>

Downloaded from a DSpace repository. https://dspace.org/

A TRAVELLER'S GUIDE TO THE GEOLOGY OF EVEREST (A TRAVERSE FROM LUKLA TO EVEREST)

René Carlo Hochreiter

A dissertation submitted to the Faculty of Science, University of the Witwatersrand, in fulfilment of the requirements for the degree of Master of Science

Johannesburg, 2016

DECLARATION

This dissertation is my own unaided work, conducted under the supervision of Professors P.H.G.M. Dirks and E.G. Charlesworth. It is being submitted for the degree of Master of Science at the University of the Witwatersrand, and has not previously been submitted for any degree or examination at any other University.

_____

René C. Hochreiter

Dated_____

ABSTRACT

In this, Part 1 of a two-part MSc, the geology of the area between Lukla and Mount Everest is described. An outcome of the MSc is the production of a field guide to this area, presented as Part 2 of this thesis.

The collision between India and Asia resulted in the Himalayan orogen, 3000 km in lateral extent, an elevated Tibetan Plateau and a crust of at least 60 km in thickness. The resulting crustal flow from under this region is in the direction of least resistance, eastwards towards the Pacific subduction zones, but there is also southwards flow towards the Indian subcontinent resulting in vertical complexity. This southwards extrusion of mid-crustal rocks through a mechanism termed channel flow explains the presence of Miocene leucogranite between Ordovician limestones comprising the summit of Everest, and granite gneiss underlying the exhumed granite. Rapid rates of denudation assisted the extrusion of crustal slabs between the South Tibetan Detachment (STD) and the Main Central Thrust (MCT).

Low-grade metamorphic rocks of the Everest Series are juxtaposed across the STD with the underlying high-grade metamorphic rocks of the Greater Himalayan Sequence (GHS). The GHS rocks in turn, are juxtaposed across the MCT with the underlying low-grade Siwaliks. Everest Series schists record temperatures of between 600 °C and 650 °C, and pressure estimates for these rocks ranging from 2.9 ± 0.6 kbar to 6.2 ± 0.7 kbar, corresponding to burial depths of between 10 km and 20 km. The GHS experienced eclogite facies metamorphism with pressures of > 14 kbar (>45 km depth) before being exhumed to granulite facies conditions of 4-6 kbar and 700-800 °C. High-temperature metamorphism of the GHS has resulted in partial melting and melt segregation and ascent to form the High Himalayan Leucogranites, a number of granitic bodies that have accumulated near the top of the GHS.

Intense erosion through the action of glaciers, rivers, landslides and earthquakes (as the 25th April 2015 magnitude 7.8, and 12th May 2015, of magnitude 7.3 earthquakes attest), balance uplift of the Himalaya.

DEDICATION

This work is dedicated to my mother, Gisela, my father, Karl, to a friend, Steve Kearney; and to Oliver Allan. May their lives and times forever be remembered in the highest places on Earth.

ACKNOWLEDGEMENTS

I would like to thank my supervisors, Prof. P.A. Dirks and Prof. E.G. Charlesworth for their patient guidance during this research.

Special thanks to Dr. L. Longridge who contributed to this work with many long hours of discussion and advice. Dr. Luke Longridge gave input and advice on sections relating to tectonics, metamorphism, the P-T-D-t history and channel-flow theory. Fruitful discussions were held with Prof. J Kinnaird, Prof. T McCarthy and Prof. M Searle, with Prof. Searle's map of Everest forming the basis for a number of the maps in this book. Comments and advice provided by Mark Austin-Cheval, a geologist who guided me on Ama Dablam, are also acknowledged.

Logistical support, sample collection on the upper slopes of Everest and some photographs were provided by Sean Disney, Pemba Gaylje Sherpa and Vaughan de la Harpe. Sean Disney, our expedition's climbing leader, provided his impressions on Stops 12 to 14, as the author developed frostbite at Camp II and did not proceed higher.

Special thanks to my wife, Gail, for her consistent and unquestioning support.

Financial assistance is acknowledged from Anglo Platinum, Implats, Aquarius Platinum, Eland Platinum, Mvelaphanda Resources, Eland Platinum, and Salene Mining, with thanks.

Proceeds from the sale of the Guidebook will go to the families of the Sherpas, with whom I had climbed on Ama Dablam, who died in Base Camp in the earthquake which caused the avalanche in Base Camp on 25th April 2015.

TABLE OF CONTENTS

DECLARATION i

ABSTRACT ii

DEDICATION iii

ACKNOWLEDGEMENTS iii

TABLE OF CONTENTS iv

LIST OF FIGURES vii

LIST OF MAPS xix

ABBREVIATIONS COMMONLY USED IN THIS DISSERTATION xx

CHAPTER 1: INTRODUCTION 1

1.1 Overview and background of the study 1

1.2 Rationale 1

1.3 Methodology 2

1.4 The geology of the Himalayas and the study area 3

1.5 The history of topographical and geological exploration of the Lukla-Khumbu-Everest area. 6

1.6 Geological thinking about the Himalayas: From the “axial granite core” to “crustal flow” to “channel flow” 9

CHAPTER 2: GEOLOGY OF THE MT. EVEREST REGION 15

2. 1 The tectonic zones of the Himalayas and a cross section through the Himalayas today 15

2.2 Tectonic boundaries 18

2.3 Stratigraphy 22

2.4 P-T-D-t paths and metamorphism of the Greater Himalayan Sequence and the Everest Series. 27

2.4.1 The metamorphic and deformation history of the Everest Series 28

2.4.2 The metamorphic and deformation history of the Greater Himalayan Sequence 31

2.4.3 Metamorphic and deformation zones in the Everest area 34

2.5 The tectonic history of the Himalayas 36

2.6 Leucogranite, its composition and metamorphic origin 41

2.7 Active tectonics and current thinking regarding the formation of the Himalayas 45

2.8 The Channel Flow Model 45

2.9 The relationship between erosion and the rapid exhumation of rocks 50

CHAPTER 3: GEOLOGICAL FEATURES ALONG THE ROUTE FROM LUKLA TO EVEREST 56

Map 1: Route map from Lukla to Everest (Amended after Himalayan Map House, Kathmandu, Nepal) 57

Map 2: Regional geological map of North Eastern Nepal (Drafted from maps produced by the Department of Mines and Geology, Nepal, and the Ministry of Geology and Mineral Resources, People's Republic of China). 58

Map 3: Geological map of the Lukla to Ama Dablam area (After Searle (2007), modified, based on 2006 and 2008 field work by the author) 59

3.1 Granite gneiss, migmatite and the Namche migmatites 60

3.2 Sillimanite-biotite schist, P-T-D-t path and the age relationship to the Everest Series 66

3.3 Tourmaline-muscovite granite of Ama Dablam and the Khumbu thrust 69

Map 4: Geological map of Ama Dablam and Everest area (Modified after Searle (2007) incorporating further cross-section lines not included in this part of the dissertation) 73

3.4 Views from Kala Pattar – the Everest Series and South Tibetan Detachment 74

3.5 View from Base Camp and the Western Cwm 83

3.6 Glacial valleys/ erosion/ exhumation 87

3.7 Fossils of Everest Series/ age of sediments/ burial and exhumation/ early history of exploration/ Yellow Band 92

3.8 Top of Everest - lateral continuity of the Himalayan tectonic zones and the far-reaching effects of continental collision..... 99

CHAPTER 4: DISCUSSION AND CONCLUSIONS..... 103

4.1 Higher Himalayan Granite Gneiss, and the Namche migmatites 103

4.2 Sillimanite-biotite schist, the P-T-t-D path and the age relationship of the GHS to the Everest Series..... 104

4.3 Leucogranite, tourmaline-muscovite granite of Ama Dablam and the Khumbu thrust 105

4.4 The View from Kala Pattar towards the Everest Series and South Tibetan Detachment 106

4.5 Glacial valleys/erosion/ exhumation 107

4.6 Fossils of Everest Series/ age of sediments/ burial and exhumation/ early history of exploration/ Yellow Band 109

4.7 Top of Everest / lateral continuity / tectonic zones / far-reaching effects (Tibet / China / Burma / Pakistan, etc.) 109

References 112

LIST OF FIGURES

Figure 1.1: Over the last 80 million years, India has moved northwards towards Asia. (a) Shows the movement of India with Asia in a fixed reference frame. Reconstructed positions of India are shown in 20 Ma intervals. In (b), the rate of convergence is shown since 75 Ma. The grey bands show the timing of important events in the history of the collision. Also shown is the timing of eclogite formation and exhumation. Initial collision is thought to have begun in the western part of the region and propagated eastwards over the following 5-15 Ma (from Copley et al. 2010). 4

Figure 1.2: Major structural features including thrusts, normal faults, fold trends and strike-slip faults of the Indian, Himalayan and Tibetan regions with postulated lower crustal flow directions (after Molnar and Tapponnier, 1975). The inset shows the elevated areas of the Himalaya, the Karakoram and Tibet, shown in pink, resulting from the collision of India with Asia. 5

Figure 1.3: One of Tapponnier's plasticine experiments using a flat indenter in an apparatus called the Prandl cell. This rigid indenter, when pressed into layered plasticine as shown in this figure, closely approximates the strike-slip faulting that we see in Tibet and China today. The left hand (western) side of plasticine had resistance kept in place to approximate the Eurasian continent. The right hand (eastern) side had no resistance placed on it to approximate the low resistance that a subduction zone would offer. Hence, the resulting approximation of crustal flow was strikingly similar to the geology of the Tibetan terrane and that of southern China as shown in Figures 1.2, 2.1, 3.29 and 4.4 (after Tapponnier and Peltzer, 1988). 10

Figure 1.4: Convergence of India and Asia was accommodated by crustal flow eastwards (indicated by the arrows) into the Pacific subduction zones, which offered less resistance owing to the thinner crust and pre-existing crustal weakness compared to the thick, stable crust of the Eurasian Craton (after Clark and

Royden, 2000). Strike-slip faulting is a consequence of this crustal flow owing to differential flow rates between crustal blocks. *14*

Figure 2.1: A - Geology of the tectonic zones of the Himalayas and the Tibetan Plateau, showing their remarkable lateral consistency over more than 3000 km in an east-west direction. B – N-S section across the Himalayas and the Tibetan Plateau, showing the main subdivisions: The Sub-Himalayas, the Lesser Himalaya or Siwaliks, the area between the Main Basal Thrust (MBT) and the Main Central Thrust (MCT), the Greater Himalayan Sequence, the South Tibetan Detachment (STD), the Tethyan Himalayas, the Indus Suture Zone and Transhimalayan Batholith (modified after Dézes, 1999). Tibetan geology modified after http://www.geo.arizona.edu/~ozacar/frontp~1.htm. *16*

Figure 2.2: The location of the three main faults in Nepal, Bhutan and China. A zone about 30 km wide, bounded by the South Tibetan Detachment (STD) in the north and the Main Central Thrust (MCT) in the south, is referred to as the Greater Himalayan Sequence or High Himalaya. Further to the south from the MCT are the foothills of the Himalayas, the so-called Siwaliks or Lesser Himalaya, which are separated from the Indian lowlands by the Main Frontal Thrust (MFT) and Main Basal Thrust (MBT). The Khumbu Thrust (KT) is located very close to the STD and is not shown in this image, but is shown in Figure 2.3. The base map is an image taken from Google™ Maps. *21*

Figure 2.3: Geological cross section of the Everest massif, Tibet-Nepal showing the main faults and the detail of the STD which consists of the Qomolongma Detachment (QD) and the Lhotse Detachment (LD) with the Khumbu Thrust (KT) immediately below the LD. (modified after Jessup et al. 2008). *22*

Figure 2.4: Stratigraphy of the area from Lukla to the summit of Mount Everest, shown in relation to the geological timescale. *25*

Figure 2.5: The main features of the geology of Mt Everest: Sedimentary rocks (originally from the floor of the Tethys Sea) make up the summit of Everest. The

Qomolongma Detachment (QD) separates the summit limestone from underlying pelite or metamorphosed mudstones. The Lhotse Detachment (LD) separates the pelitic unit from the underlying sheeted sills of pegmatite and leucogranite, which were intruded between 32 and 16 million years ago (Searle et al. 2003). Near Base Camp, the Khumbu Thrust (KT) marks the top of underlying dark sillimanite-biotite gneiss. Dips are 5° to 15°N. Figure sketched by the author, after Searle et al. (2003). 26

Figure 2.6: History of metamorphism and deformation in the Everest Series schists (after Jessup et al. 2008). 30

Figure 2.7: Cross section through the Greater Himalayan Sequence showing the key relationships between deformation and metamorphism. 31

Figure 2.8: History of metamorphism and deformation recorded in the Greater Himalayan Sequence. Burial (A) to depths of >45 km results in eclogite facies metamorphism, rarely preserved. Subsequent decompression and heating to the granulite facies (B) results in the replacement of eclogitic assemblages, and the widespread development of sillimanite, as well as migmatisation. This is widely regarded as M1. Further decompression and cooling to upper amphibolite facies results in the growth of cordierite (C). Note that this is referred to as M2 in the GHS. Note that D1 in the GHS is likely to have occurred during burial (i.e. before M1), with D2 (and S2 fabric development) taking place during Exhumation, and overprinted by low-pressure cordierite (i.e. during M1 and M2) (figure drafted after Lombardo and Rolfo, 2000; Jessup et al., 2008). 33

Figure 2.9: Metamorphic zonation across the Himalaya (after Goscombe et al. 2006). 35

Figure 2.10 (previous page): Crustal sections through the collision of India with Asia (modified after Allegre et al. 1984). A. As India approached Asia during the Cretaceous period, sediments were deposited in the shrinking Tethys Sea (on top of older Palaeozoic to Mesozoic sediments) on the continental shelf of the Indian plate. A. Forearc basin developed adjacent to an Andean-type volcanic

arc on the Asian Plate, where granites were emplaced. Slivers of subducting oceanic crust were caught in the accretionary wedge, and today form ophiolites. B. As movement continued, so the Tethys Sea began to shrink. Sediments developed as the leading edges of the Asian and Indian plates were brought together. Once collision began, sediments were juxtaposed, and the Main Boundary Fault was formed along which much of the movement was taken up. C. During collision, some of the Palaeozoic to Mesozoic Sediments were taken to mid-crustal depths where they were folded and deformed, and heated up at depth to many hundreds of degrees centigrade. These hot rocks then began to melt, became ductile and were pushed out to surface along a channel, between the Main Central Thrust and the South Tibetan Detachment. D. The rocks of the Lesser Himalaya and the Higher Himalaya are of the same age and were originally deposited together on the Indian continent. They now differ greatly in metamorphic grade, having experienced significantly different histories during the collision of India with Asia. The Cretaceous sediments deposited in the Tethys Sea on the Indian Plate now form the Tethyan Sediments of Tibet. The deformed accretionary wedge and forearc basin became the Indus Suture Zone, and the Andean-type intrusions now form the Transhimalaya Batholith. Sediments eroded from the rising Himalayan mountains have been deposited on the Indian Continent as the Sub-Himalayas..... 39

Figure 2.11: Upward migration of partial melt occurs when rocks deeper down in the Greater Himalayan Sequence begin to melt, forming migmatites. This melt rises upwards and accumulates as leucogranite plutons. The exhumation of the Greater Himalayan Sequence and the leucogranites is enhanced by erosion on the orogenic front (modified after Searle et al., 1997). 42

Figure 2.12: Schematic diagram of the relationship between channel flow and extrusion of a palaeochannel (after Godin et al. 2006). 1 – Mantle, 2 – Lower Crust, 3 – Mid Crust, 4 – Upper Crust, 5 – Weak Crustal Channel, 6 – Isotherms (from Beaumont et al. 2004), 7 – Schematic velocity profiles, 8 – 750°C isotherm,

structurally below which partial melting occurs, 9 – Rheological tip of channel, if temperature is too low, channel will underthrust, 10 – Extruding crustal block, 11 – Lower thrust zone of extruding block (e.g. Khumbu Thrust or the Main Central Thrust), 12 – Upper shear zone/detachment zone of extruding block (e.g. the South Tibetan Detachment or the Qomolongma Detachment), 13 – Focussed surface denudation. 47

Figure 2.13: Granulitic lower crust subducted underneath Tibetan upper crust with limited downwards movement as its relative density is lower than that of the upper mantle. This results in a very thick crust approaching 100 km in thickness (after Jackson et al. 2008, from Dhital, 2015). 51

Figure 2.14: Interaction between surface processes and exhumation in orogenic wedges. High rates of erosion allow underplated crust to be exhumed more rapidly along thrust planes (after Malavielle et al. 2008). 53

Figure 3.1: Recumbent south-verging fold in granite gneiss near Phakding (Stop 2 on Map3). GPS co-ordinates 27°42'57.27"N, 86°42'46.51"E..... 61

Figure 3.2: Example of the Namche migmatites (near Stop 3 on Map 3). There are two generations of folds in this outcrop of biotite-sillimanite gneiss, an early recumbent F_1 fold and S_1 axial-planar fabric and an upright S_2 overprint and upright F_2 folds, which can be seen in the lower right hand side of the outcrop, as indicated. Note the lighter coloured leucosome bands (evidence for migmatisation, made up of quartz and feldspar) within the darker grey gneiss. GPS co-ordinates 27°48'57.14"N, 86°43'50.53"E. 62

Figure 3.3: Migmatite outcrop northeast of Tengboche (near Stop 4 on Map 3) showing interfingered leucosome (white segregated partial melt) within the pre-existing darker coloured sillimanite-biotite gneiss. Note the banded (stromatic) nature of the migmatite at this outcrop, suggesting that melting occurred syntectonically. Some leucosomes have been further deformed or stretched into boudins. In places, leucosome are discordant to the planar fabric defined by the neosomes.

The handle of the hiking pole is 15 cm in length. GPS co-ordinates 27°48'18.64"N, 86°43'2.66"E. 64

Figure 3.4: Recumbent folding above Namche Bazaar village. Migmatite outcrops lie above the buildings on the left side of the photograph. Photograph taken from GPS co-ordinates 27°48'19.22"N, 86°42'41.20"E, looking westwards..... 65

Figure 3.5: Photomicrograph (XPL) of sillimanite-biotite schist. A strong fabric of aligned biotite and sillimanite grains is present. Quartz (Qtz), plagioclase (Pl) and minor amounts of K-feldspar muscovite make up the remainder of this rock. Quartz and plagioclase grains may have inclusions of fine-grained sillimanite. Note the irregular shape of the quartz grains and the numerous small, rounded grains of quartz, indicating high degrees of strain (MacKenzie and Guilford, 1980). Sample of schist taken from near Laboche. GPS co-ordinates: 27°57'23"N, 86°4724"E. 67

Figure 3.6: Ama Dablam south-east ridge, at approximately 6500 m. The black rock on the left hand side is an amphibolite xenolith with tourmaline granite on the right. The black specks on the granite are tourmaline crystals. The white rock with large crystals to the right of the climbers is a pegmatite. The layering above the yellow helmet of the climber is part of a sillimanite-biotite gneiss xenolith. GPS co-ordinates 27°51'24.35"N, 86°51'17.23"E. 69

Figure 3.7 Photomicrograph (XPL) of tourmaline granite. The rock is made up of quartz (Qtz), plagioclase (Pl) and K-feldspar (Kfs), tourmaline (Tur) and minor amounts of biotite. Some of the quartz is strained, indicating deformation after crystallisation of this granite. Sample collected at GPS co-ordinates 27°51'9.95"N, 86°51'4.30"E. 71

Figure 3.8: View from Kala Pattar of Changtse, Everest and its west shoulder, and Nuptse. The Khumbu Thrust zone (KT) is located at the base of the massif in the dark gneiss. The Lhotse Detachment (LD) runs along the Lhotse Ridge and through South Col on the right edge of the south-east ridge of Everest where it meets the

Lhotse Ridge. The Qomolongma Detachment (QD) is located at the top of the Yellow band near the summit of Everest and dips northwards through the top of the Yellow Band on Changtse (Figure 3.9). Nuptse and the west shoulder of Everest are composed of leucogranite whilst Everest itself is composed of the dark dolomitic marble and limestone. The summit rocks are composed of mylonitized limestone containing calcite, with small amounts of dolomite and very small amounts of quartz and muscovite (Yin and Kuo, 1978; Sakai et al., 2005, Myrow et al., 2009). Photograph taken from the Kala Pattar summit, GPS co-ordinates 28°59'7.45"N, 86°49'39.38"E. 75

Figure 3.9: The Everest Series on Changtse to the north of Everest shows the Qomolongma Detachment (QD) positioned at the top of the Yellow Band. Photograph taken from the Kala Pattar summit, GPS co-ordinates 28°59'7.45"N, 86°49'39.38"E looking ENE. 76

Figure 3.10: More detailed view of the west face of Nuptse showing a stockwork of cream-coloured granite dykes and sills (centre) above a more massive granite pluton (bottom left) intruding sillimanite-biotite gneiss on the west face of Nuptse. The granite extends across the entire base of Nuptse below the level of the photograph. Photograph taken from the Kala Pattar summit, GPS co-ordinates 28°59'7.45"N, 86°49'39.38"E looking ESE. 77

Figure 3.11: View N across KP hill to Pumori, showing sillimanite gneiss in the foreground and the overlying leucogranite. The KT that separates the units is hidden by topography. Dark sillimanite gneiss is evident in the foreground and on the summit of Kala Pattar hill. Beyond it, the sheeted pegmatite dykes at the base of Pumori give way to leucogranite approximately two-thirds of the way up the S face of Pumori. Photograph taken from GPS co-ordinates 28°58'52.97"N, 86°49'42.95"E looking northwards..... 78

Figure 3.12: The west face of Nuptse above the Khumbu Icefall showing folding of the leucogranite sills and dykes (Searle, 1999, Fig 11 proves this). Photograph taken

from the north end of Base Camp, GPS co-ordinates 28°58'35.50"N, 86°52'45.65"E. *79*

Figure 3.13: (A) Fine-grained aplite dyke intruding two-mica granite. (B) Granite intruding sillimanite-biotite gneiss and an earlier generation of granite in moraine rock from Base Camp. Note the mylonitic zone seen near the bottom left of the photograph, indicating that granites have experienced shearing post-emplacement. Photograph taken at GPS co-ordinates 28°0'6.58"N, 86°51'49.03"E. *80*

Figure 3.14: Photomicrograph (XPL) of a mylonite sample collected near Camp I. The rock is predominantly fine-grained quartz, biotite and plagioclase. The rock is very fine grained and platy biotite and quartz are aligned in a strong fabric. Intense deformation has led to a grain size reduction through dynamic recrystallization, a texture typical of mylonite. Sample collected at GPS co-ordinates 28°0'6.58"N, 86°51'49.03"E. *81*

Figure 3.15 Photomicrograph (XPL) of strongly deformed protomylonite of leucogranitic origin collected from near Camp 2. The rock is very pale and has few mafic minerals. It is composed of quartz (Qtz), which is often strained, plagioclase (Pl), K-feldspar and lesser amounts of muscovite. Fine to medium grained muscovite mica grains are aligned to form a fabric, and quartz shows evidence of straining and grain size reduction. Note the zone of shear and intense grain size reduction cutting the sample. Sample collected at GPS co-ordinates 28°58'39.68"N, 86°53'58.89"E. *82*

Figure 3.16: The east faces of Pumori and Lingtren above the Khumbu glacier showing exhumed leucogranite intruding sillimanite-biotite gneiss. *83*

Figure 3.17: The east face of Lingtren viewed from Camp 1 (in the Khumbu Icefall) showing sheeted leucogranite sills in sillimanite-biotite gneiss below the leucogranite that forms the summit of Lingtren, and sheeted leucogranite sills and dykes on the West Shoulder of Everest. *84*

Figure 3.18: Restored Pumori – Everest profile before emplacement of the leucogranite. Crosses mark samples from Kala Pattar, 12km west of Everest (Map 4) which record pressures of 3.7, 4.1 and 4.5kb. at a true dip of 3° to 5°N measured on the N face of Everest, relative displacement is would be 180-216km (After Searle et al. 2003). *85*

Figure 3.19: The age relationship between metamorphism (M_1 and M_2), the leucogranite of the Pumori-Lingtren-Everest ridge, the Rongbuk metamorphism, the deformed sills and dykes and ductile and brittle faulting on the STD (After Searle et al. 2003). 1 – Age of maximum pressure metamorphism (M1) 32.2 ± 0.4Ma (Simpson et al. 2000). 2 – Age of low pressure cordierite metamorphism (M2) 22.7 ± 0.2Ma (Simpson et al. 2000). 3 – Anatexis resulting in melts that formed leucogranites found on Everest 20.5–21.3 Ma (Simpson et al. 2000). 4 – Youngest metamorphism 17.9 ± 0.5 Ma (Simpson et al. 2000). 5 – Deformed leucogranite sills, 16.67–16.2 Ma (Hodges et al. 1998; Murphy and Harrison 1999). 6 - Undeformed cross-cutting dykes 16.8– 16.5 Ma (Hodges et al. 1998; Murphy and Harrison 1999). *86*

Figure 3.20: The Western Cwm fold structure as seen from Camp 2. The low angle of the northwards dipping metasediments and detachments are clearly visible. Note the thrust fault and folded calc-silicate bands with a south-westerly vergence, suggested to be related to the Lhotse Detachment (Searle, 1999). Photograph taken from GPS co-ordinates 28°0'42.75"N, 86°51'24.57"E looking northwest. *87*

Figure 3.21: Earthquake epicentres and their magnitude recorded in the India-Eurasia area between 1900 and 2014. Note the greater number of earthquakes west of the Himalayas (in Uzbekistan, Tajikistan and Kyrgyzstan) and east of the Himalayas (in Burma), compared to the Himalayan Mountain chain (Pakistan, Nepal and Bhutan). *89*

Figure 3.22: Map showing lift and drop of the 7.8 magnitude earthquake of 25th April, 2015 with epicentre west-north-west of Kathmandu. The epicentre was probably located on the MCT. *90*

Figure 3.23: Oblique Google Map View of the Everest area from the south. Note the many U-shaped glacial valleys which are found in the Everest region. Glaciers are a powerful erosive force in the concentrated denudation of the high Himalayas (Egholm et al. 2009) . In the Everest massif area, 8 major glaciers can be seen in this photograph. In the foreground from the left, the Khangri Nup, the Khangri Shar, the Khumbu, the Nuptse, the Lhotse Nup and the Lhotse glaciers can be seen. North of Everest from the left, the Rongbuk and the East Rongbuk glaciers can be seen. The east Rongbuk glacier is directly behind Everest and cannot be seen here. *91*

Figure 3.24: Fossils of the Everest Series: (A) - Crinoid plate with well-preserved perforations from the summit of Everest (enlarged 17x; Gansser, 1964). (B) - Stem fragment of crinoid in fine-grained limestone from the summit of Everest (enlarged 40x; Gansser, 1964). (C) - Ammonites (left) and a bi-valve mollusc (right) which are on display in Kathmandu at the offices of the Department of Mines and Geology of Nepal). *93*

Figure 3.25: Stratigraphic column for Mt Everest and the Everest Series, showing the units where fossils are found. *94*

Figure 3.26: The Yellow Band as seen from the South Summit looking towards the Hillary Step, where two climbers are circled in red (Photograph: Sean Disney, 2006). Photograph taken from GPS co-ordinates 27°59'12.31"N, 86°55'26.76"E looking north-west towards the Everest summit. The outcrop near the summit shows the location of the summit samples taken shown in Figure 3.26. ..... *95*

Figure 3.27: Photomicrograph (PPL) of a rock sample from South Summit, within the Yellow Band. The rock is a marble and is composed almost entirely of sparry calcite with a large number of crystals showing twinning. Black carbonaceous material

is present as stylolites parallel to the fabric direction. These wavy, black carbonaceous layers may have originated from fossiliferous material on stylolite dissolution planes. The rock is medium to fine grained (<0.3 mm grains) with some coarser calcite crystals. Numerous shears cut through the sample. Calcite grains tend to form elongate lenses between the shear planes, and some calcite shows deformed cleavage bands. Sample collected at GPS co-ordinates 27°59'5.25"N, 86°55'31.17"E. 96

Figure 3.28: Photomicrograph (XPL) of rock sample RH17 from the Hillary Step (Figure 3.26). The rock is composed mostly of calcite with minor muscovite and, rarely, epidote. The sample is fine-grained although there are some coarser calcite grains present. Small carbon-rich (graphite) grains are visible. The fine-grained nature of this sample suggests it has experienced intense deformation. Sample collected at GPS co-ordinates 27°59'12.31"N, 86°55'26.76"E. 97

Figure 3.29: Photomicrograph of rock sample near the summit of Mount Everest. It is composed almost entirely of calcite grains. Small amounts of mica are also found, in addition to a number of opaque grains of pyrite and darker bands of organic-rich (carbonaceous) layers. The majority of the sample is fine grained due to shearing which has caused grain size reduction. This shearing has resulted in breccia zones with further evidence for deformation found in folded carbonate layers and bent cleavage planes in some of the calcite crystals. Sample collected at GPS co-ordinates 27°59'16.37"N, 86°55'30.23"E..... 99

Figure 3.30: Google earth image of the Tibetan Plateau showing its lateral extent of around 3000 km east-west and its north-south expanse of over 1500 km. The continental collision has resulted in a convex–to–south arc of the world's loftiest orogenic system (Dhital, 2015) and has affected 7 countries. 100

Figure 3.31: Simplified geological map of the Himalayas (from Dhital, 2015, modified from Stöcklin, 1980, Gansser, 1981, and Sorkhabi and Stump, 1993). 102

Figure 4.1: Sequence of growth of minerals of a subducted granulitic continental crust pertinent to the GHS. 104

Figure 4.2: Cross section B-B' (Map 4) from Nuptse Northwards to Hermit's Gorge. According to Searle (2003), a large leucogranite outcrop is found on the south face of Nuptse. Folded yellow calc-silicate bands on the Lhotse face are separated from this leucogranite by the Lhotse Detachment. Searle shows the leucogranite as a recumbent fold. However, it may also be possible that there has been exhumation of leucogranite and extrusion southwards in a ductile channel between the Khumbu Thrust and the Lhotse Detachment. 107

Figure 4.3: USGS map of earthquake epicentres since 1900. (From: http://earthquake.usgs.gov/earthquakes/tectonic/images/himalaya_tsum.pdf) 108

Figure 4.4: The Tibetan plateau is the largest plateau on Earth with an average elevation of 4880 m and a crustal thickness of 65 km. High elevations are shown in white (5000 m to 8850 m) red (4000 m to 5000 m) and low elevations in blue (1000 m to 2000 m) and purple (<1000 m). The Tibetan Plateau is bounded by the deserts of the Tarim and the Qaidam Basin to the north, and the Himalayan, Karakoram and Pamir mountain chains to the south and west (source: http://oak.ucc.nau.edu/wittke/tibet/plateau.html). 110

LIST OF MAPS

Map 1: Route map from Lukla to Everest 57

Map 2: Regional geological map of North Eastern Nepal 58

Map 3: Geological map of the Lukla to Ama Dablam area 59

Map 4: Geological map of Ama Dablam and Everest area 73

ABBREVIATIONS COMMONLY USED IN THIS DISSERTATION	
GHS	Greater Himalayan Sequence
LHS	Lesser Himalayan Sequence
KT	Khumbu Thrust
LD	Lhotse Detachment
MCT	Main Central Thrust
MCTZ	Main Central Thrust Zone
MCT 1	Main Central Thrust 1, the southern boundary of the MCTZ
MBF	Main Boundary Fault (south of the MCTZ).
STD	South Tibetan Detachment
Bt	Biotite
Crd	Cordierite
Kfs	Potassium feldspar
Ms	Muscovite
Omph	Omphacite
Opx	Orthopyroxene
Pl	Plagioclase
QD	Qomolongma Detachment
Qtz	Quartz
Sill	Sillimanite
Tur	Tourmaline

CHAPTER 1: INTRODUCTION

1.1 Overview and background of the study

This thesis describes the geology along the ~50km route from Lukla, Nepal, to the summit of Mt Everest (see Maps 1-3, p57-59). This route transects some of the major features of Himalayan geology, and these geological features provide insights into the dynamic processes that have resulted in what is one of the greatest mountain chains on Earth. Most travellers land at the town of Lukla and then hike through the Khumbu Valley to Everest Base Camp and some will climb to the summit of Everest. Hence, the guidebook describes this route in detail as this traverse is where almost all of the questions regarding geology will arise.

Part 1 of this thesis provides a review of the scientific literature on the area, followed by detailed descriptions of rocks along the route and their context within the current understanding of Himalayan tectonics. Part 2 consists of a completely separate guide book, where the geology along the route is described in layman's terms.

1.2 Rationale

Although a literature study was undertaken for the compilation of this thesis, personal observations were made during two South African International expeditions during 2004 and 2006. A further expedition was made to the study area in 2008 with a New Zealand expedition.

The study was undertaken on three separate visits to the study area and in all, around 5 months were spent collecting samples and making observations. On two occasions avalanches narrowly missed the author and several dozen crevasses were crossed in the Khumbu Icefall to gain access to outcrops or to gain a vantage point for an observation or photograph. The author developed frost-bite in the Khumbu Icefall, precluding him from working above Camp 2.

I wish to emphasise that this study was therefore not just an armchair literature search, but was completed with considerable physical risk to the author high up on Everest and Ama Dablam.

1.3 Methodology

The study area is located in the north-east of Nepal along a trail from Lukla to Namche Bazaar and Pangboche, then into the Khumbu Valley where the villages of Periche, Laboche and Gorak Shep are located, and finally on to Everest Base Camp (see Maps 1, 3 and 4, p57, 59 and 71). Most visitors will land at the world-famous, dangerous airstrip at Lukla and make their way 50 km to the Everest Base Camp and climbers will add a further 11 km from Base Camp to the Summit of Everest. Owing to the volume of people on this path, particularly during the climbing season of April and May each year, it was decided that this route would be a particularly appropriate one in which to explain the geological features encountered.

Maps showing the route and the geology of the area are introduced here to highlight the study area and the regional and local geology of the area discussed in the pages below.

Map 1 (page 57) shows the study area and the route taken from Lukla (stop 1) to the Everest summit (stop 14). Observations were made methodically at various points along this route. These included geological observations, photographs and the collection of rock samples. These samples were collected for later microscopic studies.

Map 2 (page 58) shows the regional geology of Nepal and Tibet. The majority of the route is underlain by the crystalline gneiss of the Greater Himalayan Sequence and, nearer to Everest, by granite and the limestone of the Everest Series.

Map 3 (page 59) shows the geology of the area between Lukla and Ama Dablam, with stops 1 to 6 showing the route taken.

Map 4 (page 73) shows the geology of the area between Ama Dablam and Mount Everest and to the north into Tibet with stops 7 to 14 showing the route taken.

Access to Nepal Geological Survey maps and the use of Google Earth images with oriented 3D images of the Himalayas assisted in the compilation of this dissertation.

1.4 The geology of the Himalayas and the study area

The Himalayas are the product of the collision between two continents – India and Asia. Starting about 180 million years ago (Ma), the supercontinent Gondwana began to break up (Copley et al. 2010, from Dhital, 2015). This breakup eventually led to the configuration of the continents as they are seen today, as South America, Antarctica, Australia, India and Madagascar moved away from Africa. India broke away from the east coast of Africa at about 115 Ma (Copley, et al. 2010).

Following the breakup of Gondwana, India began to move northwards, resulting in subduction of the denser oceanic part of the Indian plate below the less dense Asian continental plate. The record of the magnetic stratigraphy in the Indian Ocean allows accurate reconstruction of the collision between India and Asia to be made. Since the late Cretaceous period, the successive positions of India at various times from 71 Ma to present time are shown in Figure 1.1 (Copley et al. 2010). Whilst this subduction occurred, a number of small micro-continental fragments or terranes were accreted onto Asia (Van der Voo et al. 1999). India had the fastest speed of any continent moving away from Gondwanaland (Aitchison et al. 2007). Between 75 and 50 Ma, India's speed northwards varied between 10 and 16 cm/yr, slowing down to 4 cm/yr at present (Copley et al. 2010, from Dhital, 2015). Further slowing from this rate since then has seen the speed drop to around 2 cm/yr (Searle and Rex, 1989).

After more than 50 million years of northwards movement and subduction of oceanic crust, the Indian continent collided with Asia around 55 Ma to 45 Ma (Molnar and Tapponnier, 1975; Searle and Rex, 1989; Copley et al. 2010). During the collision of these two continents, some of the Indian continent was forced beneath the Asian continent. The Tethyan sea probably closed around 50 Ma, whilst the Wharton Ridge (Figure 1.1), an active spreading ridge, began to be subducted beneath Asia from approximately 70 Ma onwards (Heine et al. 2004) and was abandoned around 44 to 42 Ma (Copley et al. 2010). This subduction probably ended at about 45 Ma with the formation of eclogite and exhumation of part of the Greater Himalayan Sequence (Figure 1.1), (Copley, et al. 2010). The collision of India with Asia has resulted in a wide zone of crustal thickening across Tibet, China and west into Pakistan (Figure 1.2), forming the so-called Tibetan Plateau, an area which has an average elevation of over 4,000 m.

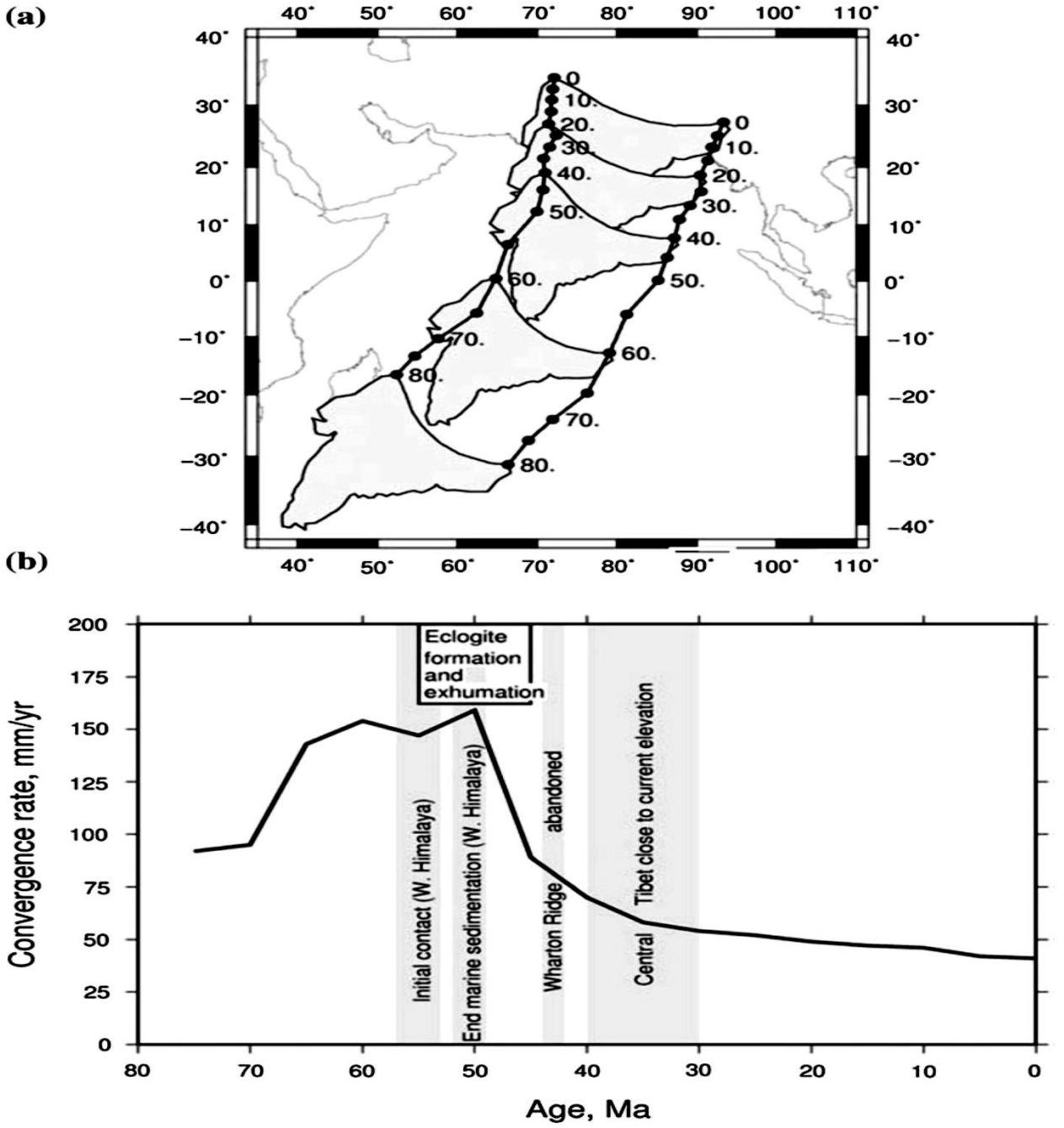


Figure 1.1: Over the last 80 million years, India has moved northwards towards Asia. (a) Shows the movement of India with Asia in a fixed reference frame. Reconstructed positions of India are shown in 20 Ma intervals. In (b), the rate of convergence is shown since 75 Ma. The grey bands show the timing of important events in the history of the collision. Also shown is the timing of eclogite formation and exhumation. Initial collision is thought to have begun in the western part of the region and propagated eastwards over the following 5-15 Ma (from Copley et al. 2010).

The collision and resulting crustal thickening formed a curved range of mountains along the northern edge of India (the Himalayas or Himalayan Front), which are between 6,000 m and 8,850 m in height. Although the speed of India has slowed, it continues to move northwards into Asia at about 2 cm/year, resulting in the continued rise of the Himalayan mountain chain (Searle and Rex, 1989).

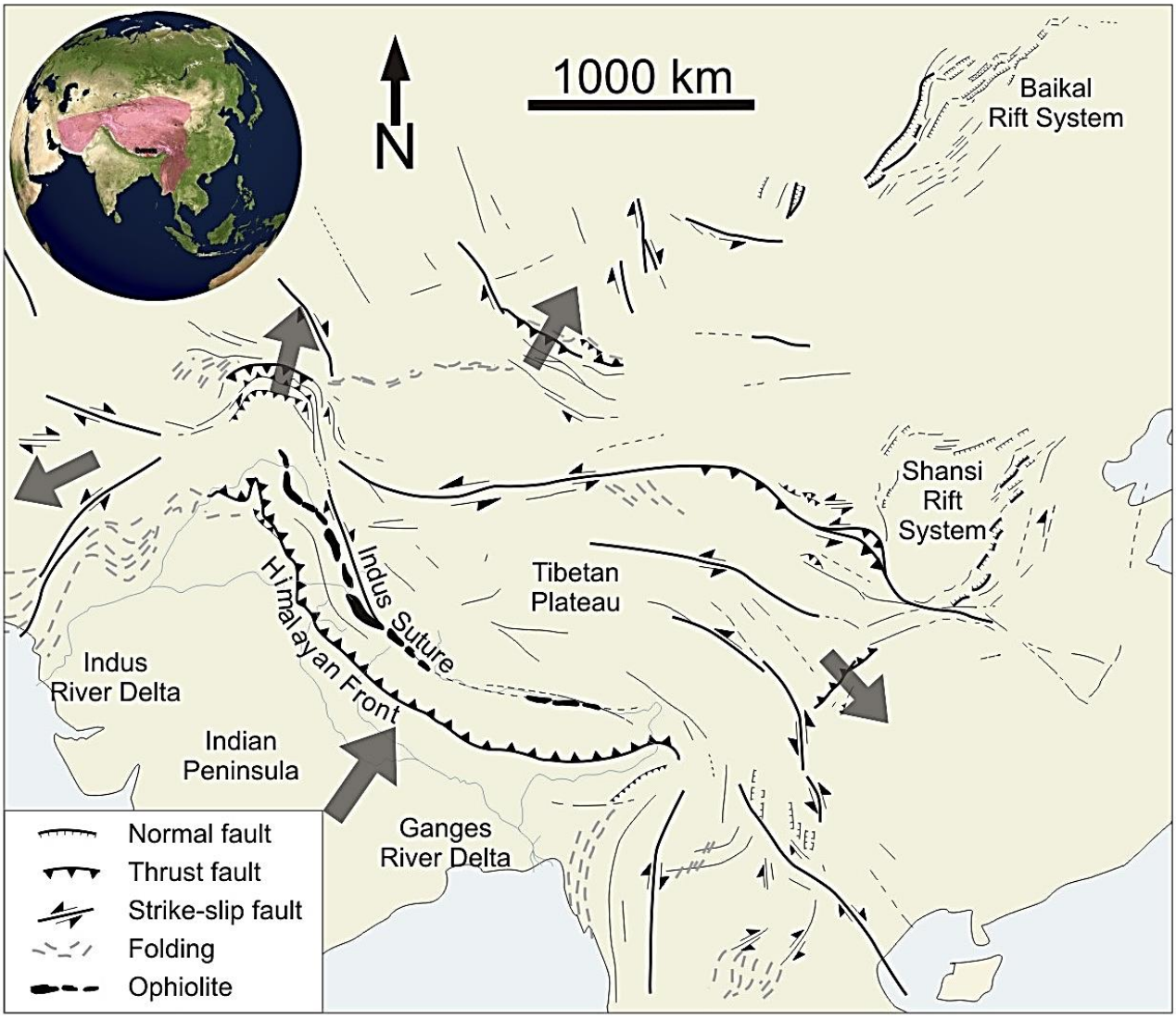


Figure 1.2: Major structural features including thrusts, normal faults, fold trends and strike-slip faults of the Indian, Himalayan and Tibetan regions with postulated lower crustal flow directions (after Molnar and Tapponnier, 1975). The inset shows the elevated areas of the Himalaya, the Karakoram and Tibet, shown in pink, resulting from the collision of India with Asia.

1.5 The history of topographical and geological exploration of the Lukla-Khumbu-Everest area.

Apart from the area's unique geology, the story of the surveyors and geologists who accompanied the early Everest expeditions is a fascinating account. These early workers endured arduous journeys through some of the most rugged terrain on Earth to bring a wealth of knowledge to the scientific world. Many of these results and interpretations are still applicable today.

In 1808, the British began their Great Trigonometrical Survey of India. One of the objectives of this study was to determine the height of the Himalayan mountain peaks. Massive 500 kg theodolites were used which needed 12 men to carry. Refusal by the Nepalese to allow the Survey to enter Nepal resulted in some measurements being taken from over 240 km away.

It took the Great Trigonometrical Survey of India until 1852 to discover Everest as the highest mountain in the world. In 1847, Andrew Waugh, the Surveyor General at the time, took observations which established Kanchenjunga as the highest peak known at that time, but noted a higher peak beyond it, some 230 km away, which he called peak "b". James Nicolson was then sent by Waugh in 1849 to determine the height of peak "b". He made over 30 observations from five stations, the closest of which was 174 km away. His rough calculation for the height of this peak was 30,200 feet (ft.) (about 9,200 m). Michael Hennessey renamed the peak, and peak "b" became Peak XV. In 1865, it was named Mount Everest after the British Surveyor General of India, Sir George Everest. The Tibetans who live on the north side of Everest call it Jomo Lungma, or sometimes Chomolongma, which means "goddess, mother of the world". On the south side, the Nepalese call it Sangamartha, which means "goddess of the sky".

Radhanath Sikhdar, a Bengali mathematician and surveyor, established Peak XV as the highest mountain in the world in 1852 when he processed Nicolson's measurements. A further four years of checking and corrections finally culminated in an altitude of 29,002 ft. (8,840 m) above mean sea level (amsl), when the altitude was officially announced in 1856. This is an amazing feat when compared to the accepted height of 29,028ft. or 8,848 m, which was determined in 1955 by an Indian survey. Is it possible that both measurements are correct and that the summit of Everest has risen 8 m in 102 years, at a rate of 8 cm a year? Some measurements suggest an annual 45

mm rise above mean sea level and 27 mm lateral movement per year, and in 1999 Mount Everest was found to be two metres higher than in 1955 (8,850m).

Investigations into the geology of the Himalayas began in the middle of the nineteenth century with a paper published in the *Quarterly Journal of the Geological Society of London* by R Strachey, entitled *The Geology of part of the Himalaya Mountains and Tibet* (Strachey, 1851). In 1864, H.H. Goodwin-Austen (after whom the famous Goodwin-Austen Glacier near K2 in the north-western Himalayas is named) published his geological notes in the *Quarterly Journal of the Geological Society of London* (Godwin-Austen, 1864), in which he described the glaciology of northern Kashmir.

However, the foundations of Himalayan geology were laid by the Irish geologist H.B. Medlicott who, in 1857, surveyed the Himalayas between the Ravi (or Ravee) and Ganges Rivers, and in 1864 published a paper *On the geological structure and relations of the southern Himalayan ranges between the Ganges and the Ravee* in the *Memoirs of the Geological Survey of India* (Medlicott, 1864). He also published *Notes on the geology of Nepal* in 1875 in the same journal (Medlicott, 1875).

In 1866, F. Stoliczka produced what were, arguably, the first cross sections through the Himalayan mountains (Stoliczka, 1866), and the geological knowledge of India and the Himalayas was brought together in *A Manual of the Geology of India*, published in four parts between 1879 and 1887 (Medlicott and Blanford, 1879; Medlicott and Blanford, undated; Ball, 1881; Mallet, 1887). In addition to the basic strata and structure of the Himalayas, fossils found in these strata have been key in determining the age of the rocks. A variety of fossils was mentioned in Strachey's 1851 paper, and a number of other notable papers refined the classification of Himalayan fossils (e.g. Middlemiss, 1885; von Mojsisovics, 1900).

Although geological work on the Himalayas began in the mid-nineteenth century, investigations into the geology of the area around Everest and to the north into Tibet only began with Sir Henry Hayden's pioneering investigations when this geologist accompanied the famous Tibet Expedition of 1903-1904, led by Sir Francis Younghusband. Hayden went on to become the Director of the

Geological Survey of India between 1910 and 1921. In 1907, H.H. Hayden and S.G. Burrard published their paper on the geography and geology of the Himalayan mountains and Tibet, which included the first geological map of the Himalayas, and which was revised by Burrard and Heron in 1934 (Burrard and Hayden, 1907; Burrard and Heron, 1934).

In 1921, A.M. Heron accompanied Mallory's expedition to Mount Everest. The expedition was unfortunately called off after an avalanche just below the North Col killed six porters. However, Heron was able to report on the geology of the sedimentary rocks north of Everest in a 1922 paper in the *Geological Journal* (Heron, 1922).

It was Noel Odell, a geologist on the fateful 1924 Everest expedition, who focused on the crystalline rocks to the south of Everest; and who was the first geologist to examine outcrops of the dark limestone, fossils and the Yellow Band near the summit of Everest (Odell, 1925, 1943, 1948). For many years, Odell was the most famous "Everest Geologist", and he published the first geological map of the district surrounding Everest (Odell, 1925). Throughout the 1930s, L.R. Wager continued work on the Everest region, publishing a paper on the age of the Everest rocks and adding to Odell's map (Wager, 1934). In 1935, C.E. Wegmann published "*The meaning of the migmatites*" (Wegmann, 1935). Odell returned to Everest in 1938 and made an extensive collection of the rock types in the area, but the entire collection was stolen by Tibetans. An even greater blow was struck in 1941 when all Odell's field notes, diaries, maps and partially completed papers, covering 14 years of work, were lost on a voyage to India. Amazingly, Odell still managed to publish notes on the geology and geophysics of the Himalaya from memory, and noted the major fault below Lhotse and into the base of Everest itself, a key feature of the geology of the mountain (the Lhotse Detachment - see Figures 2.3 and 2.5). Odell also detailed the geology of the granites and gneisses south of Everest in his 1943 paper: *The so-called 'Axial Granite Core' of the Himalayas: its actual exposure in relation to its sedimentary covering* (Odell, 1943). In 1964 *The Geology of the Himalayas* was published by Augusto Gansser, a compilation of all the work on the Himalayas which to this day remains one of the key reference books for the geology of the region (Gansser, 1964). Another is T. Sharma's study of the Mount Everest region (Sharma, 1988) undertaken for the Nepalese Geological Survey. After the *Ascent of Everest* (Hunt, 1954) was published by John Hunt, who was the leader of the British Expedition that headed the successful

Hillary/Norgay summit team, geological research proliferated. Recent investigators include M.P. Searle, R.D. Law, L. Godin, K.D. Nelson, M.J. Jessup, and R.A. Jamieson, to name but a few.

To name even some of the many geological investigators would “alone demand a lengthy treatise” as Augusto Gansser wrote in his 1964 book. Interestingly, the closure of Nepal to foreigners for many years inhibited geological exploration of the Khumbu valley, and most expeditions to the Everest area approached from the northern (Tibetan) side. Today, however, the Nepali side of Everest is more easily accessible, and forms the focus for this thesis and guide. The proliferation of work on Everest throughout the nineteen seventies and eighties culminated in an explosion of research in the nineties, which continues to this day. This included the International Deep Profiling of Tibet and the Himalayas (INDEPTH) programme, a major geophysical transect of the Himalayas led by Doug Nelson of the University of Syracuse. The programme showed that the Indian and Tibetan crusts were mixed, extruded southwards towards India, and crystallised into the great leucogranite mountains such as those of Lingtren and Ama Dablam (Pognante et al. 1993; Nelson et al. 1996; Searle, 1999). This led to the evolution of ideas on channel flow, and ductile extrusion and exhumation in the Himalayas at the turn of the century. These models attempt to explain how young rocks presently on surface could have been created at many kilometres depth and brought to surface over a relatively short period of time (Searle, 1997; Law et al. 2006; Jessup et al. 2006).

1.6 Geological thinking about the Himalayas: From the “axial granite core” to “crustal flow” to “channel flow”

Very early geological hypotheses on the formation of the Himalayas focused on the crystalline axis of the Himalayas (Stolizka, 1866) comprising an igneous and/or a metamorphic core versus a sedimentary cover underlain by Indian shield rocks (Dhital, 2015). There were also suggestions that the Himalayas were of geosynclinal origin (Gansser, 1964), and then counter-suggestions that they developed from a reactivated platform sequence (Dhital, 2015).

In the 1960s, the theory of plate tectonics developed and geological thinking then centred on the formation of the plutonic belts of the trans-Himalaya as the product of continental collision. Molnar and Tapponnier (1975) thought of the collision of India with Asia as a continent-on-

continent impact and used plane indentation experiments to model the resulting intracontinental deformation and the evolution of strike-slip faulting in eastern Asia and Tibet. Plasticine was used to show how faults developed (Tapponnier et al. 1982). They suggested that crustal flow towards the east where the Pacific subduction zones offered less resistance was a way of accommodating the convergence of the two continents. Tapponnier et al; (1982) demonstrated the deformation resulting from the indentation of India into Asia by using the Prandl cell, consisting of a number of differently shaped rigid indenters that were pressed into plasticine. The indenter that closely approximates what we see in Tibet and China today was that shown in Figure 1.3, a flat-topped indenter similar to what the northern margin of India could have looked like when it initially impacted Asia.

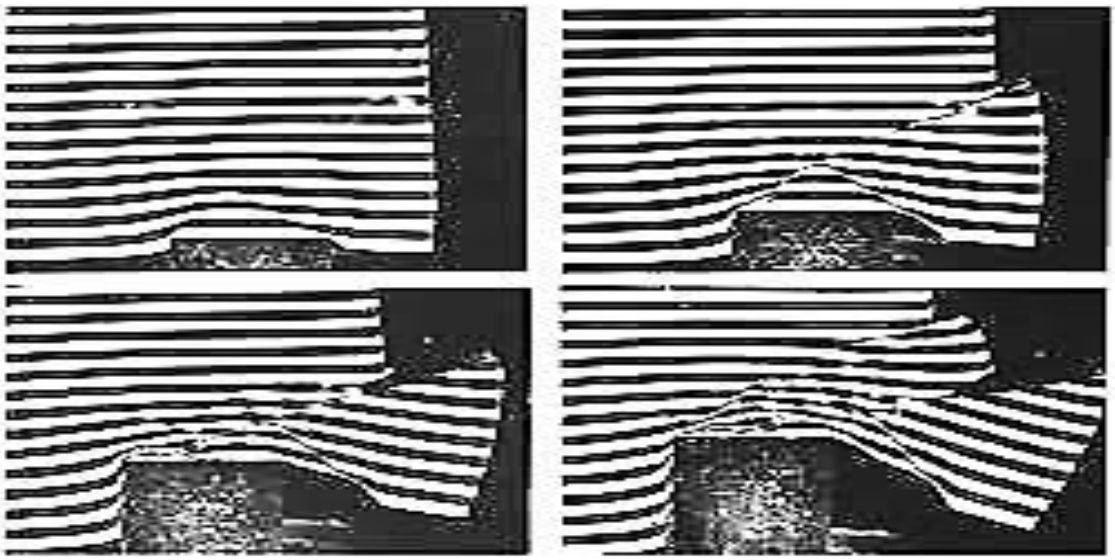


Figure 1.3: One of Tapponnier's plasticine experiments using a flat indenter in an apparatus called the Prandl cell. This rigid indenter, when pressed into layered plasticine as shown in this figure, closely approximates the strike-slip faulting that we see in Tibet and China today. The left hand (western) side of plasticine had resistance kept in place to approximate the Eurasian continent. The right hand (eastern) side had no resistance placed on it to approximate the low resistance that a subduction zone would offer. Hence, the resulting approximation of crustal flow was strikingly similar to the geology of the Tibetan terrane and that of southern China as shown in Figures 1.2, 2.1, 3.30 and 4.4 (after Tapponnier and Peltzer, 1988).

The experiments suggest that the penetration of India into Asia rotated (≈25°) and extruded (≈800 km) Indochina to the south-east along the then left-lateral Red River fault in the first 30 to 20 Ma of the collision (Tapponnier et al. 1982). Several left-lateral strike-slip faults are suggested to have been activated, one at a time, with vast lateral movement on some of the faults. For example, southern China is estimated to have moved hundreds of kilometres eastwards. The model has credibility in that there is very little magmatic product in the Himalayan collision zone; the model, however, neglected vertical complexity.

The Transhimalayan batholiths were formed on initial impact of the Indian crust with the Tibetan/Asian crust, and subduction of the lithosphere beneath Tibet, circa 38 Ma (Searle et al. 1987) strike-slip. As the leading edge of the Indian plate was subducted beneath the Asian plate (Lhasa terrane, Figure 2.1A), the heat source rising above the Indian plate generated magma that erupted from volcanoes, and created the Transhimalayan batholiths (Molnar 1986, Dhital, 2015, Figure 2.1B). These are found in Tibet, approximately 200 km north of the South Tibetan Detachment and adjacent to the Indus Suture Zone (Figure 2.1). They are distinct from the leucogranite found near the Everest massif.

Geological thinking then turned to the leucogranite plutons and sheeted sills at the top of the Greater Himalayan Sequence (GHS) and also attempted to explain how these had evolved. Le Fort et al. (1987) suggested that migmatisation of the underlying gneisses in the thickest zones of the Tibetan Slab caused the granite axial core to evolve but they did not explain the mechanism of emplacement of the leucogranite. Many of the high Himalayan peaks are composed of leucogranite or have leucogranitic material underlying them. Hence, the crux of the geology must be how these granites came to be on the surface. Early models suggest anatexis initiated by slip along a thrust, with viscous minimum melts emplaced close to their source allowing upward transport of slices of crust (Harrison et al. 1997). Other high-temperature granites were interpreted as buoyant or less viscous enough to ascend into the low-grade Tethyan rocks (Le Fort et al. 1987).

The Himalayan Mountains and elevated region of Tibet are not the only consequences of crustal thickening following the collision of India with Asia. Crustal thickening has also affected the deep crust. A layer of partially molten material containing aqueous (water-rich) fluid exists at 15-20 km depth in the crust beneath the Himalayas and Tibet (Nelson et al. 1996; Alsdorf et al. 1999). This was discovered by the INDEPTH project, a major geophysical transect across the Himalayas (Zhao et al. 1993; Nelson et al. 1996).

Data gathered by a study of shear-coupled teleseismic P waves recorded by temporary broadband networks across Tibet suggests that the crust of the northern plateau is partially melted due to high temperatures, and that a relatively cool mantle extends from the Himalayas northwards under the centre of Tibet (Owens et al. 1997; Kosarev et al. 1999). A magnetic and gravity low over Tibet indicates hot crust and in-situ partial melting at depth (Alsdorf et al. 1999) in an area about 250 km north of Everest (Searle et al. 2003) where leucogranite bodies are in the process of being formed today (Nelson et al. 1996).

What this means is that crust from the Indian Plate, which has been forced below the Asian Plate, has been heated to temperatures sufficiently high to cause the plate to melt. The heating of rocks that have been forced to great depths in collisional zones is a common phenomenon (Allegre, et al. 1984). This occurs primarily because of radioactive decay of small amounts of uranium, thorium and potassium within rocks that causes them to heat up. Because rocks have low thermal conductivities, this radiogenic heat escapes more slowly than it is generated when crustal thickening occurs, causing rocks to heat up. The temperature increase that occurs is related to the degree of crustal thickening, the conductivity of the rock, the amount of radioactive material present in the rock, and the time before exhumation occurs (England and Thompson, 1984). Other heat sources may play a role (e.g. magmatic heating, heat from the mantle, shear heating, etc. – Harley, 1989) and the conduction of heat may be enhanced by fluid movement (England and Thompson, 1984), but radiogenic heating of thickened crust remains the primary source of elevated temperatures and regional metamorphism in collisional orogens. Rocks will initially begin to melt above 650 °C, but significant partial melting does not really occur until at least 750-800 °C, depending on the rock type (Vielzeuf and Montel, 1994). The molten material formed at these

high temperatures segregates and accumulates to form granites; consequently, granites are common products of collision zones (Searle et al. 2003).

Another effect of the collision of India with Asia is the movement of rocks from the Asian continent laterally to the east and west. This is because, as India has moved northwards it has dented into Asia, and large blocks of Asian crust have been displaced sideways. These displaced rocks have “escaped” laterally (Tapponnier et al. 1986), and this lateral movement of large blocks of crust has been accommodated by a number of major strike-slip faults to the east and west into China and Afghanistan, respectively (Figure 1.2). Most of the convergence was, however, accommodated by the eastwards movement of Tibet. Eastwards movement of the subducted Indian crust into the subduction zones of the Pacific (Figure 1.4) offered less resistance than westwards movement into the Eurasian Craton (Molnar and Tapponnier, 1975). Royden et al. (1997) noted that there is clear evidence for east-west extension within the Tibetan plateau and no shortening across the eastern margin of Tibet in the last 4 million years, but there has been clockwise rotation. Their model has the lower crust weaker than the upper crust such that it flows independently from upper crustal deformation and oozes out from under the middle of the plateau towards the edges.

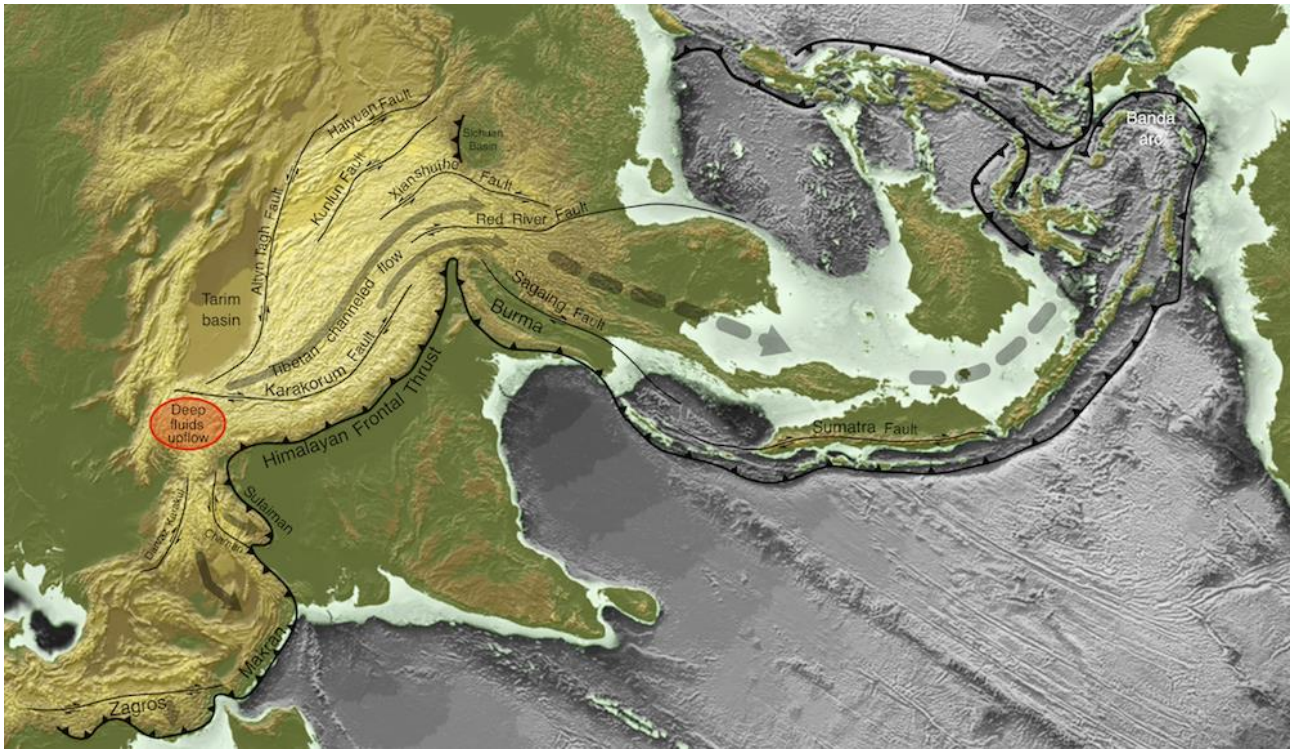


Figure 1.4: Convergence of India and Asia was accommodated by crustal flow eastwards (indicated by the arrows) into the Pacific subduction zones, which offered less resistance owing to the thinner crust and pre-existing crustal weakness compared to the thick, stable crust of the Eurasian Craton in the west (after Clark and Royden, 2000). Strike-slip faulting is a consequence of this crustal flow owing to differential flow rates between crustal blocks. The orange area is annotated as being a zone of deep fluids upflow.

Many earthquake epicentres have been recorded along the line of the Himalayan Front, as well as along these strike-slip faults (*(http://earthquake.usgs.gov/earthquakes/tectonic/images /himalaya_tsum.pdf)*, Figure 4.3). This is due to the continued movement of the Indian sub-continent underneath Tibet, and the escape of material away from the Himalayas (Figure 1.4). The recent earthquakes (discussed in section 3.6 and Figures 3.21 and 3.22) near Kathmandu in Nepal (25th April and 12th May, 2015) are examples of the continued relative movement of the two continental blocks.

CHAPTER 2: GEOLOGY OF THE MT. EVEREST REGION

2. 1 The tectonic zones of the Himalayas and a cross section through the Himalayas today

On a broad scale, the Himalayas have been divided into a number of tectonic zones (Figure 2.1A), consisting of (from south to north) the Sub-Himalayas, the Siwaliks, the Greater Himalayan Sequence, the Tethys Himalayas, the Indus Suture Zone and the Transhimalaya Batholith (Hodges, 2000). These tectonic units are separated by a number of major shear zones, and each zone reflects specific tectonic processes taking place within different portions of the crust over the life of the orogen, now juxtaposed along the faults into the configuration that is seen today. This tectonic zonation and structure of the Himalayas is remarkably consistent along the entire Himalayan range, which stretches for over 3,000 km. A cross section through the tectonic zones of the Himalayas (Figure 2.1B) shows the basic architecture of the orogen. To the north of the Greater Himalayan Sequence, a series of terranes from the Lhasa Terrane through the Qiangtang, the Songpan-Ganze and the Kunlun Terranes are thrust over the North China Terrane (Figure 2.1A). The sizes of continental fragments accreted to Asia range from continent-sized blocks to small slivers (Molnar, 1989). These terranes are remarkably similar in shape and size to the youngest “terrane”, the Greater Himalayan Sequence. Figure 2.1B shows these terranes in cross section, separated by faults. This implies that previous continent-continent collisions may have occurred over a long time period, with the North China Terrane having been subducted below the Kunlun Terrane, which appears to have been thrust over the former (Figure 2.1A), very much like the Greater Himalayan Sequence being thrust southwards over the subducting Indian Plate.

The Transhimalaya Batholith and Indus Suture Zone (Figure 2.1) occur on the northern margin of the Himalayas. The Indus Suture Zone defines the boundary between the Indian and Asian plates where these two plates were sutured by the collision. The period of subduction of India below the Asian continent prior to collision resulted in an Andean-type arc, and long-lived magmatism in this arc resulted in the intrusions that make up the Transhimalaya Batholith (Klemperer, 2006).

The rocks that make up these northernmost two zones record the geological history of the Asian plate prior to the collision of the Indian and Asian continents. The Indus Suture Zone contains a

number of slivers of oceanic crust and sediments (ophiolites) that were caught up in the collision between India and Asia (Dewey et al. 1988; Hodges, 2000).

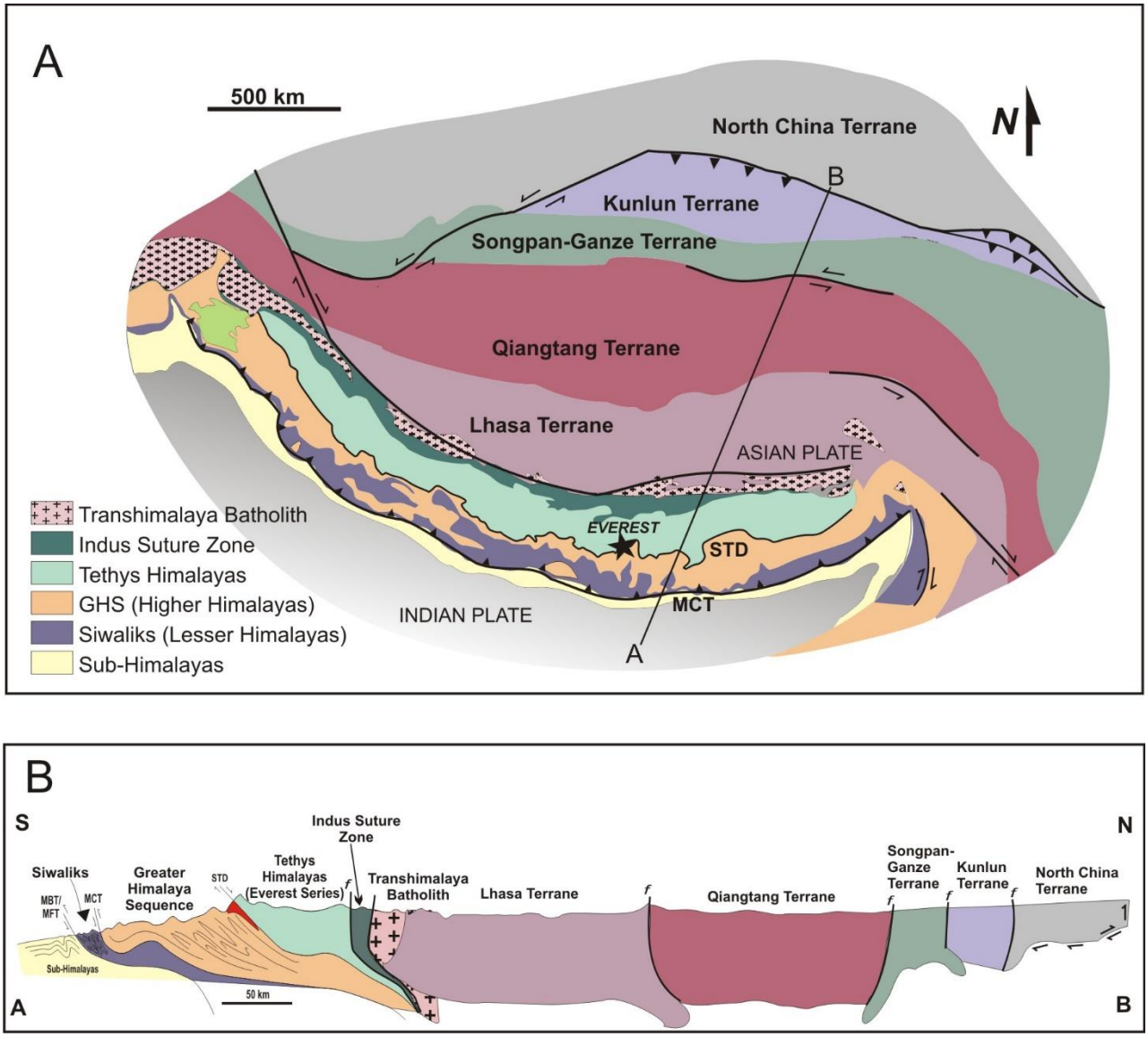


Figure 2.1: ***A*** *- Geology of the tectonic zones of the Himalayas and the Tibetan Plateau, showing their remarkable lateral consistency over more than 3000 km in an east-west direction.* ***B*** *– N-S section across the Himalayas and the Tibetan Plateau, showing the main subdivisions: The Sub-Himalayas, the Lesser Himalaya or Siwaliks, the area between the Main Basal Thrust (MBT) and the Main Central Thrust (MCT), the Greater Himalayan Sequence, the South Tibetan Detachment (STD), the Tethyan Himalayas, the Indus Suture Zone and Transhimalayan Batholith (modified after Dézes, 1999). Tibetan geology modified after http://www.geo.arizona.edu/~ozacar/frontp~1.htm.*

To the south of the Indus Suture Zone, the platform Tethyan Sediments or so-called Tethys Himalayas occur. These sediments were deposited in the Tethys Sea during the Ordovician era along the shoreline of the Indian Plate as it moved northwards prior to collision (Crawford, 1974; Gansser, 1981). These low-metamorphic-grade sediments are separated from the more southerly, high-metamorphic-grade Greater Himalayan Sequence, also known as the Higher Himalaya, by the South Tibetan Detachment, a major extensional shear zone (Searle et al. 2003).

The Greater Himalayan Sequence is a sequence of high-grade metamorphic rocks that form the core of the orogen. Similar to the rocks which were deposited in the Tethys Sea, some of these rocks were originally deposited as sediments on the northern margin of the Indian Plate before being subducted, deformed, heated and exhumed to their present position (Gansser, 1981; Searle et al. 2003; Myrow et al. 2009). The high-temperature mineral sillimanite, stable at temperatures of >500 °C at relatively low pressure (Yardley, 1989), is commonly found in the Greater Himalayan Sequence (Hodges et al. 1993; Dézes, 1999; Carosi et al. 1999), and widespread migmatisation (partial melting) has led to the formation of numerous leucogranites, which are also a common feature of the Greater Himalayan Sequence (Visona and Lombardo, 2002). These high-grade rocks have been thrust upwards to the south along the Main Central Thrust (MCT), which separates the Greater Himalayan Sequence from the lower-grade Siwaliks (or Lesser Himalaya).

The Siwaliks are a sequence of Precambrian to Miocene sedimentary rocks that have been metamorphosed at low- to moderate-grade and intensely folded and thrusted, before being juxtaposed against the Greater Himalayan Sequence by thrusting along the MCT (Burchfiel and Royden, 1985; Searle et al. 2003). Minerals such as kyanite, staurolite and garnet (which grow under specific temperature and pressure conditions, in this case ~600 ˚C and 7-9 kbar or 22-30 km depth (Goscombe et al. 2006) are common in the Siwaliks, and can be used as tools in determining the geological history of these rocks, which differs from the history recorded in the Greater Himalayan Sequence. They differ both in terms of P-T path, degree of metamorphism (high T, low P in the GHS but low T and high P in the Siwaliks) and timing of the metamorphism (older in the GHS, at 20-24 Ma, and younger in the Siwaliks, at 6-18 Ma – Goscombe et al., 2006). They are bounded to the north by the MCT, and to the south they are thrust over the Sub-Himalayas along the Main Basal Thrust or Main Frontal Thrust (Jessup et al. 2008).

The Sub-Himalayas form the most southerly of the tectonic zones of the Himalayas, and rocks in this area are made up of relatively unmetamorphosed coarse clastic sediments, forming a Molasse deposit that was derived from the erosion of the uplifted Himalayan Mountain front, and deposited on the foreland of the Himalayas (Dhital, 2015). These young sediments, deposited in basins at the foot of the mountains, have been overthrust and over-ridden from the north by the Siwaliks along the Main Basal Thrust and Main Frontal Thrust, and are folded along their northern margin (Dhital, 2015).

The northward movement of India and its eventual collision with Asia involved a number of stages, and took place over the last 50 million years. At 40 Ma, India was 1,250 km further south than it is today and the Tethys sea that existed between the Indian and Asian continents, had by then dried up but not closed up (Figure 2.10B; Allegre et al. 1984). Rock that now forms the highest mountains of Tibet was oceanic crust covered by platform sediments along the northern Indian shoreline (Figure 2.10B and C) which was part of the Tethys Sea. At approximately 15 Ma, the sea closed up completely, deforming the sediments (Rowley, 1996). By 5 Ma, the high Himalayas were forming and rising as they are today. Currently they continue to rise and are eroded by the Indus and Ganges drainage systems (Rowley, 1996). This sequence of events and their relationship with the tectonic zones of the Himalayas is shown in Figures 1.1 and 2.10 and is explained in the following tectonic history of the Himalayas.

2.2 Tectonic boundaries

The main structures in the Himalayas comprise the Main Boundary Thrust (MBT), at the base of the orogen, followed by the Main Central Thrust (MCT), the Khumbu Thrust (KT), and the South Tibetan Detachment (STD) which comprises the Lhotse Detachment (LD) at the base of the STD and the Qomolongma Detachment (QD) at the top of the STD near the summit of Everest (Figures 2.1, 2.2, 2.4 and 2.5). The MBT and the MCT are located south of Lukla and are the faults where much of the movement was taken up following the collision of India and Tibet (Figure 2.10D); they are considered to be a part of a large-scale zone accommodating the strain caused by the collision of India and Asia to form the Himalayas (Searle, et al. 2006). The MCT zone, for example, is a zone of high strain between 3km and 5 km thick which dips 10° to 30° to the north (Hubbard, 1988). An

important thrust called the Khumbu Thrust was postulated by Searle (1999a) to explain the presence of the leucogranitic layer between the dark sillimanite gneiss layer, pervasive in the Khumbu valley and near Everest Base Camp, and the LD. In fact, there is much evidence of movement along this layer with the presence of rafts of dark brown sillimanite gneiss in the overlying leucogranites and layers of dark gneiss intercalated with migmatitic rocks (Searle, 1999a). In numerous places along the route to Everest where the Khumbu Thrust is observed, dark brown sillimanite-biotite schists are typically juxtaposed with pale grey leucogranite bodies along the thrust. This relationship characterises the Khumbu Thrust and makes it an easily recognisable feature of the geology along the Khumbu valley (Searle, 1999a).

What makes the Khumbu Thrust significant is that it is a plane along which the Higher Himalayan leucogranites have been exhumed (Searle, 1999a). Structural and geochronological evidence suggests that thrusting along the MCT and the KT was taking place at the same time as extension along the STD (Searle et al. 2003), with the hangingwall of the STD moving down towards the north at the same time as the hanging walls of the MCT and KT were being thrust to the south (Figure 2.3). This means that although extension is evident in the STD, no net extension occurred across the Himalayan Mountain belt as the environment was purely compressive, and any extension across the STD was less than contractional thrusting across the MCT, MBT and KT. This implies the channel-flow-type mechanism that allowed for the extrusion of rocks between the STD and the MCT.

At the same time as the Higher Himalayan Leucogranites were thrust over the sillimanite-biotite schists of the Greater Himalayan Sequence, the STD (above the leucogranites) brought the Tethyan sediments to lower stratigraphic levels, adjacent to the leucogranites and Greater Himalayan Sequence.

The main tectonic boundaries that separate the geological units across the Himalayas and dominate the geology of the area, (Figure 2.2) are:

1. The South Tibetan Detachment (STD): This zone of normal dip-slip movement separates the Greater Himalayan Sequence from the Everest Series, and two major faults define it near Everest – the Lhotse Detachment (LD) and the Qomolongma Detachment (QD).

2. The Main Central Thrust (MCT): This thrust separates the Greater Himalayan Sequence from the Siwaliks (Lesser Himalaya) to the south of Lukla (and thus is not crossed on the trek to Everest). It is an important tectonic boundary and played a major role in the exhumation of the Greater Himalayan Sequence.

3. The Khumbu Thrust (KT): This is a large fault located below a zone of granites near the upper parts of the Greater Himalayan Sequence near Everest postulated by Searle (1999a).

4. The Main Frontal Thrust (MFT): This is a large fault located at the base of the extruding wedge (and the base of the Lesser Himalayan Sequence and the Siwaliks) and at the top of the subducting Indian upper crust.

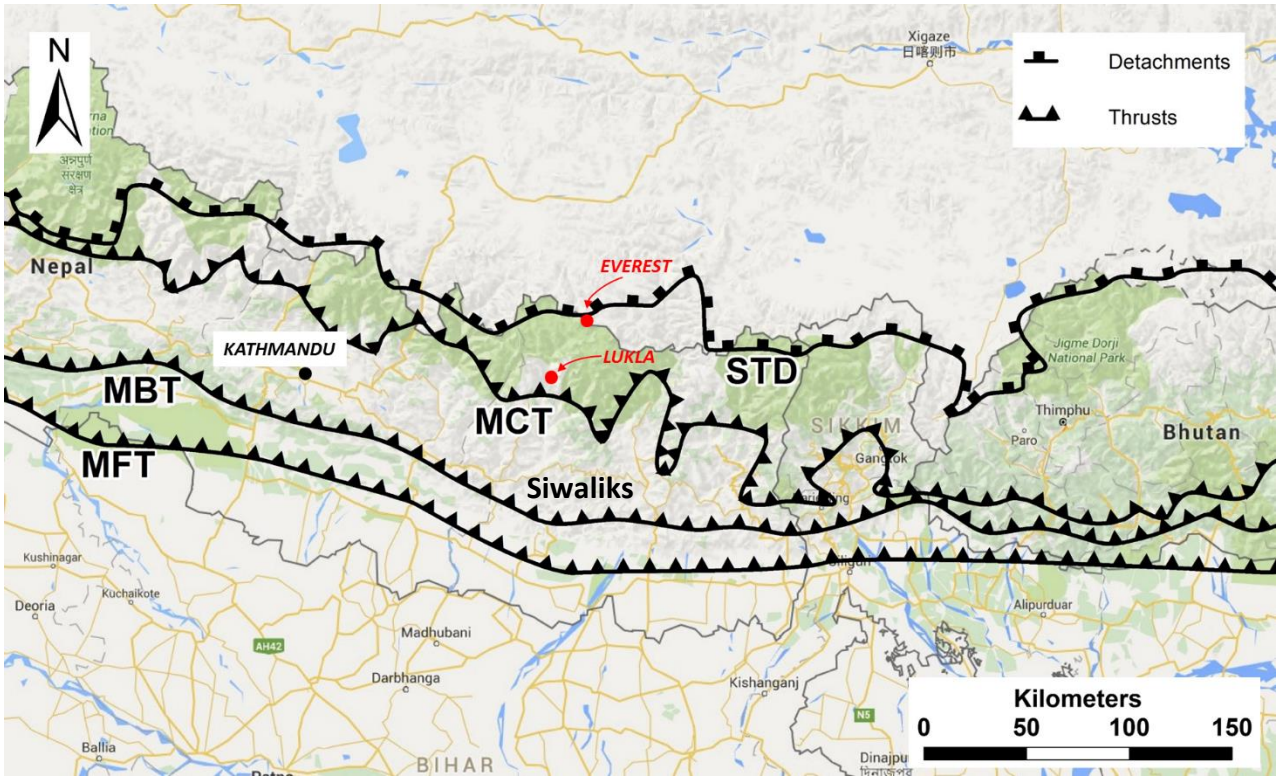


Figure 2.2: The location of the three main faults in Nepal, Bhutan and China. A zone about 30 km wide, bounded by the South Tibetan Detachment (STD) in the north and the Main Central Thrust (MCT) in the south, is referred to as the Greater Himalayan Sequence or High Himalaya. Further to the south from the MCT are the foothills of the Himalayas, the so-called Siwaliks or Lesser Himalaya, which are separated from the Indian lowlands by the Main Frontal Thrust (MFT) and Main Basal Thrust (MBT). The Khumbu Thrust (KT) is located very close to the STD and is not shown in this image, but is shown in Figure 2.3. The base map is an image taken from Google™ Maps.

These large-scale faults are all roughly east-west striking and dip towards the north at shallow angles, subparallel to the general northward dip of strata in the Himalayas (Figure 2.3).

The northern limits of the Greater Himalayan Sequence occur immediately south of Mt Everest and the GHS extends to the south past the town of Lukla towards the foothills of the Himalayas (Figure 2.3). It comprises a 10 km thick sequence of crystalline orthogneiss (the Namche migmatites) and sillimanite-biotite gneiss (Jessup et al. 2008). Large- and small-scale recumbent

folds (with subhorizontal to shallow northwards-dipping fold axial planes) were observed along the route.

The slopes of Mt Everest itself are made up of two distinct units: The lower parts of the Everest massif, below the STD, are made up of the high-grade gneiss of the Greater Himalayan Sequence, intruded by many pegmatites and leucogranites. The upper parts of Everest and Lhotse, above the STD (Figure 2.3), are made up of the lower-grade metasediments of the Everest Series.

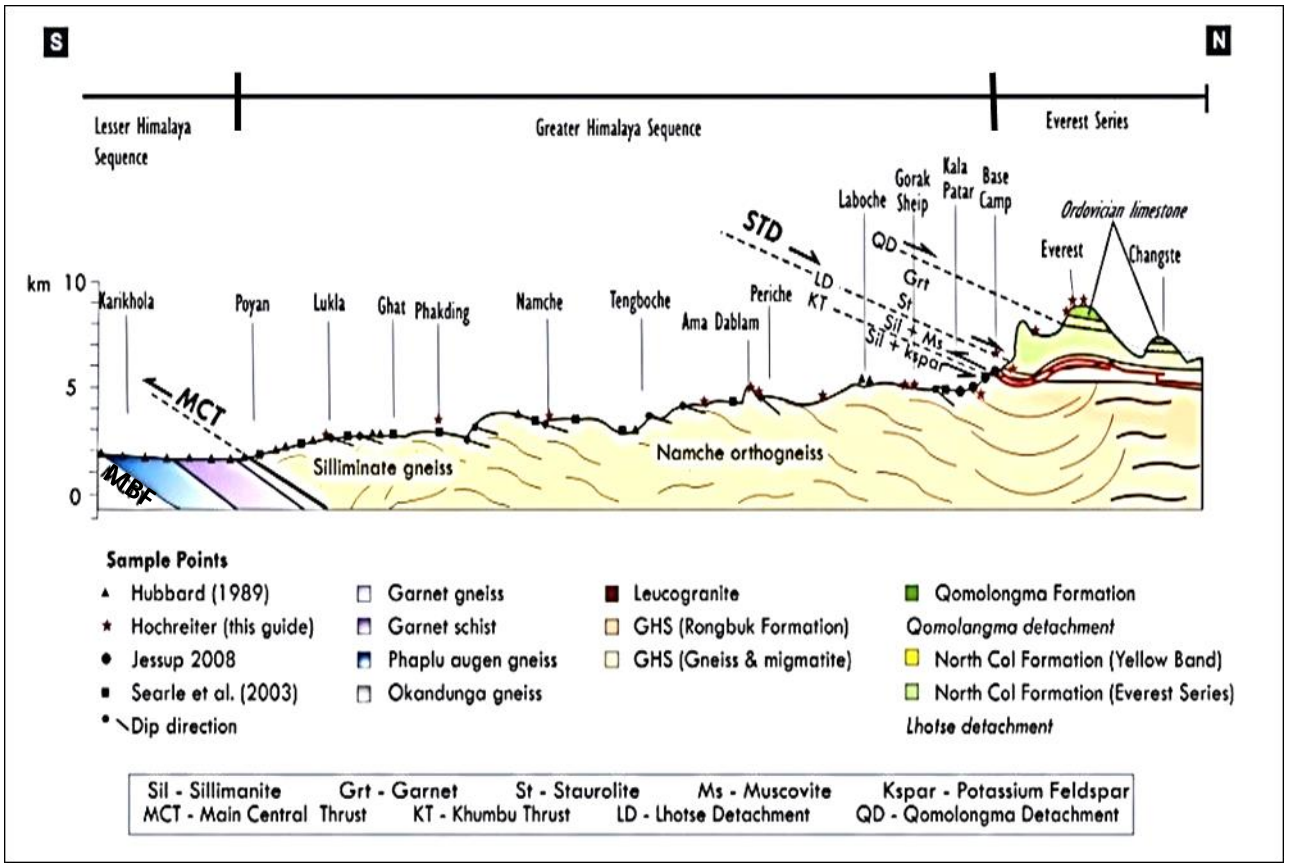


Figure 2.3: Geological cross section of the Everest massif, Tibet-Nepal showing the main faults and the detail of the STD which consists of the Qomolongma Detachment (QD) and the Lhotse Detachment (LD) with the Khumbu Thrust (KT) immediately below the LD. (modified after Jessup et al. 2008).

2.3 Stratigraphy

The Greater Himalayan Sequence (Figures 2.1, 2.2 and 2.3) occurs south of Mount Everest, between the base of the mountain (south of the town of Lukla) and the foothills of the Himalayas.

It comprises a crystalline gneiss sequence approximately 10 km thick with metamorphic minerals including sillimanite, biotite, kyanite and staurolite (Searle et al. 2003). Recumbent folds with horizontal fold axes and shallow, north-dipping fold planes occur in the Greater Himalayan Sequence with limbs from a few centimetres to many kilometres in length. The northern limit of the Greater Himalayan Sequence occurs on the slopes of Mount Everest itself, which can be divided into two distinct units. The lower portion of Everest consists of high-grade gneisses of the Greater Himalayan Sequence and Higher Himalayan leucogranites, whilst the upper parts of the mountain are made up of the lower-grade metasediments of the Everest Series. The two are separated by the STD, a zone which consists of the Qomolongma Detachment at the top of the famous "Yellow Band" and, further down, the Lhotse Detachment (Figure 2.3 and 2.4). The Greater Himalayan Sequence and the Everest Series have been further sub-divided into the Rongbuk, North Col and Qomolongma Formations (Yin and Kuo, 1978; Sakai et al. 2005; Myrow et al. 2009).

The Rongbuk Formation lies below 7,000 m altitude on Everest, and is part of the Greater Himalayan Sequence. It consists of sillimanite-biotite and K-feldspar schist and gneiss, calc-silicates and amphibolites, which have been intruded by dykes and sills of leucogranite. These dykes and sills range from a few centimetres to tens of metres in thickness and some of the larger leucogranites are sheets up to 1,500 m in thickness (Sakai et al. 2005; Searle, 1999b). The Rongbuk Formation is separated from the overlying North Col Formation by the Lhotse Detachment (LD) which forms part of the South Tibetan Detachment (STD) (Figures 2.4) (Yin and Kuo, 1978; Sakai et al. 2005, Myrow et al. 2009).

The lower portions of the North Col Formation, between 7,000 m and 8,200 m, consist of interlayered, deformed, marble and biotite-, sericite-, chlorite- and epidote-bearing schist and phyllite (Figure 2.5). The upper parts of the North Col Formation (above 8,200 m) are formed by the distinctive Yellow Band, a 400 m thick unit of rock comprising intercalated beds of middle Cambrian diopside- and epidote-bearing marble and lesser muscovite-biotite phyllite that weathers to a distinctive yellow-brown colour. Almost five percent of the Yellow Band was found to consist of "ghosts" of recrystallized crinoid ossicles, i.e. fossils (Gansser, 1964).

The North Col Formation has a tectonic contact along the Qomolongma Detachment with the overlying Qomolongma Formation (Figure 2.5). This uppermost unit extends from 8600 m to 8850 m, and is composed of Ordovician limestone, calcareous shale and siltstone. The top 10 m of Mount Everest consists of deformed re-crystallised calcite with minor occurrences of cubes of pyrite (FeS) and carbonaceous material (Yin and Kuo, 1978; Sakai et al. 2005; Myrow et al. 2009).

The North Col and the overlying Qomolongma Formation are separated by the Qomolongma Detachment which is also part of the STD. The uppermost 5 m of the Yellow Band (Figure 2.4) is found to be highly deformed adjacent to the Qomolongma Detachment, and a fault-breccia zone between 5 cm and 40 cm thick probably represents the zone where much of the recent movement between the two formations has occurred (Yin and Kuo, 1978).

The Qomolongma Formation (also low-grade metasediments of the Everest Series) extends from the top of the Yellow Band at 8,600 m above sea level to the summit of Mt Everest (Figures 2.4 and 2.5). This unit has also been called the Everest Formation or the Jomo Lungma Formation. This formation is composed of Ordovician limestone, calcareous shale and siltstone, which are dark grey through light grey to white in colour. The limestones are laminated and bedded, and interlayered with siltstone and recrystallised limestone beds that have gritty or argillaceous laminae (Yin and Kuo, 1978).

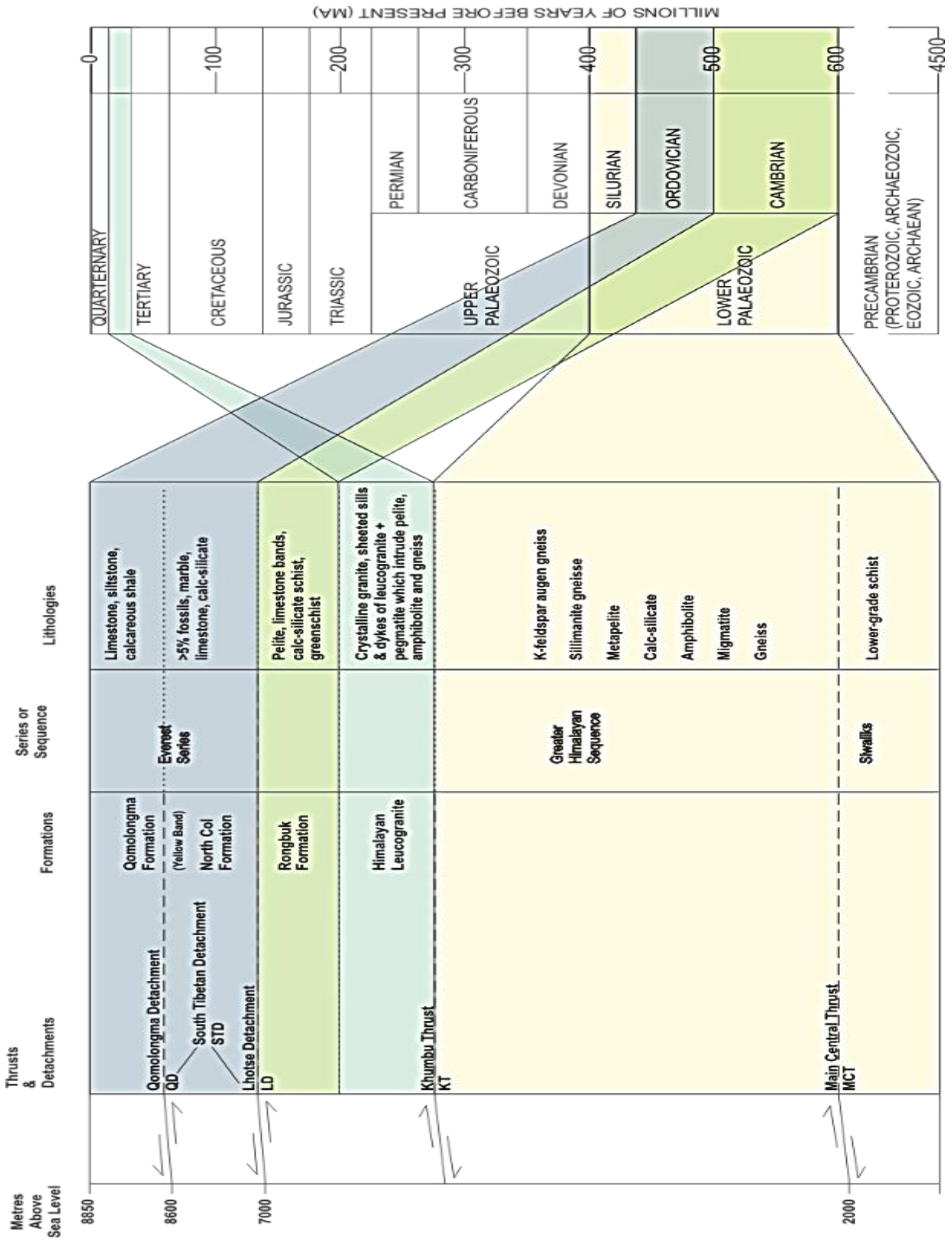


Figure 2.4: Stratigraphy of the area from Lukla to the summit of Mount Everest, shown in relation to the geological timescale.

In Figure 2.5, the main geological features are superimposed on a sketch of Mount Everest in order to give a better illustration of the geology of Everest and to show the physical stratigraphy on the mountain itself.

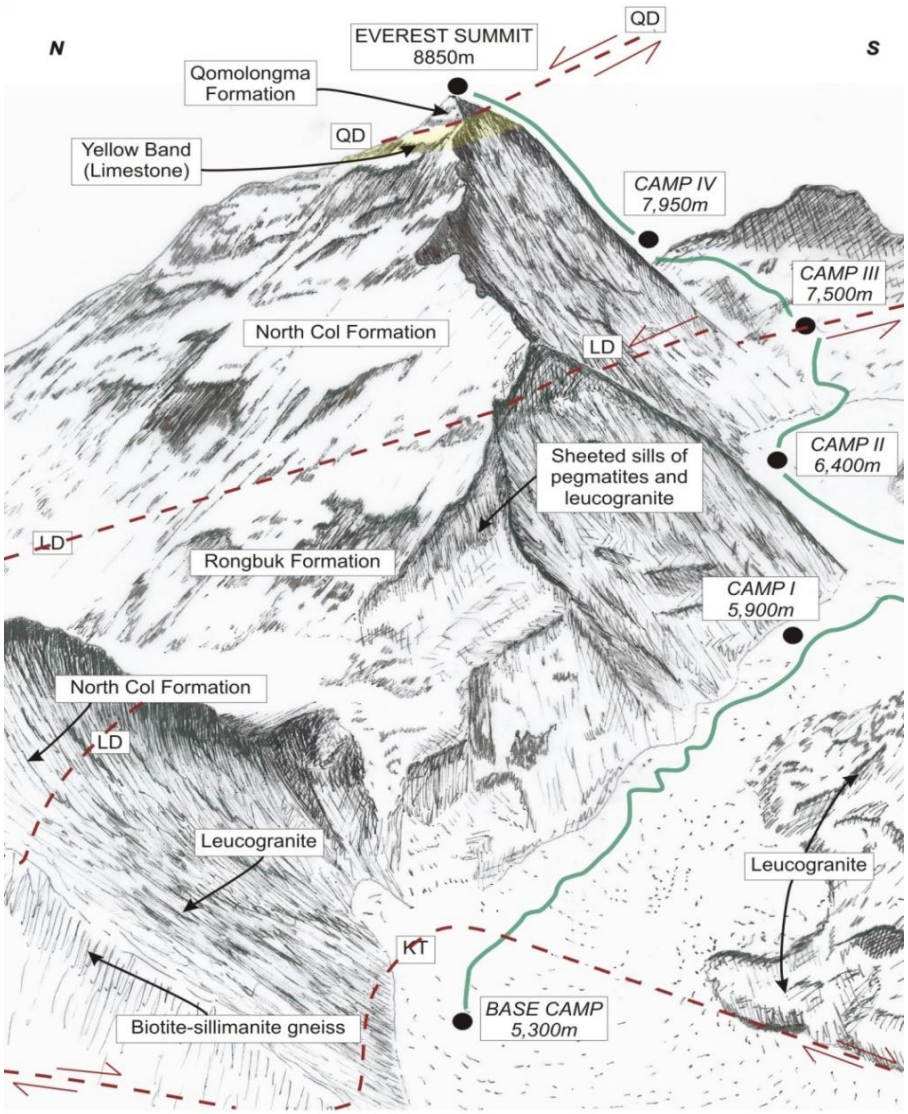


Figure 2.5: The main features of the geology of Mt Everest: Sedimentary rocks (originally from the floor of the Tethys Sea) make up the summit of Everest. The Qomolongma Detachment (QD) separates the summit limestone from underlying pelite or metamorphosed mudstones. The Lhotse Detachment (LD) separates the pelitic unit from the underlying sheeted sills of pegmatite and leucogranite, which were intruded between 32 and 16 million years ago (Searle et al. 2003). Near Base Camp, the Khumbu Thrust (KT) marks the top of underlying dark sillimanite-biotite gneiss. Dips are 5° to 15°N. Figure sketched by the author, after Searle et al. (2003).

Augusto Gansser in his book *The Geology of the Himalayas* first reported finding microscopic fragments of crinoids in marble taken from the upper portions of Everest (Gansser, 1964). These fossil fragments were later identified as being pieces of trilobites, crinoids and ostracods that had been partly sheared and recrystallized during low-grade metamorphism. At the base of the third step on the north-east ridge of Everest is a 60 m thick, white-weathering unit called a thrombolite bed. This contains sediments cemented and bound together by biofilms of micro-organisms that lived in a shallow marine environment (Gansser, 1964). This unit extends to within 10 m of the summit.

The Qomolongma Formation is broken up by several high-angle faults that end at the base of the formation along the main low-angle Qomolongma Detachment. These are secondary normal faults that are related to extensional movement on the Qomolongma Detachment (Yin and Kuo, 1978). Like the Yellow Band of the North Col Formation, the rocks five metres immediately overlying the Qomolongma Detachment are highly deformed (Yin and Kuo, 1978; Sakai et al. 2005; Myrow et al. 2009).

2.4 P-T-D-t paths and metamorphism of the Greater Himalayan Sequence and the Everest Series.

The high-grade rocks of the Greater Himalayan Sequence and the lower-grade schist and metasediments of the Everest Series and Lesser Himalaya each preserve a sequence of events that reveal much about how the Himalayas formed. These juxtaposed rocks have led to the development of the so-called crustal channel flow model for the formation of the Himalayas (Beaumont, et al. 2001).

Crucial to evaluating this model is the Pressure-Temperature-Deformation-time (P-T-D-t) path of the Greater Himalayan Sequence. P-T-D-t paths are generally constructed for metamorphic rocks that may record the changes in pressures and temperatures that a rock has experienced during burial and later uplift or exhumation.

2.4.1 The metamorphic and deformation history of the Everest Series

One of the fundamental differences between the Greater Himalayan Sequence and the Everest Series is the metamorphic grade. Everest Series schists record maximum temperatures of between 600 °C and 650 °C (Jessup et al. 2008), lower than those of the GHS, which exceed 700 °C (Searle et al. 2003). Pressure estimates for the Everest Series are more variable, ranging from 2.9 ± 0.6 kbar to 6.2 ± 0.7 kbar (Jessup et al. 2008), which corresponds to burial depths of between 10 km and 20 km for these rocks, whilst the GHS records eclogite facies metamorphism with pressures of > 14 kbar (>45 km depth) before being exhumed to granulite facies conditions of 4-6 kbar.

Critically, the rocks that give lower pressure conditions have preserved retrograde reaction textures, proving that they record decompression from higher pressures and temperatures (i.e., the rocks reached 20 km in depth and were then exhumed back to shallower depths of ~10 km during metamorphism). Additionally, Everest Series schists preserve prograde zoning in metamorphic minerals. Such zoning forms because of a progressive change in the reacting bulk composition and, consequently in the chemical composition of metamorphic minerals during their growth. Thus, rocks of the Everest Series preserve a record of burial and heating, peak metamorphism, and their subsequent exhumation and cooling.

Early in the metamorphic history of the Everest Series, muscovite and biotite were aligned by intense shearing and isoclinal folding of the original sedimentary layering in the rock during D_1 (Figure 2.6A) (Jessup et al. 2008). This early deformation event occurred during early collisional thrusting and the burial of these sediments (Jessup et al. 2008). This resulted in the formation of the early S_1 fabric, which was subsequently overgrown by garnet and staurolite as the temperature and pressure increased (Figure 2.6B). The term 'S_1' refers to the earliest schistosity formed (i.e. that formed during the D_1 deformation event). As a result, both garnet and staurolite have inclusions that are aligned with the S_1 fabric. In these samples, garnet contains prograde compositional zoning (Figure 2.6C), and may be intergrown with staurolite, suggesting that staurolite grew through a reaction which consumed garnet (Jessup et al., 2008) on the prograde path (i.e. during burial, when pressures and temperatures were increasing).

Following the growth of staurolite at maximum pressures, the S_1 fabric was crenulated (folded) by D_2 (the second deformation event, coincident with exhumation). Larger biotite grains grew along the S_2 plane as a result of recrystallization. Shearing along the S_2 plane then took place which rotated garnet and staurolite grains. A stretching lineation developed during this shearing and staurolite porphyroblasts were displaced by extensional shear bands (Figure 2.6D).

Some Everest Series schists that record lower pressures post-dating D_2 have overgrowths of cordierite on staurolite, and andalusite is also found (Figure 2.6E). Both these minerals are indicative of fairly low pressures (<15 km depth), and show that the rocks were being exhumed during D_2. This cordierite and andalusite growth over the S_2 fabric was the final phase in the P-T-D-t history (Figure 2.6E).

The P-T path thus involved a prograde pressure and temperature increase followed by a peak-to-retrograde pressure decrease (at or near peak temperatures), and is consistent with a continuously evolving history from burial to exhumation. The D_2 features are related to shearing on the LD/QD, which has been linked to exhumation (Jessup et al. 2008). The switch from D_1 to D_2 is likely the point at which channel flow starts. The P-T-t-D path discussion in Jessup et al 2008 suggests that the M_1 and M_2 (coincident with D_1 and D_2) are related to burial via thrusting and decompression/exhumation, respectively. The orientation of S_1 and S_2 are both sub-horizontal and resulted from the D_1 and D_2 episodes.

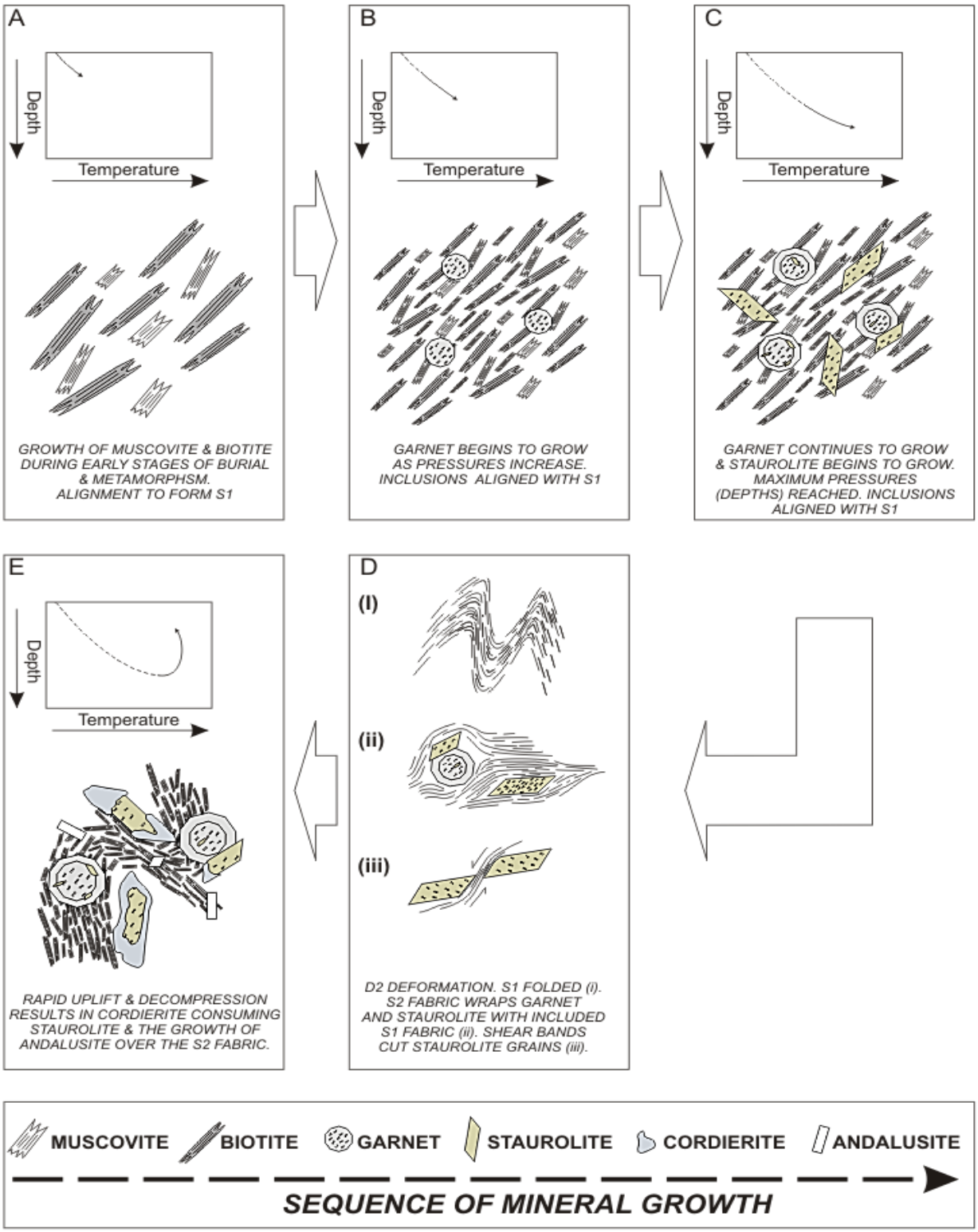


Figure 2.6: History of metamorphism and deformation in the Everest Series schists (after Jessup et al. 2008).

2.4.2 The metamorphic and deformation history of the Greater Himalayan Sequence

In contrast to the Everest Series, the sillimanite-biotite schist of the Greater Himalayan Sequence records conditions of >700 °C (Searle et al. 2003), and relatively low pressures of 4-6 kbar (Jessup et al. 2003). Garnet in these rocks has no compositional zoning, indicating that the rocks reached temperatures high enough for compositional re-equilibrium to remove prograde growth zoning. This is confirmed by the fact that much of the Greater Himalayan Sequence has been migmatised (partially melted at high temperatures) (Figure 2.7).

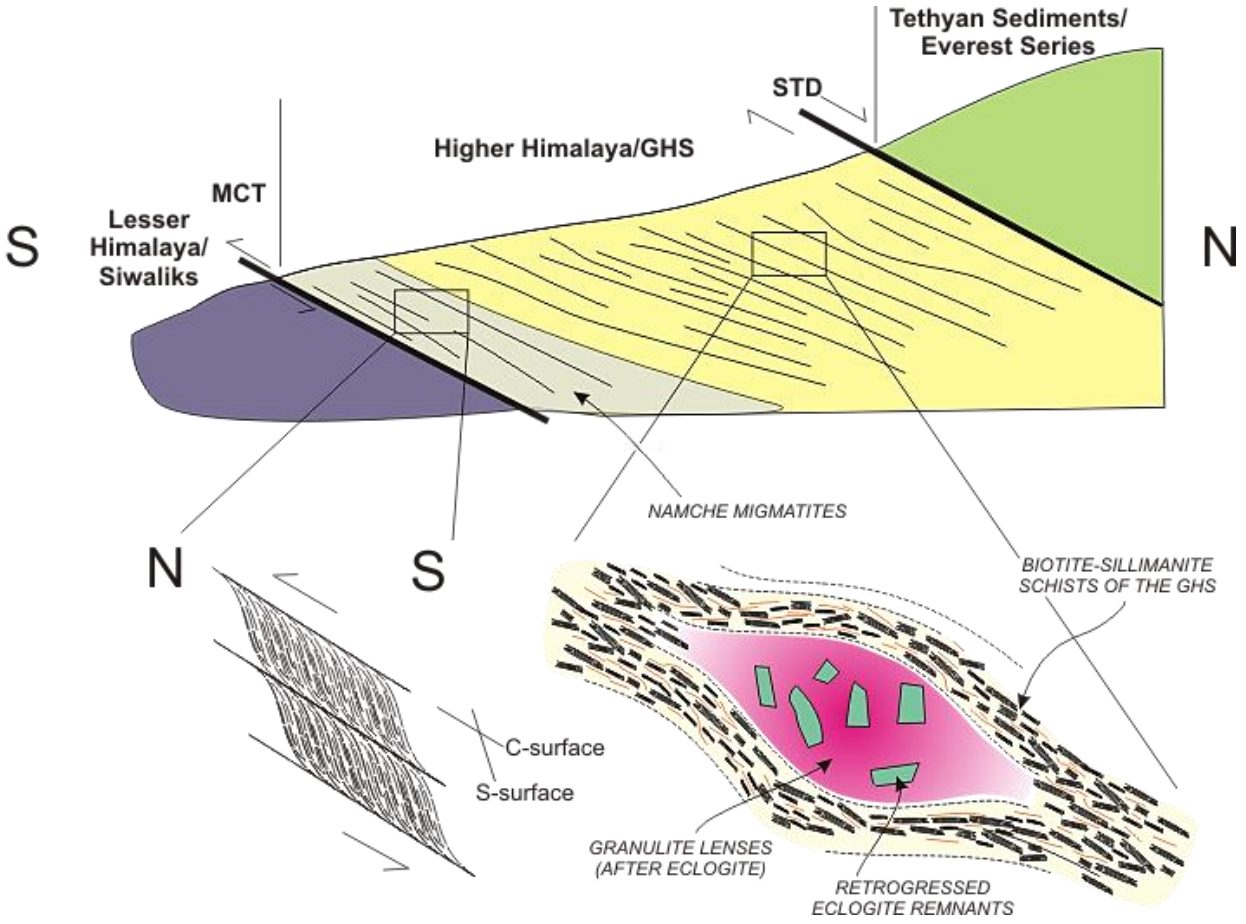


Figure 2.7: Cross section through the Greater Himalayan Sequence showing the key relationships between deformation and metamorphism.

However, although fairly high-temperature, low-pressure conditions are recorded throughout the Greater Himalayan Sequence, inclusions of granulitised eclogites have been found locally as lenses in sillimanite-biotite gneiss from the Greater Himalayan Sequence (Lombardo and Rolfo, 2000) (Figure 2.7 and 2.8). Eclogite is a rock formed at very high pressures (>14 kbar, i.e. >45 km), and this high-pressure metamorphism has resulted in the growth of omphacite (Na-rich pyroxene) and Ca-rich garnet (Figure 2.8A).

Following burial to extreme depths, these eclogites were subsequently exhumed and heated, resulting in a partial granulite facies metamorphic overprint in which omphacite has been replaced by clinopyroxene-plagioclase symplectites, and Ca-rich garnet has been surrounded by coronas of hornblende, orthopyroxene, biotite and plagioclase (Lombardo and Rolfo, 2000) (Figure 2.8B). It is likely that the S1 fabric formed during burial or at high pressures, and S1 fabrics in the GHS overgrown by staurolite and garnet are thought to be related to crustal thickening via folding and thrusting that culminated in Barrovian metamorphism (Jessup et al., 2008).

Further decompression resulted in upper-amphibolite- to granulite-facies conditions of 700-800 °C and 4-6 kbar, forming the sillimanite-biotite assemblage that is common throughout the Greater Himalayan Sequence. Locally, cordierite also grew during the latter parts of this decompression stage, which was accompanied by deformation to form the S_2 fabric in these gneisses (Figure 2.8C).

Near the base of the Greater Himalayan Sequence, in a group of stromatic (banded) migmatite and gneiss as referred to as the Namche migmatites, S-C fabrics indicate top-to-south verging movement (Figure 2.7) i.e., movement of the Greater Himalayan Sequence southwards over the Siwaliks (Searle et al. 2003). It is likely that the S_1 fabric formed during burial (as per Jessup et al. 2008) and S_2 (which includes the S-C fabric) was the start of exhumation. Higher up in the Greater Himalayan Sequence, widespread extensional shear bands indicate top-down-to-the-north movement. Sillimanite grew into extensional structures in these rocks, suggesting that deformation occurred at peak temperatures (Searle et al. 2003). Additionally, there is little or no retrograde overprint (in contrast to the Everest Series), indicating either rapid exhumation of the

Greater Himalayan Sequence (Searle et al. 2003), or a lack of retrograde fluids owing to the high-temperatures reached in the Greater Himalayan Sequence.

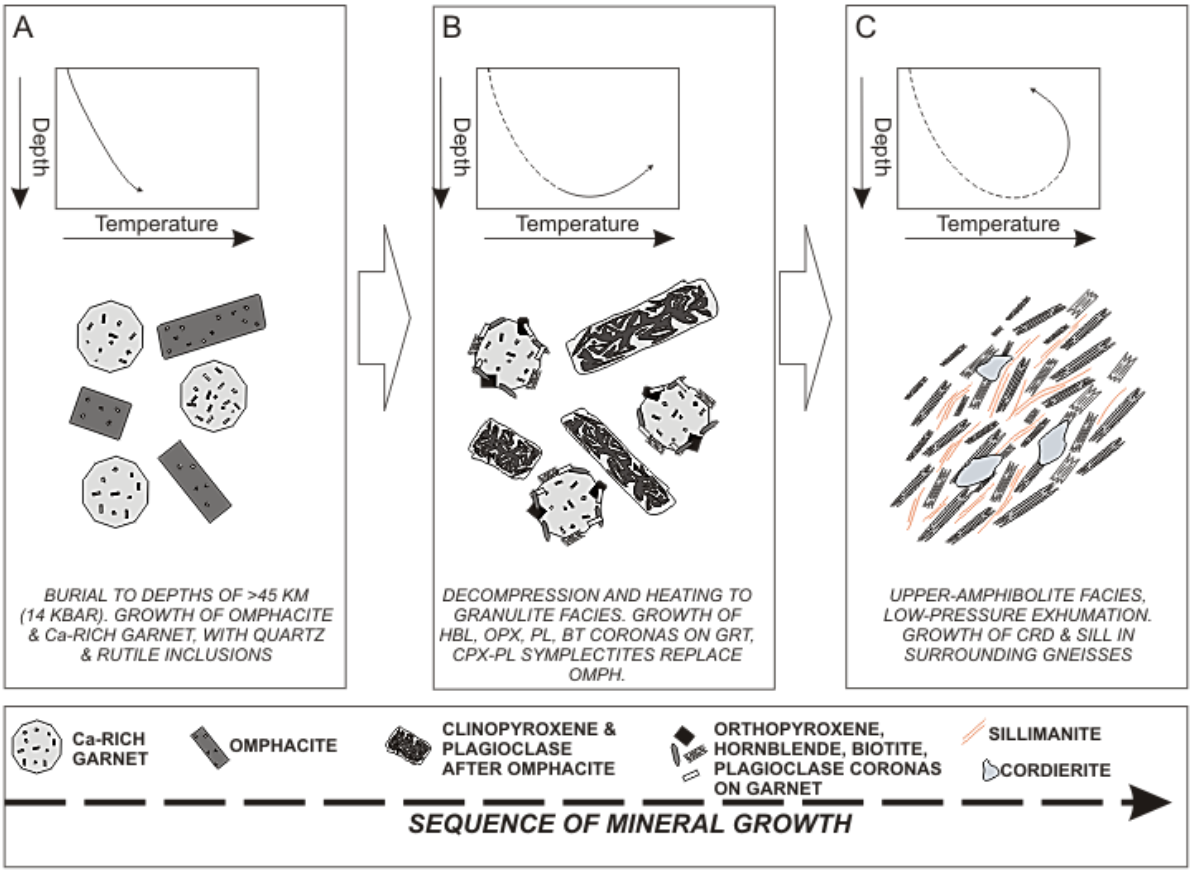


Figure 2.8: History of metamorphism and deformation recorded in the Greater Himalayan Sequence. Burial (A) to depths of >45 km results in eclogite facies metamorphism, rarely preserved. Subsequent decompression and heating to the granulite facies (B) results in the replacement of eclogitic assemblages, and the widespread development of sillimanite, as well as migmatisation. This is widely regarded as M1. Further decompression and cooling to upper amphibolite facies results in the growth of cordierite (C). Note that this is referred to as M2 in the GHS. Note that D1 in the GHS is likely to have occurred during burial (i.e. before M1), with D2 (and S2 fabric development) taking place during Exhumation, and overprinted by low-pressure cordierite (i.e. during M1 and M2) (figure drafted after Lombardo and Rolfo, 2000; Jessup et al., 2008).

2.4.3 Metamorphic and deformation zones in the Everest area

The Greater Himalayan Sequence forms the high-grade core of the Himalayan orogen and, as such, there is a clear metamorphic zoning on both the south and north sides of the Greater Himalayan Sequence (Goscombe et al. 2006). This zonation shows that the highest-grade rocks are found in the central portions of the Greater Himalayan Sequence. Metamorphic grade decreases northwards until the low-grade metasediments of the Everest Series are reached and, similarly, decreases southwards towards the low-grade schists of the Siwaliks (or Lesser Himalaya). This pattern is observable on metamorphic zonation maps, showing metamorphic minerals and, by implication, their P-T conditions (Figure 2.9) and is one of the characteristic features of the geology of the Himalayas. A general model for orogens would place the highest-grade rocks centrally in the orogen on the basis that the greatest thickening led to highest grades of metamorphism at depth, and the greatest subsequent exhumation (Harley, 1989). In the Himalayas, however, although the grade varies laterally (from low-grade in the Siwaliks, to high-grade in the GHS, and back to lower grades in the Everest Series, the orientation of structures and the relationships between these high-grade zones means that the metamorphic grade also varies considerably vertically, with temperatures decreasing both upwards and downwards from the higher-grade GHS. This unique vertical zonation, and particularly the inverted metamorphic profile across the MCT, is one of the key geological features that has given rise to the Channel Flow model (Beaumont et al. 2001).

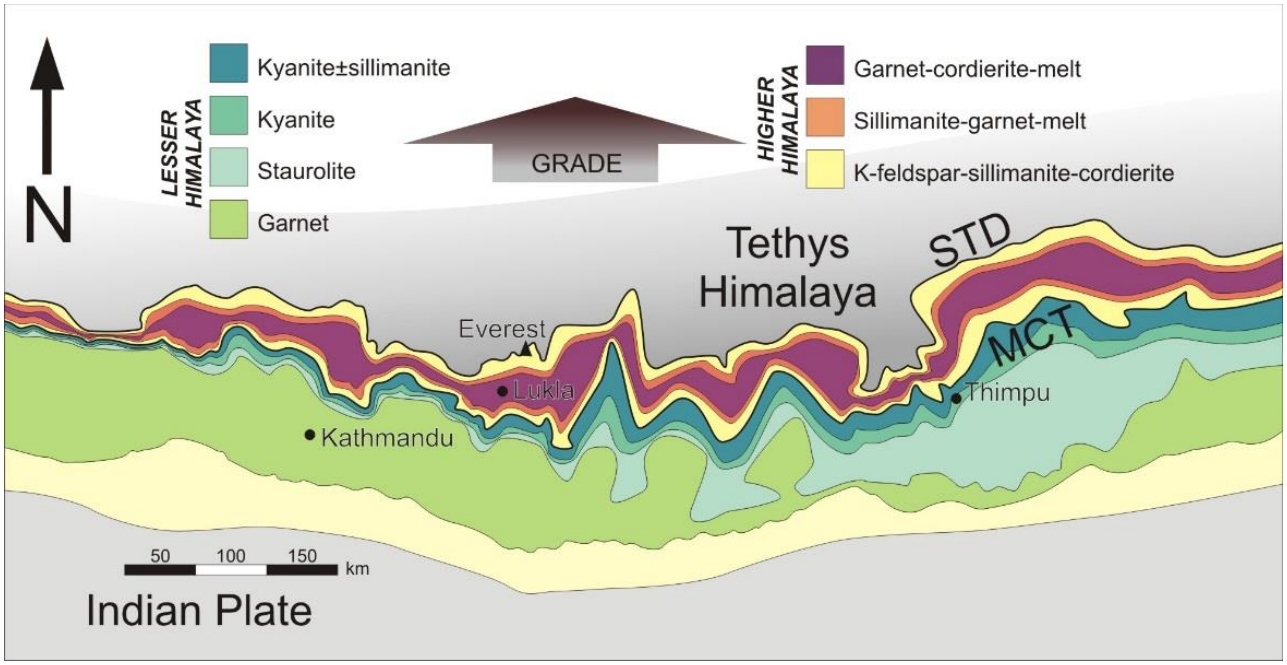


Figure 2.9: Metamorphic zonation across the Himalaya (after Goscombe et al. 2006).

Critically, what this shows is that at the top of the Greater Himalayan Sequence (adjacent to the Everest Series) there is a normal metamorphic gradient (i.e. grade decreases upwards, with lower grade rocks structurally above higher-grade rocks), whilst at the base of the Greater Himalayan Sequence there is an inverted metamorphic gradient (high-grade Greater Himalayan Sequence rocks are structurally above the low-grade Lesser Himalaya). This metamorphic zonation is further emphasised by the pattern of deformation across the Greater Himalayan Sequence and into the adjacent Siwaliks and Everest Series i.e. the contrasting shear direction, top-to-north, normal dip-slip faulting in the north (juxtaposing the GHS and the Everest Series) vs. top-to-south thrusting in the south (juxtaposing the GHS and Siwaliks) and the nature of the shearing (extension in the north vs. thrusting in the south).

At the base of the Greater Himalayan Sequence, a major zone of thrusting is found – the Main Central Thrust (MCT), along which the Greater Himalayan Sequence has been thrust over the Siwaliks. It is across this zone that the inverted metamorphic gradient is found. Additionally, S-C fabrics in the Namche Migmatites (Figure 2.7), the southern parts of the Greater Himalayan

Sequence, indicate top-to-south vergence, consistent with the thrusting along the MCT (Goscombe et al. 2006). The retrograde mineral growth is linked to the shearing/thrusting (the S_2 and S-C fabrics) through late retrograde minerals cordierite and sillimanite (Figure 2.8).

In contrast to this, the upper parts of the Greater Himalayan Sequence show extensional (as opposed to thrusting) movement (Goscombe et al. 2006; Jessup et al. 2008). Numerous extensional shear bands are found in the Greater Himalayan Sequence, with a top-down-to-the-north sense of movement (Figure 2.3). This movement culminates in the South Tibetan Detachment (STD) which is a major zone of extensional shearing where the low-grade metasediments of the Tethys Himalaya (the Everest Series) have been brought alongside the high-grade Greater Himalayan Sequence. If one looks at a cross section of the vergence of deformation and metamorphism (Figures 2.3 and 2.7), one can see that the highest-grade rocks in the core of the Greater Himalayan Sequence have moved upwards the most, relative to both the Siwaliks and the Everest Series.

Granites generated by partial melting in the hot lower crust have risen and accumulated at the top of the Greater Himalayan Sequence. Because the partial melting occurred only after the burial of the Greater Himalayan Sequence, the granites post-date early D_1 deformation, but may show some signs of later, ductile D_2 deformation related to exhumation of the Greater Himalayan Sequence (Figure 2.3).

2.5 The tectonic history of the Himalayas

The distinctive zones of the Himalayas are the result of active tectonic processes. These processes began over 50 Ma when India was still moving towards Asia and the oceanic crust was subducting below the Asian continental margin. This subduction continues today as high-grade mid-crustal rocks are exhumed along active faults. To understand the current geology of the Himalayas, the tectonic history of the orogen must be understood.

At roughly 75 Ma (Figure 2.10A) the Indian continent was moving towards Asia, and the two landmasses were separated by the Tethys Sea. Along the northern margin of the Tethys Sea, subduction of oceanic crust beneath Asia resulted in a magmatic arc (Figure 2.10A), with a forearc basin and an accretionary wedge in front of the arc. On the Indian continent, a thick package of Palaeozoic sediments composed of limestone, siltstone and calcareous shale had accumulated; these were then covered by Cretaceous sediments (mudstone and siltstone).

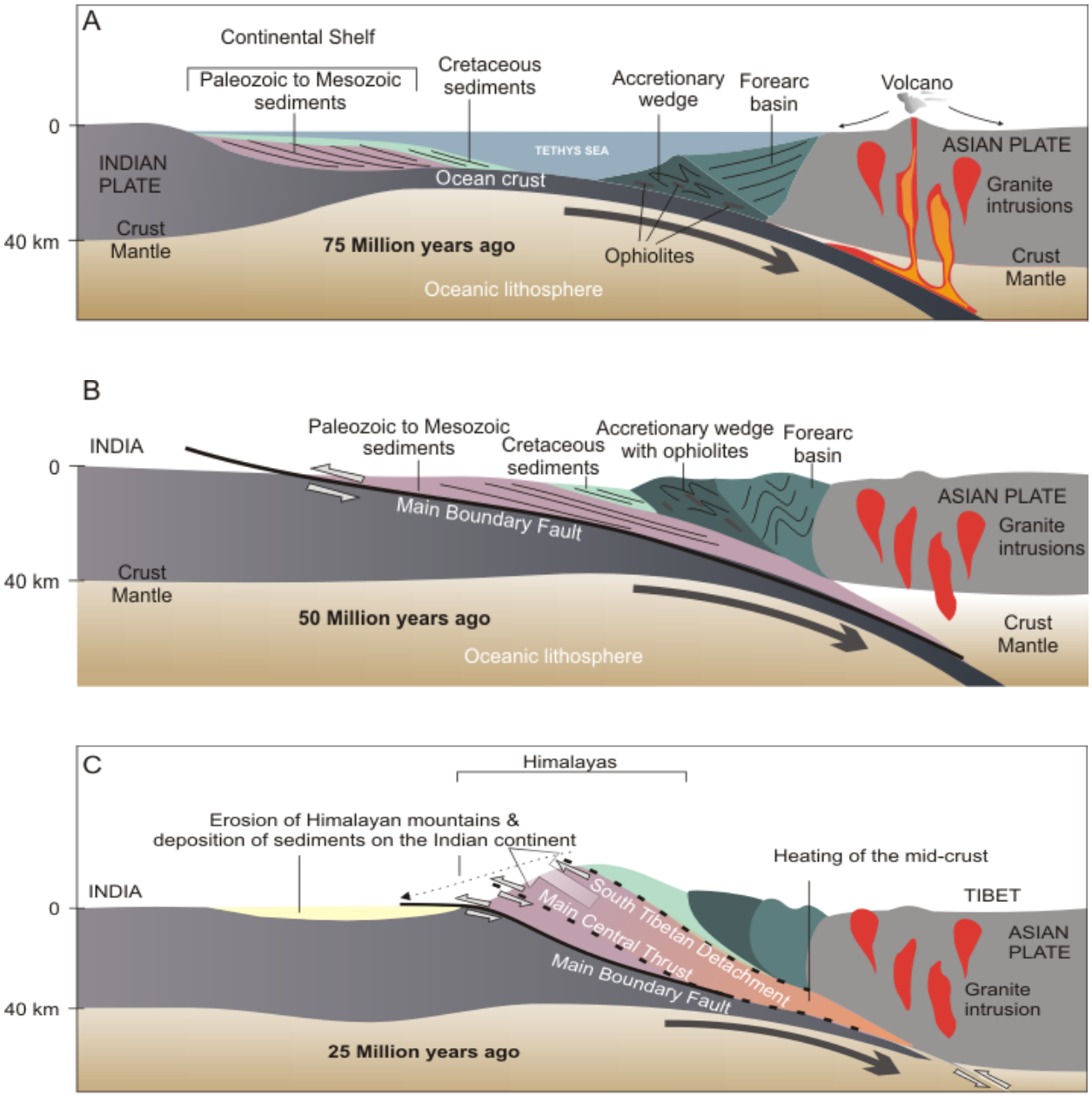
At approximately 50 Ma (Figure 2.10B) India and Asia began to collide. The accretionary wedge and forearc basin (relatively immature arkoses and siltstones derived from the volcanic arc) were caught up between the two continents. Indian continental crust and Palaeozoic sediments were also thrust below Asia, and the Main Frontal Thrust began to form.

Approximately 25 million years later (Figure 2.10C), sediments deposited on the leading edge of the Indian continent had been buried to mid-crustal levels by the collision and began to heat up. The metamorphism of these sediments to high grades (i.e. high temperatures and pressures) caused them to partially melt, and to become highly ductile. These hot, ductile sediments then began to escape from mid-crustal levels towards the surface between the incipient Main Central Thrust (MCT) and South Tibetan Detachment (STD). The exhumation of these high-grade rocks was driven by high levels of erosion along the Himalayan mountain chain, and the eroded sediments were deposited in basins on the Indian Craton.

The present-day setting (Figure 2.10D) is a result of these processes. The high-grade Greater Himalayan Sequence, also known as the Higher Himalaya, has been exhumed along the MCT and the STD.

To the south of the MCT, the Siwaliks (Lesser Himalaya) are formed from the same Proterozoic to Mesozoic sediments as the Greater Himalayan Sequence (Higher Himalaya). These rocks, however, were not subducted, heated and exhumed, and have generally experienced only low-grade metamorphism, although there is a smooth and continuous increase in metamorphic grade upwards towards the MCT, progressively across the kyanite-in, staurolite-in and -out, K-feldspar-in, muscovite-out and sillimanite-in isograds up to the top of the MCTZ (Goscombe et al., 2006). At

highest structural levels, rare migmatitic segregations are noted (Goscombe et al., 2006). Similarly, the Tethyan sediments found on the summit of Everest and northwards into Tibet are formed by low-grade Cretaceous sediments that were deposited on the Tethyan sea floor. The eroded material from the Himalayan front forms the Sub-Himalayas, deposited in a foreland basin that formed on the Indian crust.



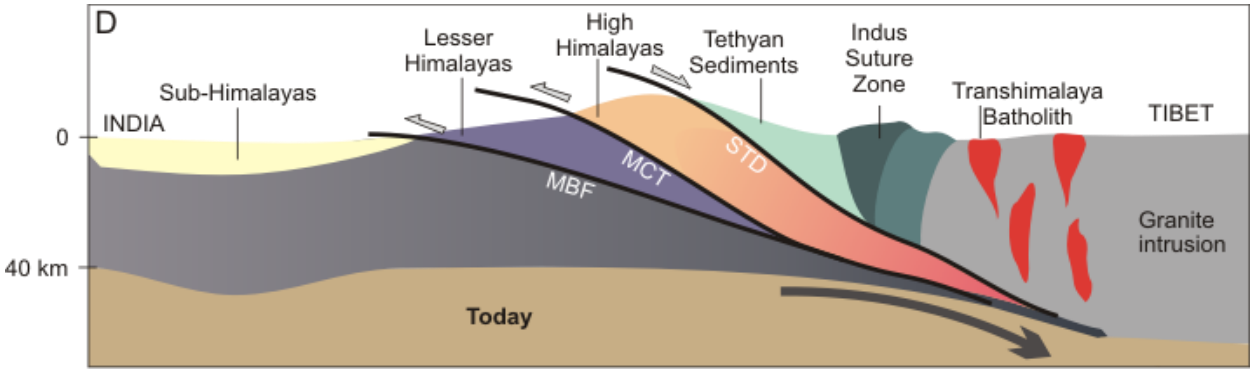


Figure 2.10 (previous page): Crustal sections through the collision of India with Asia (modified after Allegre et al. 1984). A. As India approached Asia during the Cretaceous period, sediments were deposited in the shrinking Tethys Sea (on top of older Palaeozoic to Mesozoic sediments) on the continental shelf of the Indian plate. ***A****. Forearc basin developed adjacent to an Andean-type volcanic arc on the Asian Plate, where granites were emplaced. Slivers of subducting oceanic crust were caught in the accretionary wedge, and today form ophiolites.* ***B****. As movement continued, so the Tethys Sea began to shrink. Sediments developed as the leading edges of the Asian and Indian plates were brought together. Once collision began, sediments were juxtaposed, and the Main Boundary Fault was formed along which much of the movement was taken up.* ***C****. During collision, some of the Palaeozoic to Mesozoic Sediments were taken to mid-crustal depths where they were folded and deformed, and heated up at depth to many hundreds of degrees centigrade. These hot rocks then began to melt, became ductile and were pushed out to surface along a channel, between the Main Central Thrust and the South Tibetan Detachment.* ***D****. The rocks of the Lesser Himalaya and the Higher Himalaya are of the same age and were originally deposited together on the Indian continent. They now differ greatly in metamorphic grade, having experienced significantly different histories during the collision of India with Asia. The Cretaceous sediments deposited in the Tethys Sea on the Indian Plate now form the Tethyan Sediments of Tibet. The deformed accretionary wedge and forearc basin became the Indus Suture Zone, and the Andean-type intrusions now form the Transhimalaya Batholith. Sediments eroded from the rising Himalayan Mountains have been deposited on the Indian Continent as the Sub-Himalayas.*

The following sequence of events describes the history of deformation and metamorphism experienced by the rocks of the Greater Himalayan Sequence and Everest Series:

1. ***Collision of the Indian and Asian continents between 55 and 32 Ma***. During this collision, rocks of the Indian continent were thrust below the Asian continent, resulting in crustal thickening. The deformation associated with this burial formed isoclinal folds and an S_1 fabric in the rocks of the Greater Himalayan Sequence, and also resulted in deformation in the Everest Series. During and following this D_1 event, the rocks began to heat up.

2. ***Eclogite-facies metamorphism.*** In the P-T-D-t path described by Jessup et al. (2008), Barrovian metamorphism, as a consequence of crustal thickening, is suggested as the earliest metamorphic event in the Everest Series. Although both the Greater Himalayan Sequence and the Everest Series experienced similar 'clockwise' P-T loops (i.e. burial followed by heating), the granulitised eclogites found in the Greater Himalayan Sequence indicate that these rocks were buried to much greater depths than the Everest Series rocks and experienced an early (pre-M_1) eclogite-facies metamorphic event. (M_1 refers to the first metamorphic event in these rocks.) The timing of this high-pressure metamorphism in the Everest area is unclear (Cottle et al. 2009), but may be similar to the 54-46 Ma eclogite event described from the western Himalayas (Lombardo and Rolfo, 2000; Parrish et al. 2006; Leech et al. 2005).

3. ***Heating – 'M_1' metamorphism***. Following burial, rocks were heated to upper-amphibolite facies (on the edges of the Greater Himalayan Sequence) or granulite facies (in the centre of the Greater Himalayan Sequence) conditions. These conditions were likely reached between ~32 Ma (Jessup et al. 2008) and ~13 Ma (Cottle et al. 2009). At the peak of metamorphism, granites began to form from the anatexis of these rocks. At the thermal peak, rocks also began to be exhumed. Owing to the fact that the Everest Series was far less deeply buried, it only experienced amphibolite-facies metamorphism.

4. ***Exhumation.*** Following heating, rocks of the Greater Himalayan Sequence were exhumed. Because they were hot and contained melt, these rocks were ductile. Thrusting along the Main Central Thrust brought these hot, ductile rocks up over the lower-grade Siwaliks, whilst

extensional movement along the South Tibetan Detachment brought lower-grade rocks of the Everest Series into contact with the higher-grade Greater Himalayan Sequence. Movement along both structures appears to have been coeval, with exhumation younger than 16 Ma (Jessup et al. 2006).

2.6 Leucogranite, its composition and metamorphic origin

Granites are intrusive magmatic rocks composed almost entirely of quartz and feldspar, with minor amounts of biotite or other mafic minerals. These rocks form from the partial melting of high-temperature metamorphic rocks, concentrating the lighter elements (Si, K, Na, and Ca) in the melt, whilst other elements (Fe and Mg) tend to remain behind in the (unmolten) residue (Visona and Lombardo, 2002). The molten material will accumulate, segregate and rise to form intrusive igneous bodies (or extrusive volcanics if they rise to the surface). Because of the partial melting process, the new magma is enriched in the elements Si, K, Na and Ca, and therefore it crystallises to form granite. Granites are also enriched in other trace elements that are not compatible in the crystal structures of common rock-forming minerals (and which will, thus, accumulate in the melt during partial melting). These incompatible elements include B, Zr, Rb, Li, U, Th, and the Rare Earth Elements, among others (Le Fort et al. 1987). When only a very small degree of partial melting occurs, the melt produced will be deficient in minerals containing Fe and Mg (and enriched in the lighter elements). Such granite is known as a leucogranite. Boron (B) is an element which is found in the mineral tourmaline; this mineral is very common in the leucogranites of the Everest region (Le Fort et al. 1987).

The Himalayan leucogranite that can be seen in the upper Khumbu valley is an example of the magma injection forming giant sill complexes (Searle, 1999a). In continental collision zones, rocks are buried, melted, extruded in ductile form, and exhumed (Jessup et al. 2006). The process in the Himalayas was a combination of both molten intrusion into shallower zones and mechanical emplacement along fault zones (Jessup et al. 2005; Hodges, 2006; Hodges et al. 1998). The location of these granites, near the top of the Greater Himalayan Sequence, alludes to the fact that buoyant, low-density melt always migrates upwards in the crust, and in this case has

accumulated in a zone at the top of the Greater Himalayan Sequence, where it was trapped and prevented from further upward migration by the South Tibetan Detachment (STD) (Figure 2.11).

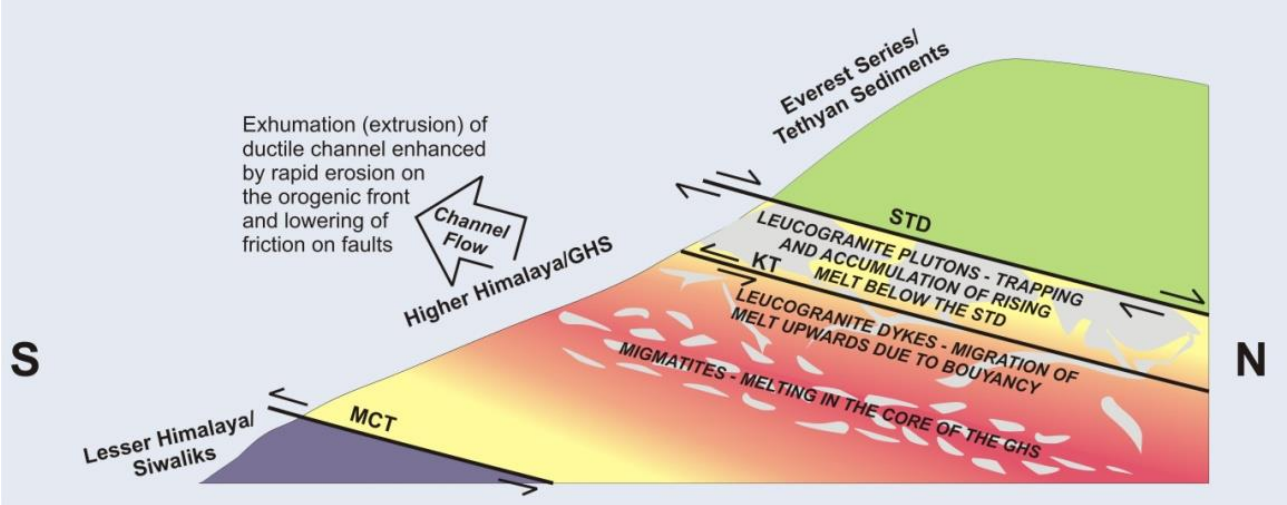


Figure 2.11: Upward migration of partial melt occurs when rocks deeper down in the Greater Himalayan Sequence begin to melt, forming migmatites. This melt rises upwards and accumulates as leucogranite plutons. The exhumation of the Greater Himalayan Sequence and the leucogranites is enhanced by erosion on the orogenic front (modified after Searle et al., 1997).

The Everest massif contains probably the largest proportion of outcropping leucogranites in the Himalayas, individually up to 1500 m thick sills and 3000 m thick intrusions, such as on the Kangshung east face of Everest or the south face of Nuptse. These leucogranites, from Cho Oyu through Everest, Nuptse, Makalu and Chomolonzo, form part of the same sheet lying immediately below the South Tibetan Detachment (Searle et al. 2003). This sheet of leucogranite, known as the Higher Himalayan Leucogranite, forms most of the high peaks in this region of the Himalayas. Around 14 principal leucogranitic plutons outcrop from Makalu in the east to Nanga Parbat in the west (Le Fort et al. 1987), a distance of some 2000 km. More than 20 such plutons were reported by Searle et al. (1997). The leucogranite sheet is the result of a low degree of partial melting of the Greater Himalayan Sequence deeper in the crust below the Tibetan plateau (Inger and Harris, 2007; Guillot et al. 1995). It has accumulated at the top of the Greater Himalayan Sequence, and is separated from the overlying low-grade Everest Series metasediments by the gently northwards-

dipping Lhotse Detachment, the lower detachment of the STD. The base of the leucogranites is formed by the Khumbu thrust (Figure 2.11) (Searle, 1999a).

These leucogranite plutons are very uniform in mineralogical composition and have some metasedimentary inclusions mainly at their margins (Le Fort et al. 1987). Studies show that the leucogranite plutons near the top of the high Himalaya crystallines in the Everest – Makalu region, are composed of two types: a two mica granite (2mg) and a tourmaline granite (Tg) (Scaillet et al. 1990; Searle et al. 1997). Two-mica granites typically have ~71% SiO_2 (30 – 35% quartz, ~10% muscovite and biotite) and ~15% Al_2O_3 (~60% K-feldspar and plagioclase), whilst the tourmaline granites are composed of ~73% SiO_2 (27 – 30% quartz, up to 4.1% muscovite, <1% biotite) and similar amounts of Al_2O_3 (~60% K-feldspar and plagioclase), but up to 4.8% tourmaline (Le Fort et al. 1987). Both types of granite resulted from melting at andalusite–sillimanite facies grade (Visona and Lombardo, 2002). The tourmaline granites were locally derived, having not travelled far from their source, and emplaced syntectonically, showing weak fabrics (Guillot and Le Fort 1995). They were produced by muscovite dehydration melting in a muscovite rich metapelite (Le Fort et al. 1987). The tourmaline content of these granites is usually > 2.2% (Le Fort et al. 1987). The two-mica granites (tourmaline content < 2.6%), were generated by melting in biotite-rich gneiss, resulting in hotter magmas. These intruded upwards by a network of dykes and sills, and solidified below the cooler rocks of the STD (Visona and Lombardo, 2002).

Additionally, other leucogranites, such as that of Shisha Pangma, are composed of plagioclase, K-feldspar, tourmaline, muscovite and biotite, with lesser amounts of sillimanite, red garnet, monazite, zircon, apatite and xenotime. This peraluminous composition also indicates a pelitic source (Searle et al. 1997). Field relations, geochemistry and isotopic studies show that the leucogranites are sourced from the high-grade metasedimentary gneisses of the GHS, and occurred during the latest stages of metamorphism (Searle et al., 1997). From here the melt moved upwards along structurally weak zones, forming the plutons found in many parts of the Himalaya. Deformed leucogranites containing sillimanite along shear fabrics confirm that the leucogranites were emplaced syn-tectonically during D2, and were likely emplaced into sillimanite-grade rocks already at high temperature, and were emplaced before final movement along the STD, as no leucogranites have been intruded along the STD (Searle et al., 1997).

A late phase, metasomatic, volatile-rich, leucogranite resulted in a layered stockwork of pegmatite sills and dykes at the top of the Nuptse-Everest leucogranite pluton (Searle, 1999b, Weinberg and Searle, 1999).

Metamorphic assemblages from the Himalayas show an increase in temperature from the MCT (500-600 °C) to 700 °C approximately 2 km above the MCT to the dark gneiss (Khumbu Thrust) immediately below the leucogranite (Searle et al. 2003). The temperatures remain constant at 700 °C in the leucogranite layer to the Lhotse Detachment, above which they fall to 600 °C and decrease further to 500-550 °C in the North Col formation (Carosi et al. 1999). In the leucogranite layer, metamorphic studies using the computer program THERMOCALC indicate P-T conditions immediately below the STD (from cordierite bearing samples) of 660 °C and circa 4 kbar (~15 km depth) (Searle et al. 2003). The Makalu granite (20km southeast of Everest) P-T conditions indicate higher temperatures of 837 ± 59 °C and pressures of 6.7 ± 1.0 kbar (~20 km depth) where garnet, cordierite and sillimanite assemblages have overgrown low pressure quartz, sillimanite and spinel assemblages (Searle et al. 2003). Hence, this appears to support the contention of Harrison et al. (1997) that there were two temperatures at which leucogranites were intruded into the upper parts of the high Himalayan crystallines.

Examples of leucogranite can be found on Lingtren and Pumori, to the east of Everest Base camp, and in the Western Cwm on either side of the Khumbu Icefall to the base of the Lhotse Wall (Map 4). Rafts of dark sillimanite-biotite gneiss are common occurrences in the leucogranite in the Base Camp area.

The Rb/Sr age of the paragneiss in the Everest-Lhotse region is 449 ± 56 Ma (Ferrara et al. 1983). Early estimates of the age of leucogranites of the Everest region suggested it is early to middle Miocene, 20 to 10 Ma (Heim and Gansser, 1939, Gansser 1964), which has been confirmed by recent studies of granites that show that earlier biotite granites were emplaced at ~20Ma, and that younger tourmaline-muscovite granite formed at 17 Ma (Searle et al., 1997) . There are some leucogranite dykes in the Nanga Parbat–Haramosh massif in Pakistan that are as young as 7 to 2.3 Ma (U-Pb analyses of Zircons) (Zeitler and Chamberlain, 1991).

2.7 Active tectonics and current thinking regarding the formation of the Himalayas

The major tectonic zones and the structures that separate each of the tectonic zones have long been recognised by geologists working on the Himalayas (Heim and Gansser, 1939; Burchfiel and Royden; 1985, Searle et al. 2003). In recent decades, investigations have concentrated on the structure of the Himalayas, and in particular on the structure and origin of the Greater Himalayan Sequence, and how it was exhumed (e.g. Searle and Godin, 2006). Recent work has also produced a detailed geological map of the area surrounding Everest (Searle, 2003: Map 3).

This work has revealed much about the closure of the Tethys Sea, the dynamics of collisional tectonics, the evolution of the Greater Himalayan Sequence, faulting and displacement along the South Tibetan Detachment (STD), the magmatic evolution of the Everest massif and the timing of movement along major structures in the Himalayas (such as the STD and the MCT). One of the key ideas from this recent (and on-going) research is the idea of "channel flow" as a result of continental collision. Burchfiel and Royden (1985) were the first to suggest that the Himalayas formed from the extrusion of a wedge from beneath the Tibetan plateau, and it is now widely accepted that the zone containing the highest peaks of the Himalayas (the Greater Himalayan Sequence, originally recognised as the Axial Granite Core by Odell, 1943) resulted from a shallowly dipping extruding channel of ductile material, bounded to the south (below) by the MCT and to the north (above) by the STD (Nelson et al. 1996; Grujic et al. 1996, 2002; Beaumont et al. 2001).

2.8 The Channel Flow Model

Over the years several different models for the extrusion of high-grade gneisses and leucogranites from the mid-crust to the surface have been put forward. These include: The channel flow model (Nelson et al. 1996), the Nanga Parbat–Haramosh Massif (NPHM) as a fault-related antiform at the lateral tip to major Himalayan thrusts (Coward et al. 1988); a zone of north-west shortening in response to orogen parallel extension around the Himalayan arc (Seeber and Pecher, 1998); upwelling of crustal gneiss domes (Pecher and Le Fort, 1999, Koons, et al. 2002); crustal scale buckling (Burg and Podladchikov, 2000); and north-south constriction/transgression above a thrust tip (Butler, et al. 2000). The Channel Flow model has been widely accepted as explaining the

principal geological features across the Himalayas, and the other models are not discussed in detail here, although they may be locally applicable.

Burchfield and Royden (1985) suggested that the Himalayan wedge had been extruded from between the South Tibetan Detachment (STD) system of normal faults and the Main Central Thrust (MCT) system of reverse faults. The concept of channel flow arose when geophysical surveys (Nelson et al. 1996) suggested that there was a molten layer in the crust beneath Tibet.

The recent exhumation of the Higher Himalayan Leucogranites and the gneisses of the Greater Himalayan Sequence from beneath Tibet have been explained by this channel flow model. Searle, et al. (2003) used structural geology, thermobarometry and geochronology to evaluate models for channel flow and ductile extrusion of the crust.

Channel flow describes the protracted flow of a weak, viscous crustal layer between relatively rigid, yet deformable, bounding crustal slabs (Godin et al. 2006). This weak crustal layer (the Higher Himalayan Leucogranites and the Greater Himalayan Sequence) flows almost laterally owing to a lithostatic pressure gradient caused by the very thick Tibetan crust and the normal crustal thickness in the Indian foreland (Godin et al. 2006; Klemperer, 2006). High rates of focussed denudation/erosion on the mountain front can enhance the exhumation of channel material. If both channel flow and denudation are acting at the same time, then extrusion of the mid-crustal channel material can occur with a normal-sense fault at the top (i.e. the STD) and a thrust-sense fault at the bottom of the channel (i.e. MCT) (Godin et al. 2006), as shown in Figure 2.12.

Beaumont et al. (2001) suggested that there were two driving forces which allowed a channel of material to be extruded to surface. Partial melting of the hot lower crust of Tibet decreases the density and viscosity of a channel of material that is the more buoyant than its surroundings and attempts to move upwards through a zone of least resistance. This zone is provided by intense denudation and weathering at the rangefront (Figure 2.12, points 9 and 10) and a system of normal and reverse faults at the top and base of the channel (Figure 2.12, points 11 and 12). Hot material flows under gravitational forcing - in the case of the Himalayas, south towards where

there is an east-west line of granite gneiss outcrops. These outcrops are the result of crustal channel flow drawn towards the surface as extremely active erosion reduces the overlying burden of material, giving an escape route through the channel for material from the mid-crust.

This model successfully explains concurrent north-south shortening across the MCT and north-south extension across the STD (Beaumont et al. 2001). It also explains inverted metamorphic gradients, and different protoliths and different grades of metamorphism in the Greater and Lesser Himalayan Sequences (GHS and LHS).

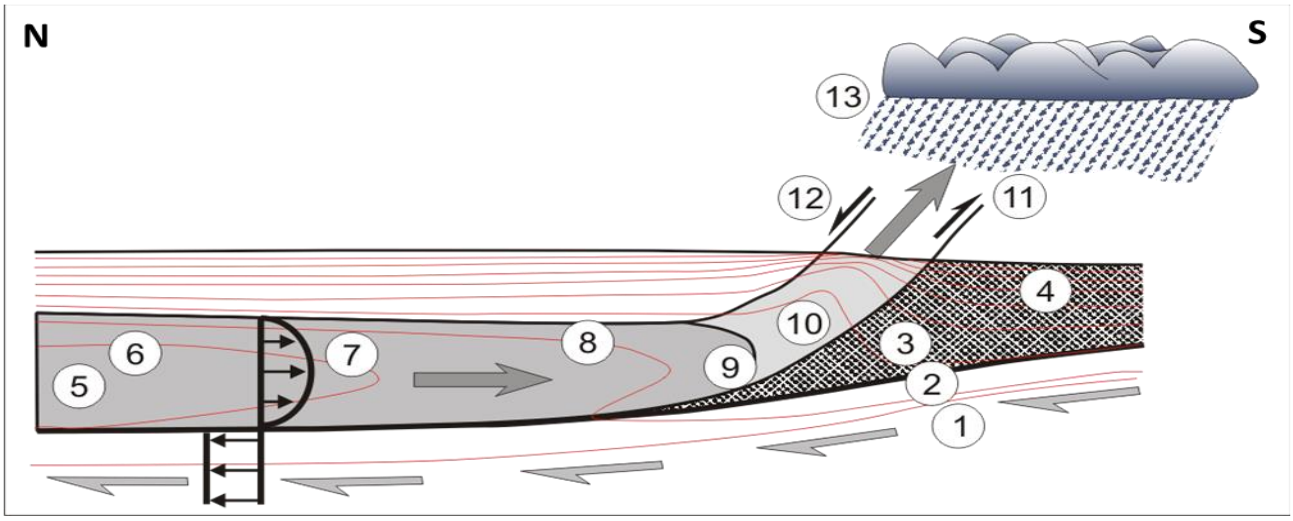


Figure 2.12: Schematic diagram of the relationship between channel flow and extrusion of a palaeochannel (after Godin et al. 2006). 1 – Mantle, 2 – Lower Crust, 3 – Mid Crust, 4 – Upper Crust, 5 – Weak Crustal Channel, 6 – Isotherms (from Beaumont et al. 2004), 7 – Schematic velocity profiles, 8 – 750°C isotherm, structurally below which partial melting occurs, 9 – Rheological tip of channel, if temperature is too low, channel will underthrust, 10 – Extruding crustal block, 11 – Lower thrust zone of extruding block (e.g. Khumbu Thrust or the Main Central Thrust), 12 – Upper shear zone/detachment zone of extruding block (e.g. the South Tibetan Detachment or the Qomolongma Detachment), 13 – Focussed surface denudation.

Evidence in support of the channel flow model includes:

- Simultaneous normal dip-slip (extensional) movement along the STD and thrusting along the MCT (Burchfiel et al. 1985, 1992; Hodges et al. 1992). Large-scale (40 km) recumbent folding of the metamorphic isograds (Figure 2.9) mapped by Searle et al. (1988), Searle and Rex, (1989), Walker et al. (1999) and Stephenson et al. (2001), showed that the thrust motion on the MCT was temporally linked to the normal motion on the STD. This has been confirmed by geochronological studies (e.g. Kellett et al. 2010) – i.e. both shear zones bounding the Greater Himalayan Sequence were active simultaneously and are still active today (Hubbard, 1989; Harrison et al. 1999; Hodges et al. 1992, 1993; Walker et al. 1999; Murphy et al. 1999; Simpson, 2002).

- Inverted and right-way-up isograds occur at the base of the MCT and at the STD, respectively. Pressure-Temperature (P-T) profiles have been shown to be remarkably consistent (Figure 2.9) along the orogen (Hubbard, 1988, 1989; Goscombe et al. 2006), with inverted isograds below the Greater Himalayan Sequence (i.e. below the MCT), and a wide zone of high temperatures recorded in the sillimanite gneiss and migmatites towards the middle of the Greater Himalayan Sequence. Notably, metamorphic pressures and temperatures drop off rapidly northwards across the STD.

- Recognition of major structures continuing at depth, associated with high-grade, partially molten rocks. This zone of high-grade rocks (the Greater Himalayan Sequence) has been confirmed by geophysical studies. During the INDEPTH geophysical profiling of the Himalayas, deep seismic reflectors were matched to the STD and MCT, indicating that movement along these structures continues at depth northwards, beneath Tibet (Nelson et al. 1996). Additionally, geophysical anomalies in the crust beneath Tibet are attributed to partial melting and granite formation at deep levels (Searle, 1999b). These granites are forming as horizons which are at structurally similar levels to those in which the Himalayan leucogranite present in Ama Dablam, Makalu, Lingtren and other major outcrops formed in the Miocene period (23 to 5.3 Ma) and, which were subsequently extruded to the south (Searle, 1999b).

Numerical modelling has also contributed to a better understanding of the channel flow model. Researchers have examined channel flow models with variable properties such as extrusion velocities (Grujic et al. 1996; Grujic, 2006) and types of shearing (simple vs. pure shear - Beaumont et al. 2001, 2004, and 2006). This numerical modelling has helped link theoretical models with the

various geological processes currently taking place (including rapid crustal-scale buckling, melting of rocks owing to high-grade metamorphism, generation and segregation of felsic magmas, and the emplacement of granite plutons). They concluded that gravitationally driven mid-crustal channel flows are most likely to occur in the Tibetan-Himalayan system (Beaumont et al. 2006).

The hypothesis of channel flow and extrusion of the Himalayas continues to be tested using structural geology, thermobarometry and geochronology (e.g. Jessup et al. 2006, Kellet et al. 2010). In the Everest massif area, there is much evidence for the extrusion of the Greater Himalayan Slab between the STD and the MCT. Assuming simultaneous movement along both faults, a southward extruding channel can be modelled. Vorticity of flow measurements from rocks of the Yellow Band showed a *Wm* (mean kinematic vorticity number) of 0.74-0.91 equating to 45-28% pure shear (Jessup et al. 2006). Below the STD, amphibolite facies schists and gneisses of the Rongbuk valley on the north side of Everest showed *Wm* numbers of 0.57-0.85 or 62-35% pure shear. Associated microstructures indicate that flow occurred at close to peak metamorphic conditions (Jessup et al. 2006). Flow partitioning in the GHS resulted in the juxtaposition of amphibolite facies rocks, recording early stage exhumation, alongside greenschist and unmetamorphosed rocks, recording later stage exhumation (Jessup et al. 2006).

Searle et al. (2006) suggested that the GHS is a mid-crustal channel flow of low viscosity, semi-molten Indian plate crust which was, and is, extruding southwards between two major ductile shear zones. Crustal melting occurred at depths of 15-19 km (4-5 kbar), assisted by radiogenic uranium-bearing minerals, whose source was Proterozoic black shales. Crustal melting triggered channel flow, which effectively resulted in the exhumation of the leucogranites following their emplacement and intrusion below the STD at *circa* 17-16 Ma. This model (Searle et al. 2003) shows that the crust in the Everest to Lukla area is rheologically layered, with several major low-angle detachments and thrusts that separate layers of crust and upper mantle.

There are other examples of channel flow that have been studied in the Himalayas. The Majba Dome in southern Tibet has been interpreted as having been formed through a middle crustal flow of Oligocene-Miocene age. Mid-crustal ductile horizontal extension was dated as beginning at 23.1 ± 0.8 Ma, with cooling below 115 °C at 9.5 ± 0.6 Ma (Lee et al. 2006) and is synchronous with

similar events in the Himalayas. In western Bhutan, a series of steep to moderately dipping shear zones within a south-easterly extruding slab of crystalline rock has been suggested by Carosi et al. (2006) as evidence of channel flow. There are well-developed, top-down-to-southeast shear sense indicators with Barrovian metamorphic minerals bent and stretched by extensional shear bands. Normal shear bands occur mostly in the upper part of the GHS, and the age of the normal shear zone formation is suggested at 17 Ma, based on parallel shearing in the leucogranite dykes (Murphy and Harrison, 1999) and the age of strongly sheared schists (16.9 ± 0.2 Ma) from immediately below the STD (Searle et al. 2003). Normal shear zones are capable of accommodating pure shear, characteristic of the inner part of an extruding slab.

Channel flow mechanisms of extrusion have been recognised in other parts of the world such as in the Canadian Cordillera where a detachment called the Selkirk Detachment (the equivalent of the STD in the Himalayas) overlies highly sheared pelitic schist and abundant leucogranite (Richard et al. 2006). In the Appalachian inner Piedmont, an orogenic channel, which has been exhumed and is strike-parallel, has been recognised as originating through a channel flow mechanism (Hatcher and Merschat, 2006). An example from the south Peloponese Hellenides in Greece shows evidence for channel flow from a 1.5 km thick extruding shear zone that formed under blueschist facies conditions (Xypolias and Kokkalas, 2006). These suggest that the channel flow mechanism has been active in orogenic collision zones in the Rockies, the Appalachians and the Alps, and is likely to be recognised in other parts of the world's orogenic belts where leucogranite and granite gneiss terranes are to be found.

2.9 The relationship between erosion and the rapid exhumation of rocks

During the collision of two continents to form mountain belts or orogens, wedges of rock from the downgoing continent are pushed below the overlying continent, a process known as underplating (Malavielle et al. 2008) also known as Ampferer or "A–type" subduction (Park, 1988). This underplating causes a thickening of the crust and elevation of the land surface. In the Himalayas, one is dealing with continental crust moving down, along and underneath continental crust. The amount of downwards movement is limited because continental crust has a relatively low density. It cannot, thus, be subducted to any significant extent. One continent will "under-ride" the other

for a short distance, after which subduction ceases completely (Molnar and Gray, 1979)). The net effect is thickening of the continental crust through underplating and hence buoyancy upwards (Figure 2.13).

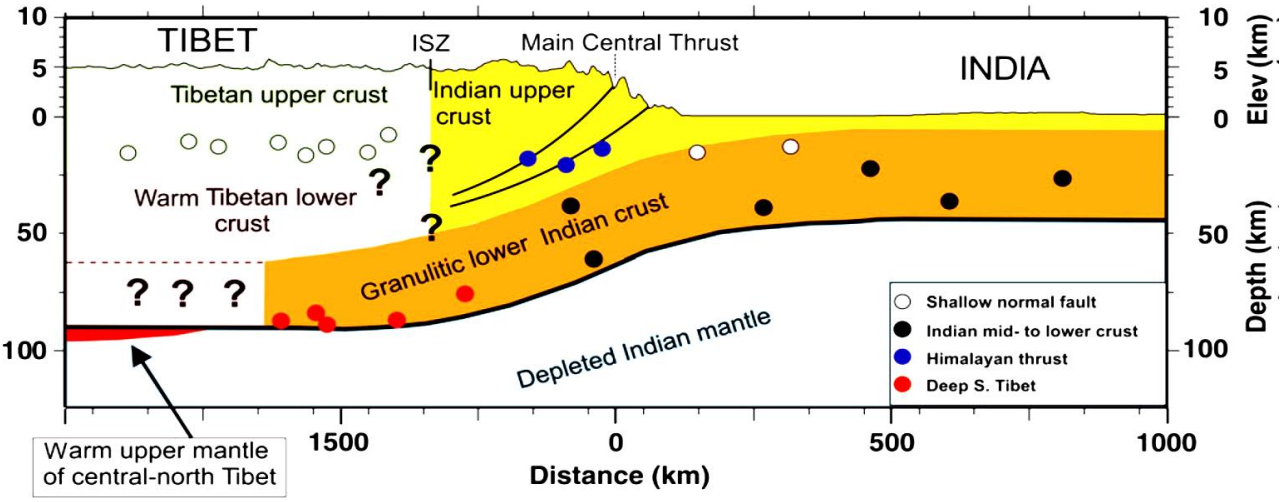


Figure 2.13: Granulitic lower crust subducted underneath Tibetan upper crust with limited downwards movement as its relative density is lower than that of the upper mantle. This results in a very thick crust approaching 100 km in thickness (after Jackson et al. 2008, from Dhital, 2015).

The state of equilibrium of the Earth's crust (known as isostasy) elevates landmasses and balances them with gravitational force that commonly depresses landmasses. Once crustal thickening and uplift have taken place, isostatic equilibrium is re-established through erosion (and exhumation of the mid-crust). The difference between uplift and exhumation is that uplift is the result of gravitational balance, whereas exhumation is associated with tectonic processes (in this case, channel flow), often assisted by erosion. Exhumation can also occur through tectonic processes such as thinning of the crust along extensional faults, or even by ductile flow. Crustal thickening of Tibet and the Himalayas, resulting from the subduction, thrusting and underplating of the Indian continental rocks beneath Tibet, results in uplift. Subduction is the downward movement of the Indian continental crust under Tibet. Underplating results from wedges of rocks being plated to the overlying crust (Figure 2.14) as the subducting slab passes by. Thrusting results from two

layers of rock moving in opposite directions separated by a thrust plane. Hence all three processes are interrelated in a mountain-building zone such as the Himalayas.

On the other hand, fragments of crust that have been pushed down are generally heated and metamorphosed at depth and are then brought back to the surface (exhumed) along thrust planes or through extensional thinning of the crust.

Exhumation is often assisted by erosion, and the rate of this exhumation and uplift is a function of the rate of erosion and of extensional unroofing of the orogenic belt (Malavielle, 2010).

A so-called 'dynamic equilibrium' exists between the rate at which crust is subducted and exhumed, and the rate of erosion of the mountain belt (Malavielle et al. 2008). If the rate of erosion is high (as in the Himalayas), the friction along thrust planes is effectively lowered, as there is less vertical pressure on the thrust planes owing to the rapid removal of overlying material through erosion. As a result of this lower friction, wedges of rock are exhumed more rapidly along thrust planes, and exhumation takes place along gently-dipping thrusts (Bose et al. 2010). The lower friction allows more rapid tectonic thickening, compensating for the extra erosion, so balance is maintained. Rapid erosion and exhumation allows material to be underplated at a greater rate (Figure 2.14).

In order to maintain the dynamic equilibrium of the orogenic wedge, the high rate of erosion in the Himalayas is balanced by high rates of uplift and exhumation (Malavielle et al. 2008). The rate of exhumation, which is typically between 2 and 4 cm/year in most orogens, is estimated at 5 to 7 cm/year in the Everest region (Malavielle et al. 2010).

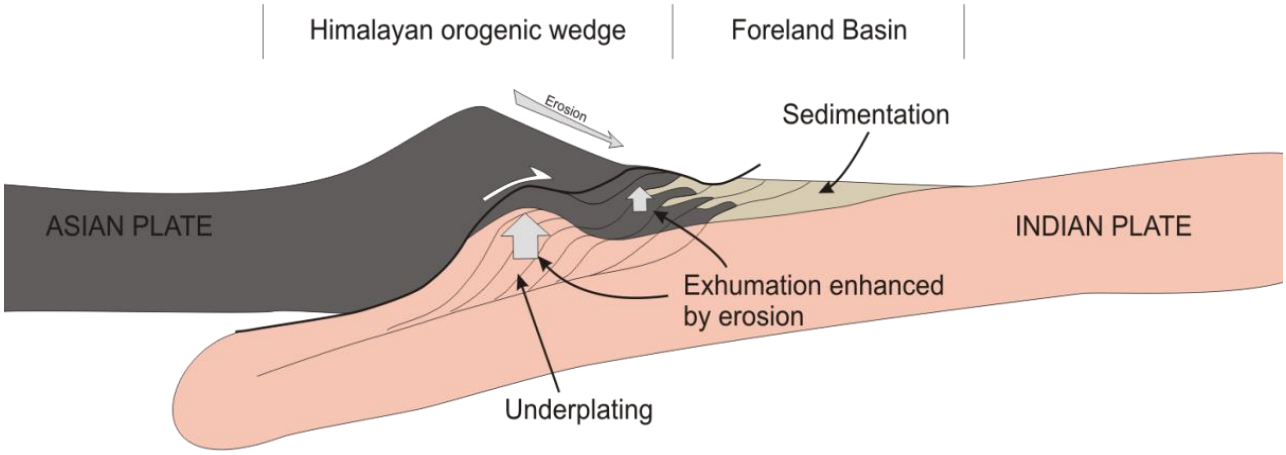


Figure 2.14: Interaction between surface processes and exhumation in orogenic wedges. High rates of erosion allow underplated crust to be exhumed more rapidly along thrust planes (after Malavielle et al. 2008).

As a mountain gets higher (because of underplating), there will be an increase in the rate of erosion to balance this mountain's growth. If the rates of erosion were lower, the higher friction on thrust planes would result in slower exhumation of buried rocks and higher mountains. Estimates of slip along the Main Frontal Thrust alone (Figure 2.2), of greater than 400 km, have been postulated (Coward and Butler 1985; Hauck et al. 1998; Murphy and Yin, 2003; Searle et al. 2003) based on balanced cross-section reconstructions. Searle et al, (2003) have estimated horizontal displacements from pressure gradients (using mineral assemblages and assuming a 3.5 km/kbar pressure gradient) of 90-108 km southwards of footwall GHS slab rocks at a 10° dip to the north, and 180-216 km southwards at a "more realistic" 5° dip to the north. The cumulative slip along all the major faults in the Himalayas is likely to be far higher. Around 20 Ma, India's speed northwards was around 9.5 cm/yr, slowing down from an initial ~21.1 cm/yr before then (Aitchison et al. 2007). This high rate of collision resulted in the rapid mountain growth. The current rate, however is estimated at 2 cm/yr.

Exhumed wedges may contain stacks of thrusts, where deeper-level rocks are progressively thrust over shallower level rocks during underplating (Figure 2.14). In the Himalayas, many low-angle, northwards-dipping planes are observed in the Greater Himalayan Sequence, which may have resulted from such a wedge-stacking process (Malavielle et al. 2008).

Surface uplift of the Himalaya and the high elevation of the Tibetan plateau are also suggested as being the cause of the initiation of the monsoon ~ 7 to 8 Ma due to this vast cold area causing changes in air flow and humidity in the surrounding areas, with far reaching effects on Africa and its climate (Searle et al. 1997). The cooling effect of the Tibetan plateau may also have had an effect on global cooling, although this is not conclusive (Raymo and Ruddiman, 1992).

2.10 Summary

The geology of the area from Lukla to the summit of Mount Everest illustrates several important geological concepts such as the collision of tectonic plates, the subduction of the Indian crust beneath the Asian plate, crustal thickening, channel flow, exhumation, prograde and retrograde metamorphism indicating the burial of some rocks to roughly 45 km and subsequent exhumation, igneous intrusions of leucogranite, and tectonic boundaries or faults such as the Main Central Thrust and the STD. The fossiliferous limestones above the STD illustrate low-grade metamorphism and an ocean floor sedimentary sequence from the Ordovician period on the summit of Everest. The initially deeply buried Everest leucogranites, at a geologically young age of 32 to 16 Ma, have been exhumed more recently between the late Miocene period and the present (Searle et al. 2003).

The Channel Flow Model explains the numerous unique features of the Himalayas, and evidence in support of this hypothesis includes the presence of leucogranite which, together with the Greater Himalayan Sequence, represents the weak crustal channel, the lower thrust zone (the Main Central Thrust and the Main Boundary Fault), the upper shear zone (or the South Tibetan Detachment), and the extruding crustal block represented by the Greater Himalayan Sequence and high Himalayan peaks such as, Nuptse, Pumori and Ama Dablam.

The reason that the Himalayas are the highest mountains in the world is a combination of rapid exhumation of both the leucogranites and the GHS. The speed with which India initially collided with Tibet almost certainly contributed to the Himalayas reaching the great height that they have.

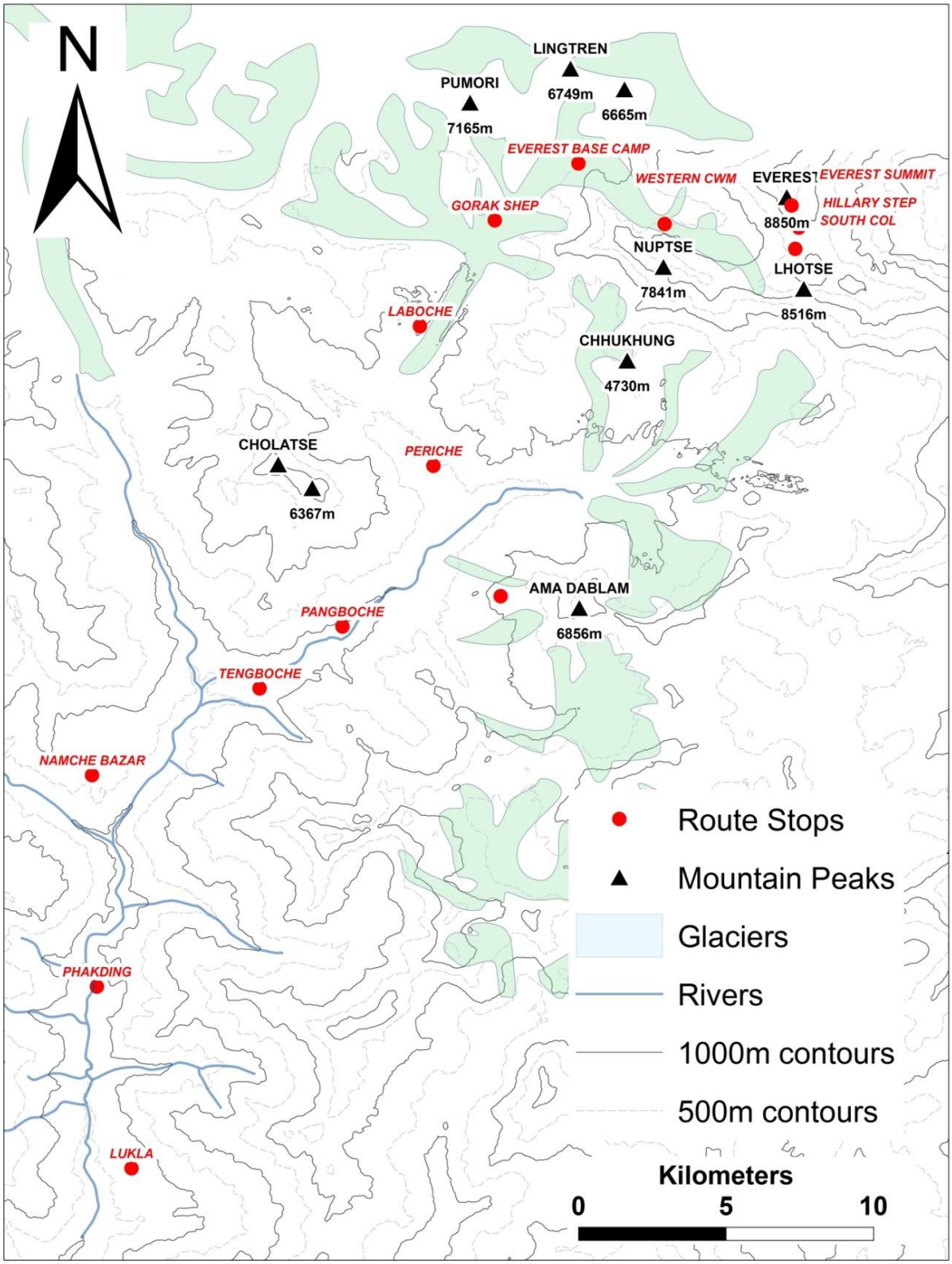
CHAPTER 3: GEOLOGICAL FEATURES ALONG THE ROUTE FROM LUKLA TO EVEREST

Introduction

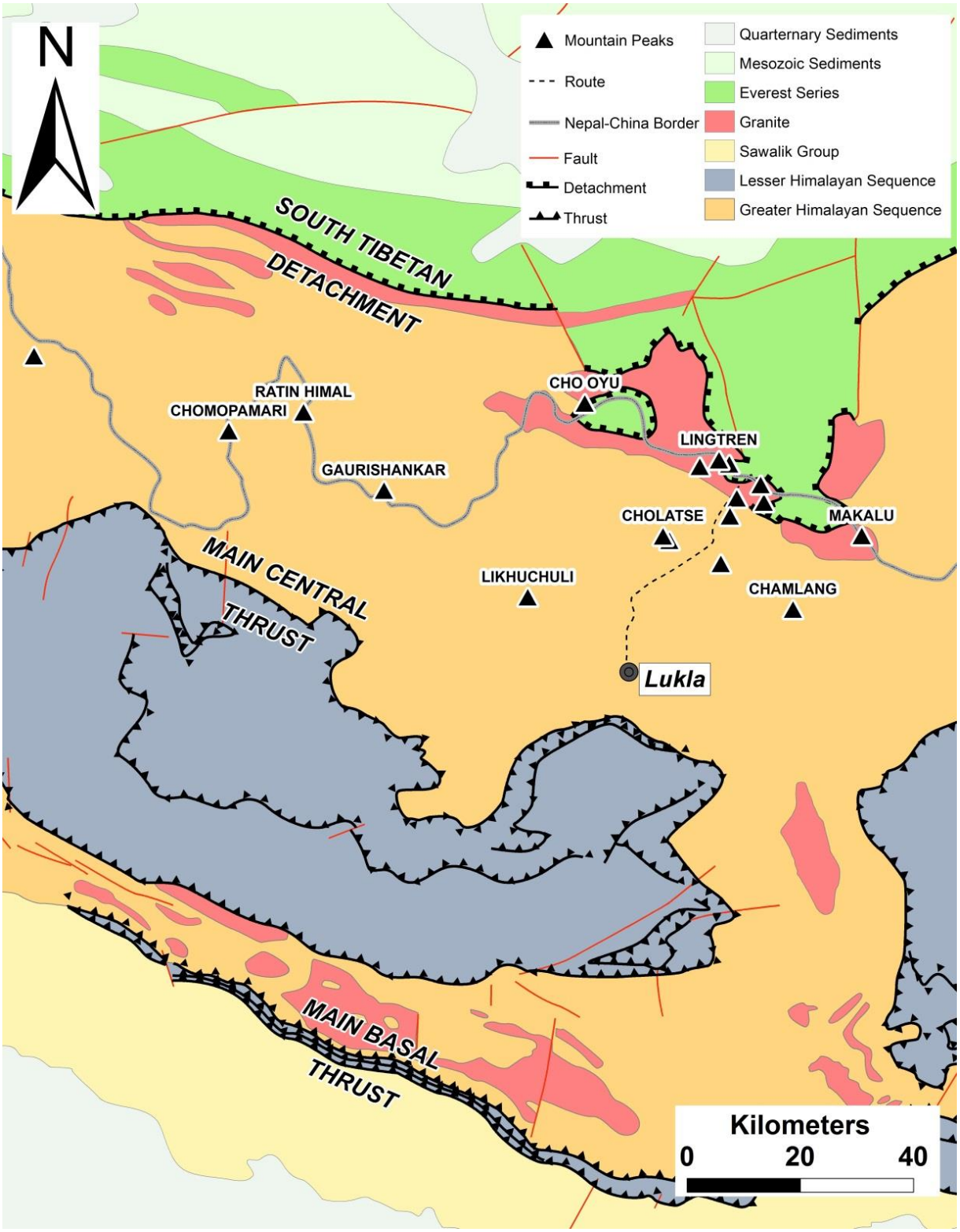
In this chapter, geological features and rock samples are described, on a traverse from the town of Lukla to the summit of Mt Everest (Maps 1, 2). Along this route, geological evidence is provided for the theories and geological histories described in Chapter 2. The route between Lukla and Everest begins in the GHS, slightly north of the MCT, and crosses the high-grade rocks of the GHS until close to Everest itself, where sheets and plutons of Higher Himalayan Leucogranites are found. These high-grade rocks and leucogranites are separated from the overlying Tethyan sediments and metamorphosed limestones of the Everest Series by the South Tibetan Detachment Zone (STD) which is made up in the Everest area by two major detachments, the Lhotse Detachment (LD) and the Qomolongma Detachment (QD). Along the route, a detour is made up the peak of Ama Dablam, where excellent exposures of the Himalayan Leucogranites are to be found.

Some of the major features are the migmatites of the GHS which are found near the town of Namche Bazaar (Map 3), the Leucogranites of Ama Dablam (Maps 3 and 4), the view of Everest from Kala Pattar (Map 4), the exposure of major detachments on the face of Everest and the juxtaposition of the leucogranite of the Western Shoulder with low-grade metasediments near the summit, the fossils of Everest, classic examples of glacial erosion and its relationship to exhumation, active tectonics in the Himalayas, and the lateral extent of the India-Asia collision zone.

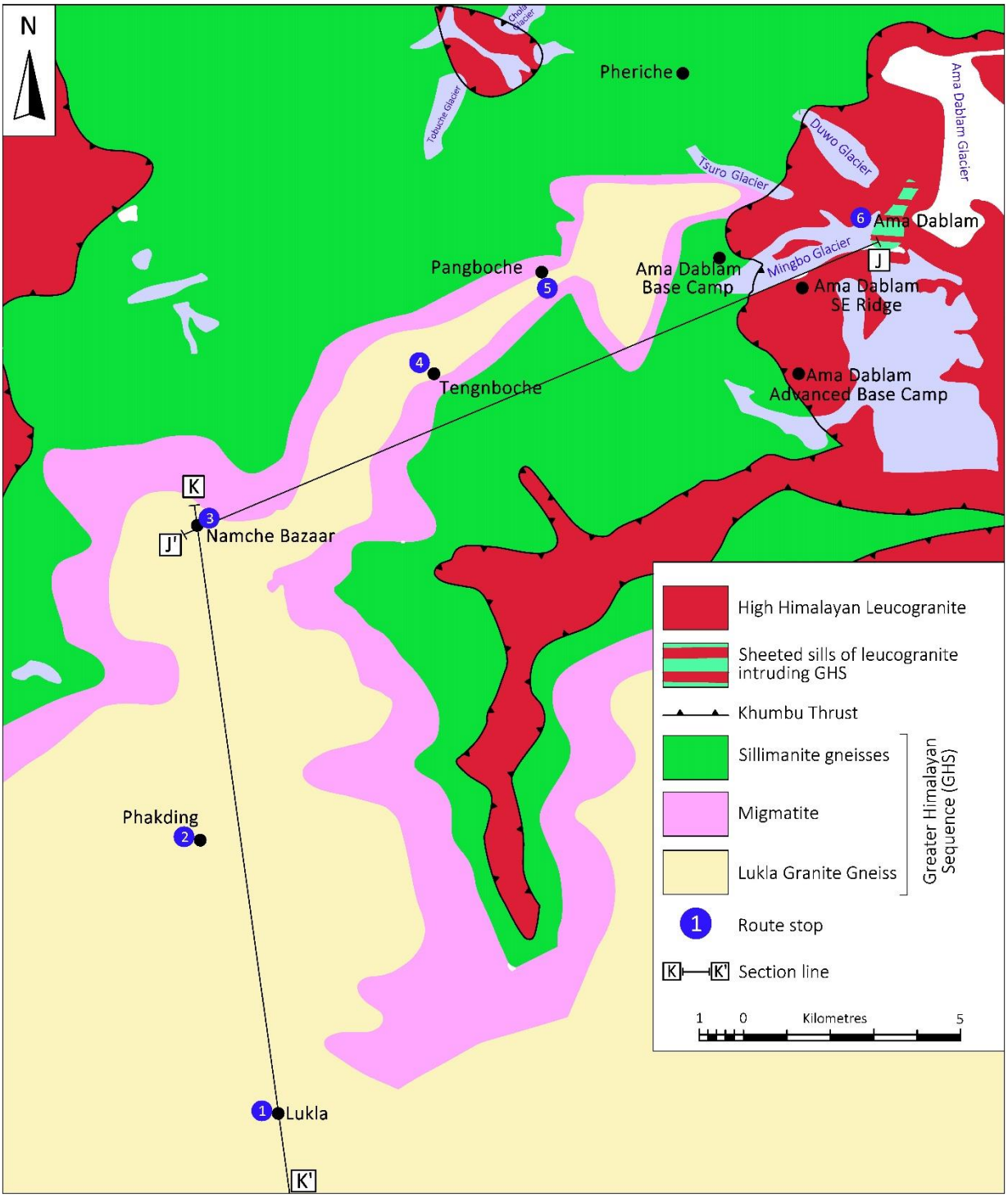
Map 1: Route map from Lukla to Everest (Amended after Himalayan Map House, Kathmandu, Nepal)



Map 2: Regional geological map of North Eastern Nepal (Drafted from maps produced by the Department of Mines and Geology, Nepal, and the Ministry of Geology and Mineral Resources, People's Republic of China).



Map 3: Geological map of the Lukla to Ama Dablam area (After Searle (2007), modified, based on 2006 and 2008 field work by the author)



3.1 Granite gneiss, migmatite and the Namche migmatites

The rocks on the route from Lukla to Namche Bazaar (Stop 3 on Map 3) are mainly granite gneiss and migmatite of the Greater Himalayan Sequence (GHS). The rock typically contains compositional banding of mafic and felsic minerals. This gneissic fabric likely represents the S_1 fabric formed during burial of the Greater Himalayan Sequence. The rock contains quartz, plagioclase feldspar, K-feldspar/microcline, biotite, and minor muscovite. Large microcline (K-feldspar) grains have small rounded inclusions of quartz and thin films of quartz are found along grain boundaries. The rounded inclusions and thin films of quartz are indicative of the rock having melted. Myrmekitic textures (a fine intergrowth of quartz and feldspar) confirm crystallization of a melt. The planar fabric of aligned biotite grains, as well as both strained and unstrained quartz found in the rock, indicate that the rock has experienced deformation followed by partial melting.

There is very little outcrop, but there are many boulders along the path and in the deeply cut rivers, showing deformation and migmatisation. Isoclinal folds are abundant, with some migmatitic melt evident in the boulders. This probably came from higher elevations. Some near-outcropping gneiss shows south-verging, recumbent folding, consistent with the sense of deformation in the GHS described by described by Carosi et al. (1999) (Figure 3.1).



Figure 3.1: Recumbent south-verging fold in granite gneiss near Phakding. The handle of the hiking pole is 14 cm in length. (Stop 2 on Map3). GPS co-ordinates 27°42'57.27"N, 86°42'46.51"E.

The migmatitic features are a highlight of this part of the route, outcropping above the town of Namche Bazaar (Figure 3.2). These are the so-called Namche migmatites, and here one can observe evidence of migmatisation in many outcrops on the trail and on the slopes above the town.

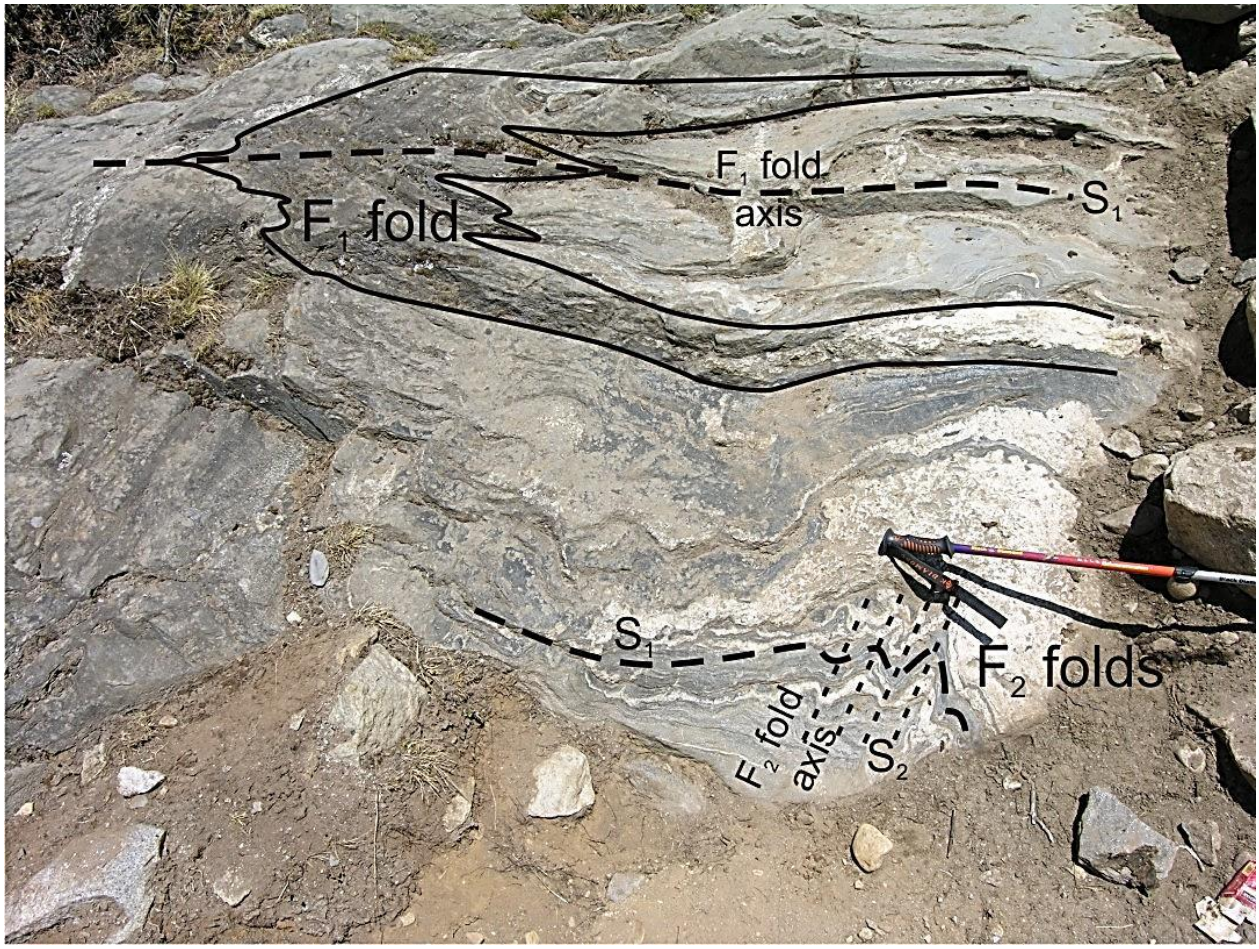


Figure 3.2: Example of the Namche migmatites (near Stop 3 on Map 3). There are two generations of folds in this outcrop of biotite-sillimanite gneiss, an early recumbent F_1 fold and S_1 axial-planar fabric and an upright S_2 overprint and upright F_2 folds, which can be seen in the lower right hand side of the outcrop, as indicated. Note the lighter coloured leucosome bands (evidence for migmatisation, made up of quartz and feldspar) within the darker grey gneiss. The handle of the hiking pole is 14 cm in length. GPS co-ordinates 27°48'57.14"N, 86°43'50.53"E.

Migmatites are folded by F2 folds (Figure 3.2), and in places display a stromatic nature, suggesting that D2 deformation continued whilst migmatisation was taking place.

Migmatisation was widespread at the time of deformation with both boudinaged and discordant veins (Figure 3.3). It has been suggested that the thick zone of partial melting in the Namche migmatites could have produced enough volume of magma to generate the large 2000 m to 3000 m thick plutons found near the top of the GHS (Searle et al. 2003).

The location of the Namche migmatites near the centre of the GHS, immediately below the Khumbu thrust and the overlying Higher Himalayan Leucogranites, suggests that this migmatite was the source of the magma that formed the Higher Himalayan leucogranites emplaced below the STD, and forming the large pluton that can be seen from Pangboche onwards to Gorak Shep in the upper Khumbu Valley (Searle, 1997). Migmatisation led to the separation of leucosome from biotite-rich restite. The buoyancy of the granite melt resulted in migration upwards into the zone between the dark sillimanite-biotite gneiss and the STD, a zone of non-coaxial simple shear (Searle, 1999). The emplacement of this granite into plutons on the west shoulder of Everest and the top of the Nuptse are seen in later stops.

The folded and stromatic nature of migmatite means that deformation continued whilst migmatisation was taking place.

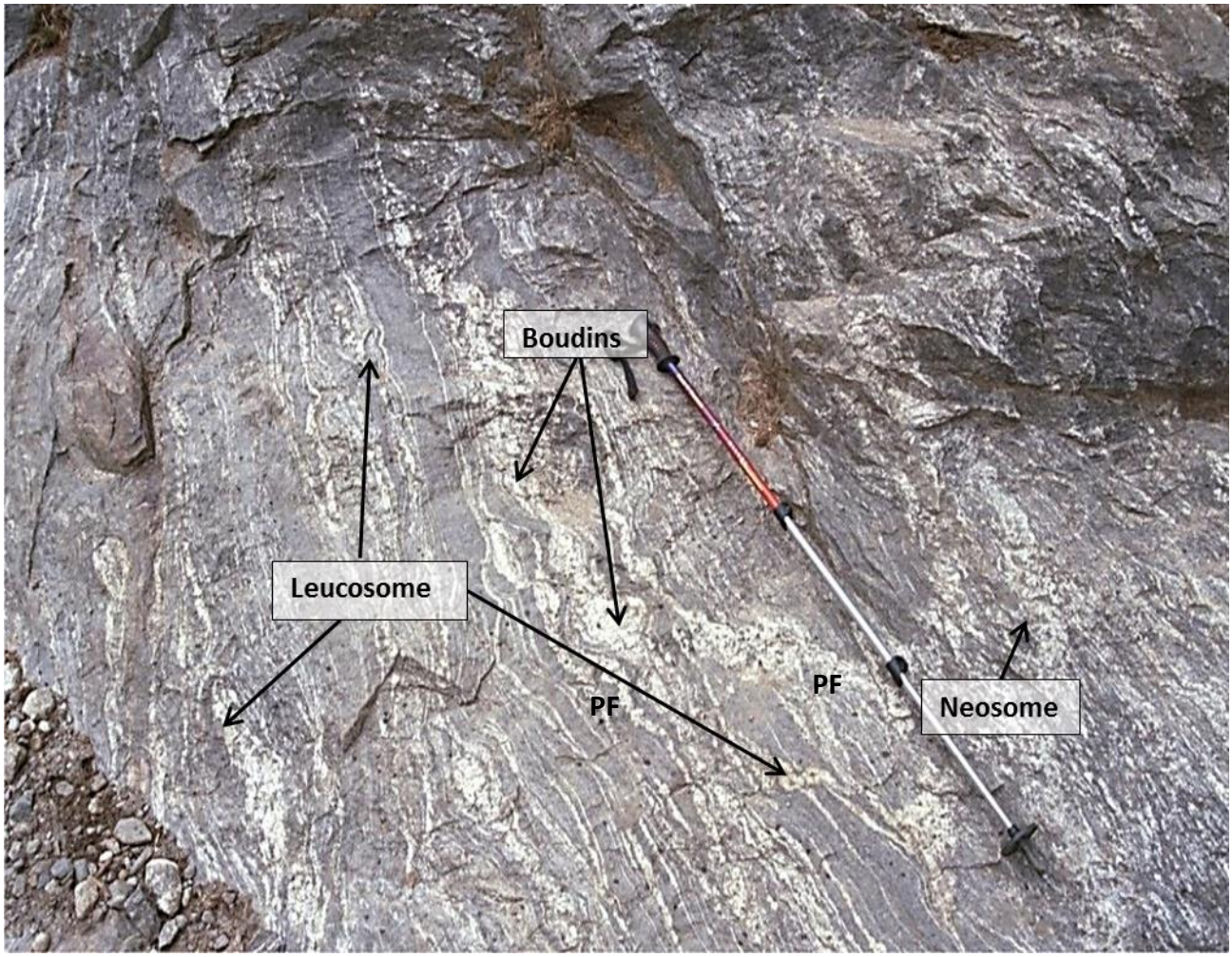


Figure 3.3: Migmatite outcrop northeast of Tengboche (near Stop 4 on Map 3) showing interfingered leucosome (white segregated partial melt) within the pre-existing darker coloured sillimanite-biotite gneiss. Note the banded (stromatic) nature of the migmatite at this outcrop, suggesting that melting occurred syntectonically. Some leucosomes have been further deformed or stretched into boudins and ptygmatic folds (PF). In places, leucosome are discordant to the planar fabric defined by the neosomes. The handle of the hiking pole is 14 cm in length. Photograph taken at GPS co-ordinates 27°48'18.64"N, 86°43'2.66"E.

Examination of the surrounding faces of the mountains shows recumbent isoclinal folding and there is evidence of large-scale folding in the east face of the ridge between Nupla and Kongde Ri west of Namche Bazaar (Figure 3.4). Here, a south-verging recumbent fold lies on a thrust plane, which could be the southwards extension of the Khumbu Thrust, exposed near Everest. This fold

may be the result of a fold-thrust association. The Namche migmatites occur throughout the granite gneiss, as well as in the sillimanite gneiss, which is capped by the KT and the leucogranite layer.

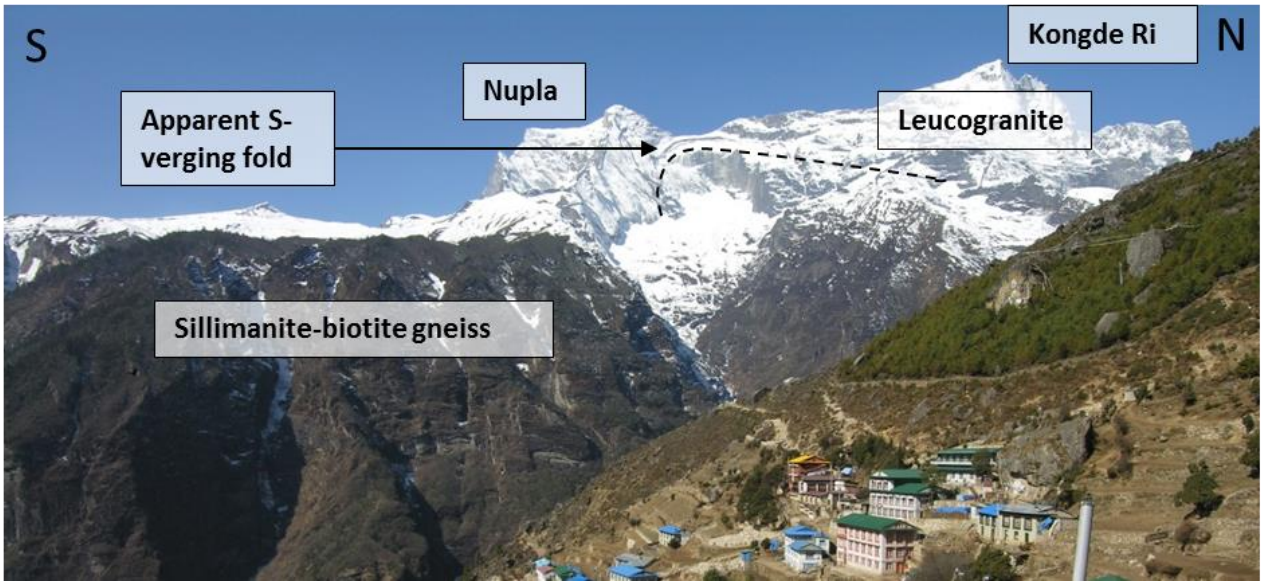


Figure 3.4: Recumbent folding above Namche Bazaar village. Migmatite outcrops lie above the buildings on the left side of the photograph. Photograph taken from GPS co-ordinates 27°48'19.22"N, 86°42'41.20"E, looking westwards.

3.2 Sillimanite-biotite schist, P-T-D-t path and the age relationship to the Everest Series

Dark biotite- and sillimanite-rich gneiss and schist is the dominant rock type northeast and north of Namche Bazaar, in a zone approximately 100m to 300m vertically above the town, and it underlies the sheet of Higher Himalayan leucogranite at the top of the GHS. The town of Namche Bazaar therefore lies at the contact of the granite gneiss and the migmatites.

The sillimanite-biotite gneiss crops out underfoot from above the migmatite layer from Namche Bazaar to Everest Base Camp, and is significant in that it is the source rock of the leucogranite melt that formed the Higher Himalayan plutons. Geochemical investigations by Le Fort et al., (1987) concluded that the Himalayan leucogranites were extracted by anatexis of the underlying Tibetan Slab gneisses. Additionally, these dark rocks are also host to the Khumbu Thrust, a zone of weakness along which the granite plutons were emplaced between the KT and the LD.

Grey/black sillimanite-biotite gneiss underlies the entire area around the foot of Ama Dablam and underlies the Khumbu glacier up to Everest Base Camp. The rock is composed of biotite, sillimanite, and quartz with minor plagioclase feldspar (Figure 3.5).The bulk of the rock is made up of strained, elongate translucent quartz and elongate brown biotite (Figure 3.5). Some plagioclase feldspar, K-feldspar and muscovite is also present. Sillimanite, a light fibrous mineral in plane polarized light, is characteristic of high metamorphic grades above 500 °C (Yardley, 1989).

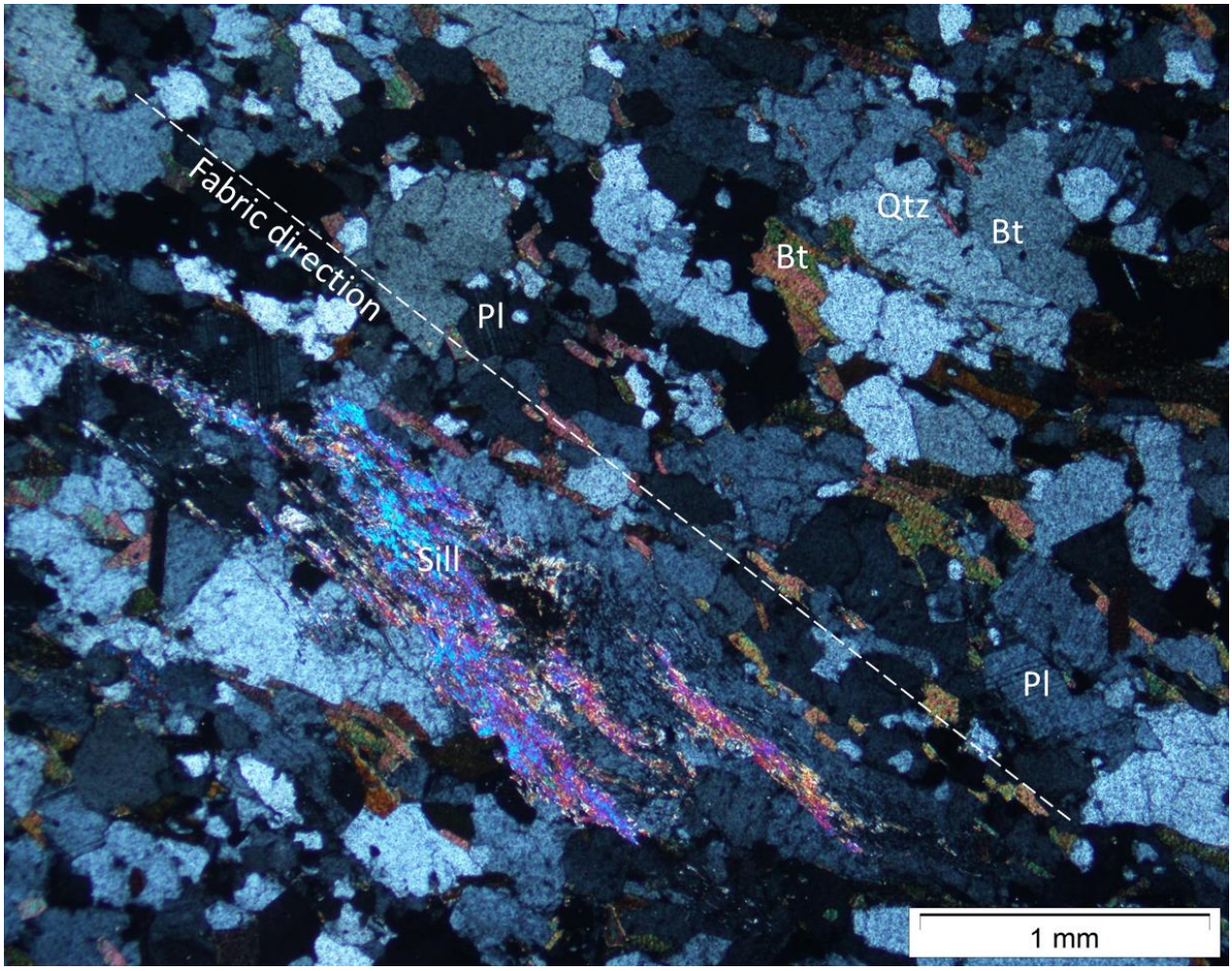


Figure 3.5: Photomicrograph (XPL) of sillimanite-biotite schist. A strong fabric of aligned biotite and sillimanite grains is present. Quartz (Qtz), plagioclase (Pl) and minor amounts of K-feldspar muscovite make up the remainder of this rock. Quartz and plagioclase grains may have inclusions of fine-grained sillimanite. Note the irregular shape of the quartz grains and the numerous small, rounded grains of quartz, indicating high degrees of strain (MacKenzie and Guilford, 1980). Sample of schist taken from near Laboche, GPS co-ordinates: 27°57'23"N, 86°4724"E.

A very strong fabric of aligned biotite and sillimanite grains is found. The bulk of the sample is coarse grained (>1 mm), but sillimanite is much finer grained, commonly occurring in the form of fibrolite. Both strained quartz and unstrained quartz are found, as well as irregular quartz and plagioclase grains with inclusions of fine sillimanite and possible cordierite. These irregular patches suggest melting at high metamorphic grades, and it has been suggested that these rocks reached conditions of 650 °C and 5 kbar (Searle, 2003). Some grains are small (<0.25 mm). The small grain

size, recrystallized quartz and a fabric indicates that intense shearing has taken place at moderate metamorphic grades (amphibolite facies). This implies that deformation was retrograde, related to exhumation of the GHS (Figure 2.8C). The movement direction is top-to-south, consistent with thrusting of the Greater Himalayan Sequence southwards over the Siwaliks.

The counter clockwise P-T-D-t history of the GHS (see Figure 2.8), of which the sillimanite-bearing gneiss is part shows that this rock has experienced burial of the original pelitic rocks, and heating to granulite facies. Decompression (exhumation) to upper amphibolite facies then saw the growth of cordierite and sillimanite in the surrounding gneiss. The fabric evident in the sample in Figure 3.5 is that resulting from D_2 deformation during exhumation. It is possible that the initial burial reached depths of >45 km or 14 kbar, i.e. reaching eclogite facies (Lombardo and Rolfo, 2000). Decompression and metamorphism then occurred with the growth of Hbl, Opx, Pl, and Bt coronas on Grt, with Cpx and Pl symplectites replacing Omph. Further decompression (exhumation) to upper amphibolite facies then saw the growth of cordierite and sillimanite in the surrounding gneiss (Figure 2.8). The fabric evident in the sample in Figure 3.5 is that resulting from D_2 deformation during exhumation, as shown in Figure 2.8C.

3.3 Tourmaline-muscovite granite of Ama Dablam and the Khumbu thrust

Ama Dablam (Stop 6, Maps 3 and 4) is composed of tourmaline granite from an elevation of 5200 m to its summit at 6856 m, a vertical exposure of nearly 2000 m. The lower slopes of the mountain consist of sillimanite-biotite gneiss. The summit of Ama Dablam consists of sheeted sills of leucogranites and granite pegmatites. Along the south-east ridge of Ama Dablam, there are numerous dark sillimanite-biotite gneiss and amphibolite xenoliths within the leucogranite to an altitude of approximately 6500 m. Black tourmaline crystals are in abundance in the granite (Figure 3.6).



Figure 3.6: Ama Dablam south-east ridge, at approximately 6500 m. The black rock on the left hand side is an amphibolite xenolith with tourmaline granite on the right. The black specks on the granite are tourmaline crystals. The white rock with large crystals to the right of the climbers is a pegmatite. The layering above the yellow helmet of the climber is part of a sillimanite-biotite gneiss xenolith. Photograph taken at GPS co-ordinates 27°51'24.35"N, 86°51'17.23"E.

The Ama Dablam granite is an example of the tourmaline granite, one of the two types of leucogranite that occur in the Everest region. The other is the two-mica granite that is prevalent in the Nuptse-Everest leucogranite. The tourmaline granite typically has >2.6% tourmaline with crystals observed up to 5 cm in length. The rock is made up mostly of quartz (~30%), plagioclase feldspar (~30%), and K-feldspar (~30%) (Figure 3.7). Very minor amounts of biotite (~5%) are found, and black tourmaline crystals (~5%) occur in the hand specimen of the sample in Figure 3.7. Both muscovite and tourmaline are common in granites generated by the melting of metasedimentary rocks such as the sillimanite-biotite gneiss near the base of Ama Dablam. They originate from in situ melting within the anatectic core of the High Himalaya. The tourmaline granite originated from muscovite dehydration melting in muscovite-rich metapelite at lower pressures (3.5 kbar) and temperatures of >640 °C, whereas the two-mica granite originated at higher temperatures (660-710 °C) and slightly lower pressures (~3 kbar) from biotite dehydration melting in biotite-rich metapelite (Visona and Lombardo, 2002). The tourmaline granite is a generally coarse-grained (>0.5 mm), massive rock and does not contain a strong fabric, although needles of tourmaline are aligned along planes dipping vertically. In places, quartz is highly strained, indicating continued deformation after the crystallization of this granite. Feldspar has been altered to sericite in places by late-magmatic fluids.

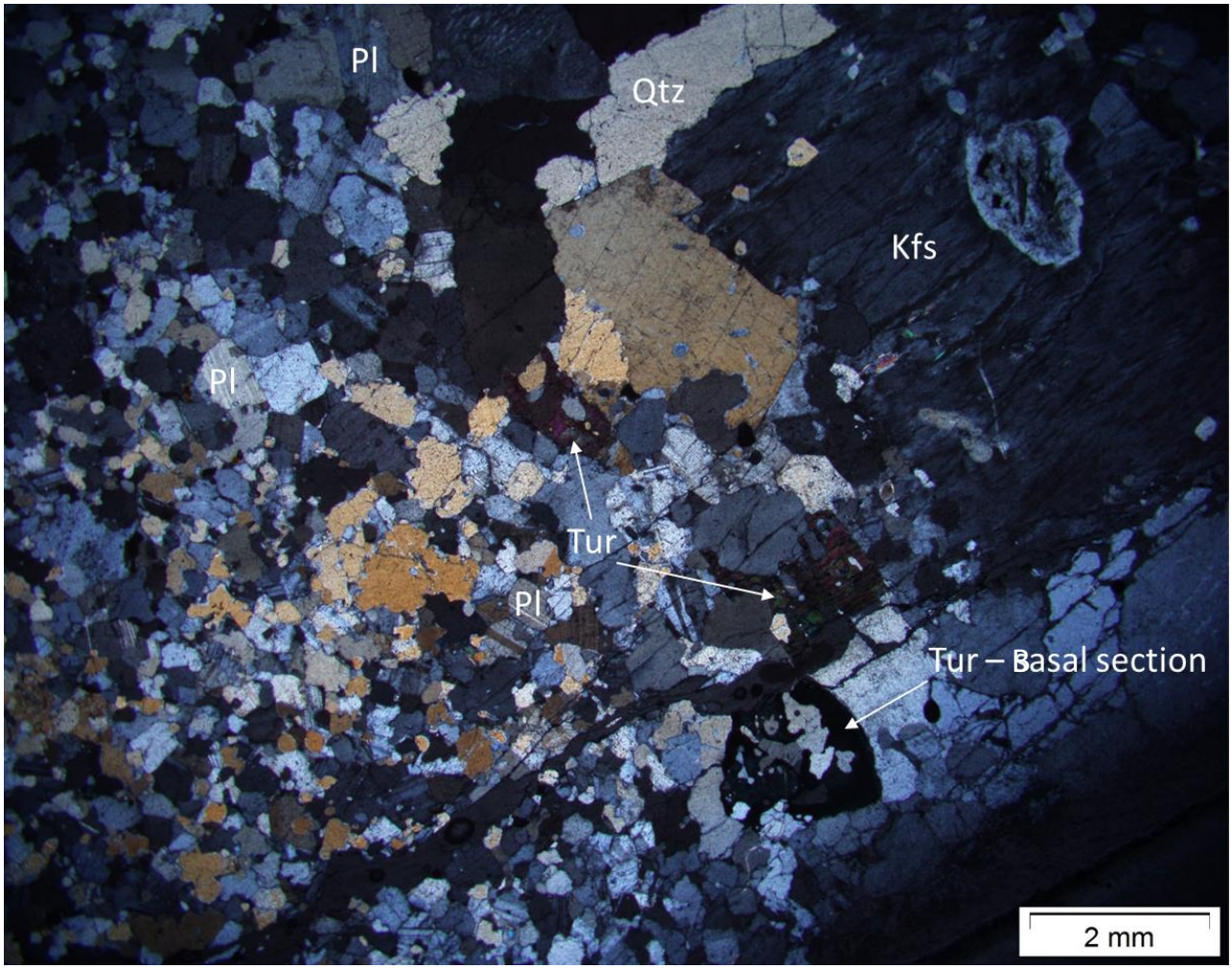
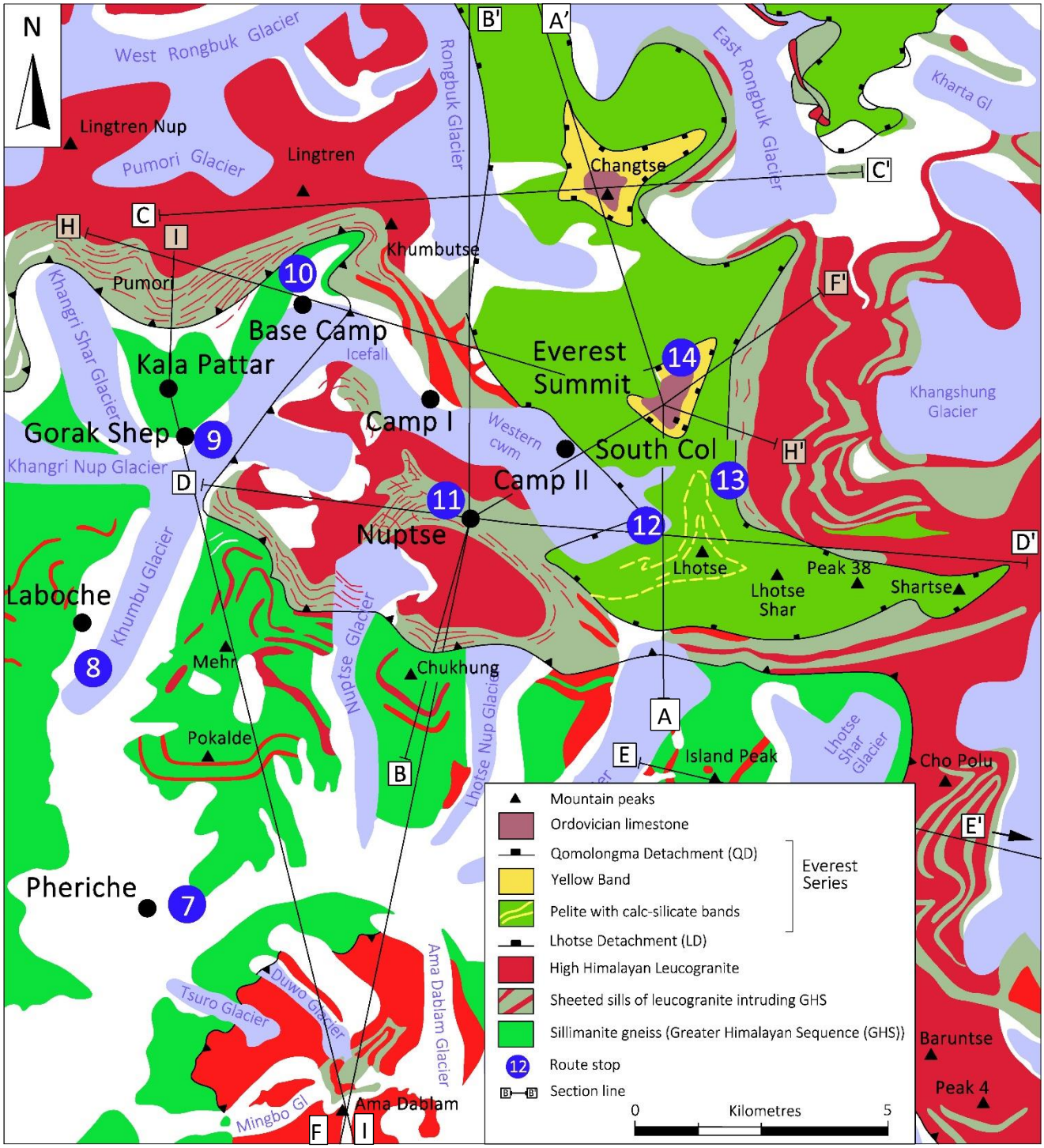


Figure 3.7 Photomicrograph (XPL) of tourmaline granite. The rock is made up of quartz (Qtz), plagioclase (Pl) and K-feldspar (Kfs), tourmaline (Tur) and minor amounts of biotite. Some of the quartz is strained, indicating deformation after crystallisation of this granite. Sample collected at GPS co-ordinates 27°51'9.95"N, 86°51'4.30"E.

Visona and Lombardo (2002) suggested that tourmaline granite was emplaced at the same structural level in which it had been generated, whilst the higher-temperature two-mica granite was transported upwards by dyking and eventually coalesced in the plutons common in the upper parts of the GHS. What this means is that large masses of granite have been generated in the Himalayas through the process of migmatisation in zones such as the Namche Migmatites, segregation of this melt, and subsequent migration upwards with emplacement along an active thrust plane or planes. The KT is the thrust plane which accommodated movement and upward

emplacement of these large masses of granite into the zone below the STD or, more precisely, below the LD (Searle, 1999). During the emplacement, rafts of underlying dark sillimanite gneiss were detached from the zone of migmatisation and included in the granite or were wedged off by merging sills in the emplacement zone (Searle, 1999). The summit of Ama Dablam is composed of sheeted dykes of pegmatite, above the thick leucogranite sheet that makes up the Ama Dablam massif, suggesting that hydraulic fracturing and emplacement of granites along a network of sills and dykes was followed by later emplacement of voluminous to form the larger the granite plutons and sheets of the Higher Himalayan Leucogranites (Searle et al. 1997). The two granites differ in terms of both grain size and mineralogy, with later intrusions observed in outcrops on Ama Dablam and at Base Camp having tourmaline suggesting that these pegmatites could represent late-stage incompatible-rich fractionates (Searle et al. 1997, Searle et al. 2003).

Map 4: Geological map of Ama Dablam and Everest area (Modified after Searle (2007) incorporating further cross-section lines not included in this part of the dissertation)



3.4 Views from Kala Pattar – the Everest Series and South Tibetan Detachment

From the top of a small hill called Kala Pattar (Map 4) immediately north of Gorak Shep, the leucogranite layer forming the uppermost part of the Higher Himalayas can be observed: to the east, the Nuptse granite with its stockwork of sheeted pegmatite dykes above the plutons of leucogranite (Figure 3.10); to the north, the west shoulder of Everest with its stockwork roof of sheeted dykes(Figure 3.8), Lingtren, with its rafts of dark sillimanite-biotite gneiss xenoliths, and the sugar-loaf pillar of the Pumori granite (Figure 3.11). The leucogranite layer is bound by the Khumbu Thrust (KT) underneath and the Lhotse Detachment (LD) above it (Figure 3.8).

To the north, above the LD, the summit of Everest and the bulk of Changtse are composed of the Everest Series rocks. The Qomolongma Detachment (QD) at the top of the Yellow Band places Ordovician sedimentary rocks above greenschist facies carbonates and shales, and the Lhotse Detachment (LD), in turn, places the Everest Series greenschist rocks above the sillimanite–cordierite gneisses with its >50% leucogranite sheets and sills (Searle 1999a, b; Searle et al. 2003). Little of the Ordovician sedimentary rocks remain at the summit of Everest and a better exposure can be seen on Changtse, to the north of Everest (Figure 3.9). The QD dips at about 10° N and hence, progressively larger outcrops of the Ordovician sediments can be seen in Tibet (Map 4).

The leucogranites are amongst the most striking geological features of the high Himalayas (Weinberg et al. 1998). An excellent example occurs on the northern and western face of Nuptse (Figure 3.10). Here the pale leucogranites intrude the darker sillimanite-biotite schist as a series of subvertical pegmatite dykes and sub-horizontal sills. These can be traced laterally into a large plutonic mass. The leucogranite plutons are likely the result of from a second phase of intrusion of melt with the surrounding stockwork pattern of sills and dykes being the result of early hydraulic fracturing and emplacement of pegmatite into the rocks surrounding the leucogranite plutons below the LD (Searle et al. 1997).

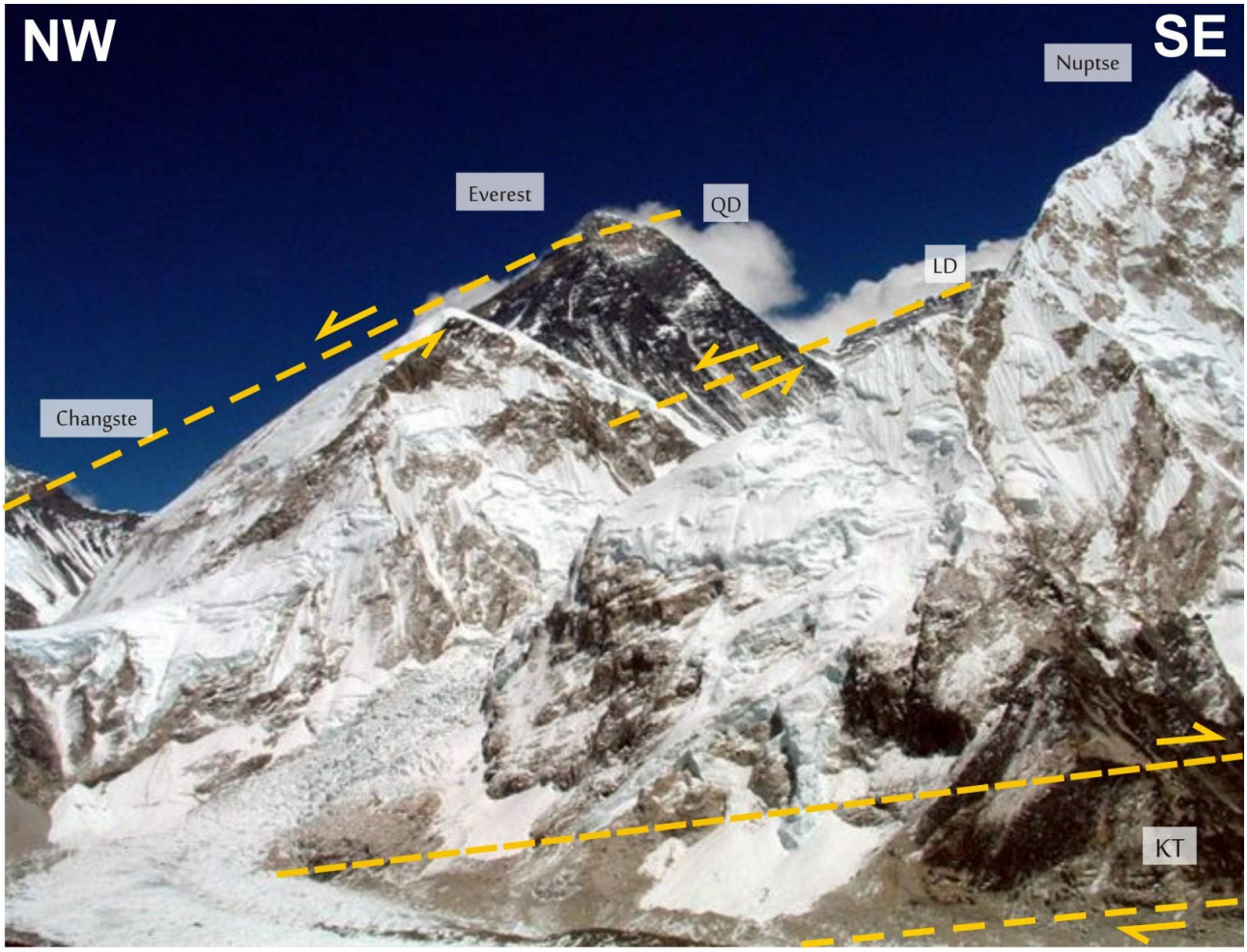


Figure 3.8: View from Kala Pattar of Changtse, Everest and its west shoulder, and Nuptse. The Khumbu Thrust zone (KT) is located at the base of the massif in the dark gneiss. The Lhotse Detachment (LD) runs along the Lhotse Ridge and through South Col on the right edge of the south-east ridge of Everest where it meets the Lhotse Ridge. The Qomolongma Detachment (QD) is located at the top of the Yellow band near the summit of Everest and dips northwards through the top of the Yellow Band on Changtse (Figure 3.9). Nuptse and the west shoulder of Everest are composed of leucogranite whilst Everest itself is composed of the dark dolomitic marble and limestone. The summit rocks are composed of mylonitized limestone containing calcite, with small amounts of dolomite and very small amounts of quartz and muscovite (Yin and Kuo, 1978; Sakai et al., 2005, Myrow et al., 2009). Photograph taken from the Kala Pattar summit, GPS co-ordinates 28°59'7.45"N, 86°49'39.38"E.

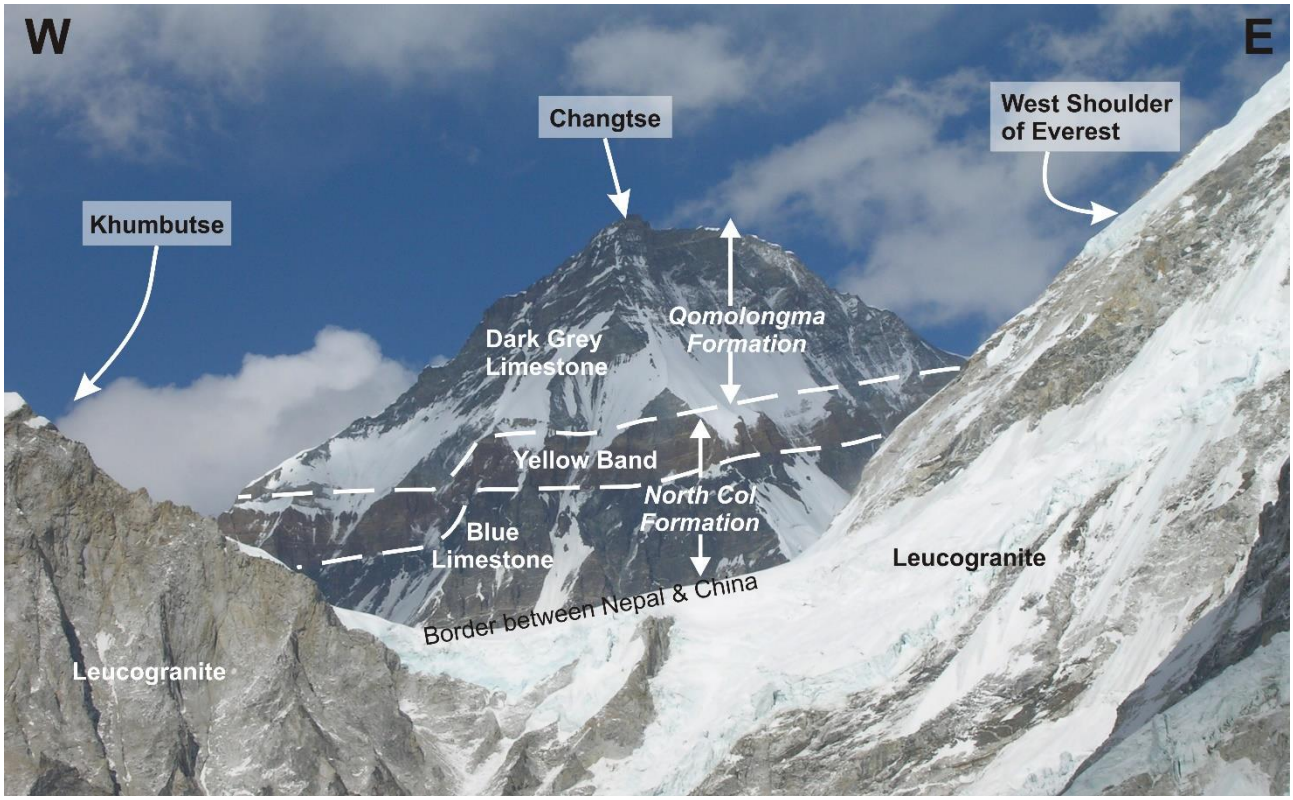


Figure 3.9: The Everest Series on Changtse to the north of Everest shows the Qomolongma Detachment (QD) positioned at the top of the Yellow Band. Photograph taken from the Kala Pattar summit, GPS co-ordinates 28°59'7.45"N, 86°49'39.38"E looking ENE.



Figure 3.10: More detailed view of the west face of Nuptse showing a stockwork of cream-coloured granite dykes and sills (centre) above a more massive granite pluton (bottom left) intruding sillimanite-biotite gneiss on the west face of Nuptse. The granite extends across the entire base of Nuptse below the level of the photograph. Photograph taken from the Kala Pattar summit, GPS co-ordinates 28°59'7.45"N, 86°49'39.38"E looking ESE.

The west shoulder of Everest, similarly, comprises a large pluton of leucogranite and pegmatite, overlain by a network of leucogranite and pegmatite sills and dykes.

Moving west of Everest, the Pumori leucogranite is located north of and above Kala Pattar (Figure 3.11). On the way to the top of Kala Pattar from the south, a small outcrop of tourmaline granite is also observed. This likely represents a dyke of tourmaline granite migrating upwards from the

migmatites of the GHS to the zone of leucogranite plutons found near the top of the GHS. The location of where this sample was taken is in the foreground of the photograph shown in Figure 3.11. The summit of Kala Pattar is composed of dark sillimanite-biotite gneiss.

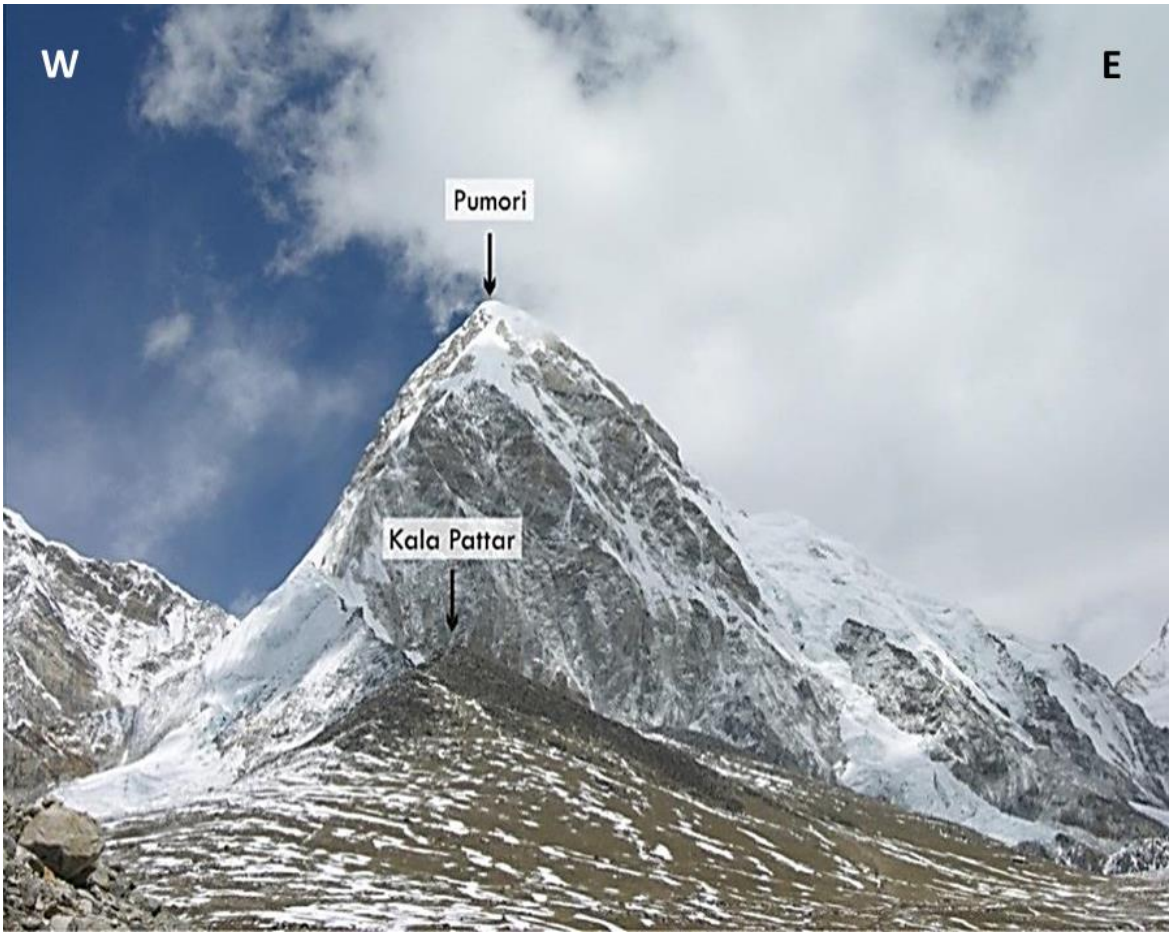


Figure 3.11: View N across KP hill to Pumori, showing sillimanite gneiss in the foreground and the overlying leucogranite. The KT that separates the units is hidden by topography. Dark sillimanite gneiss is evident in the foreground and on the summit of Kala Pattar hill. Beyond it, the sheeted pegmatite dykes at the base of Pumori give way to leucogranite approximately two-thirds of the way up the S face of Pumori. Photograph taken from GPS co-ordinates 28°58'52.97"N, 86°49'42.95"E looking northwards.

On the west face of Nuptse above the Khumbu Icefall, leucogranite sills intruded parallel to the layering in the host sillimanite-biotite gneiss (Figure 3.12), which appears to have been slightly folded (Searle, 1999). This may give the impression that leucogranite sills themselves have been folded. The folding of the layering (and possibly the leucogranite sills) is suggested to be related to shearing on the KT, which crops out near the base of Nuptse (Searle, 1999).

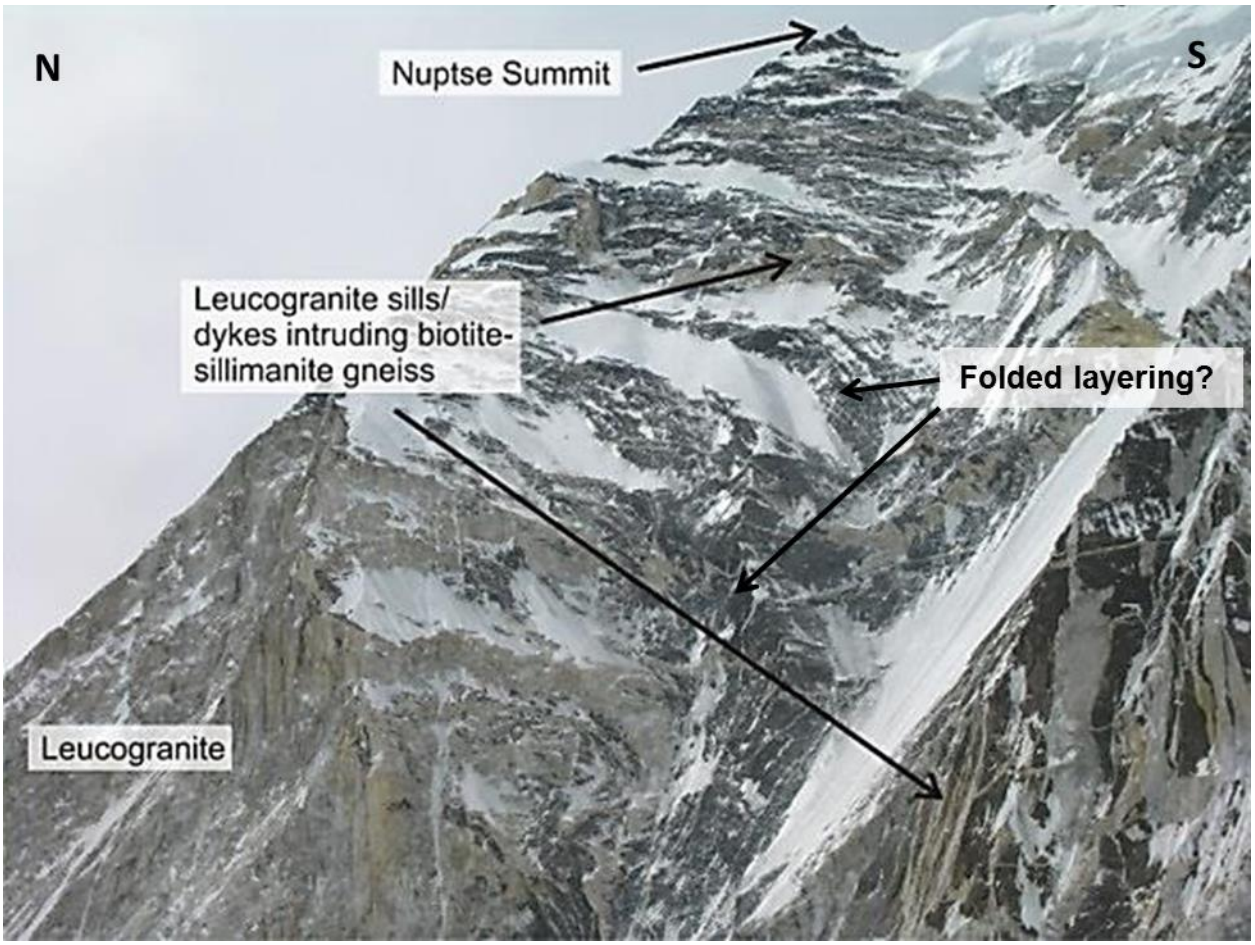


Figure 3.12: The west face of Nuptse above the Khumbu Icefall showing folding of the leucogranite sills and dykes (Searle, 1999, Fig 11 proves this). Photograph taken from the north end of Base Camp, GPS co-ordinates 28°58'35.50"N, 86°52'45.65"E.

There are also angular fragments of the darker gneiss that can be seen in the lighter leucogranite intrusive. Much of the lighter, pale rock is sheared leucogranite and mylonite (Figure 3.13). Intense

shearing in the vicinity of major thrust planes, such as the Khumbu Thrust, resulted in the widespread occurrence of mylonite. Evidence of this is from the preponderance of float samples containing mylonite from Gorak Shep, Base Camp and Camp 2.

A leucogranite outcrop 300 m east of Base Camp at the foot of Nuptse shows multiple phases of granite intrusion, with differing grain sizes and textures (Figure 3.13A). Searle et al. (1997) suggested that the crust was actively deforming during granite formation as the early two-mica granites, and even the later tourmaline granites, are foliated. Alternating compression and dilation of anastomosing shear zones drove the ascent of leucogranite melts (Searle et al. 1997). This must have occurred rapidly and in multiple stages as one of the moraine rocks at Base Camp (Figure 3.13B) shows angular fragments of dark gneiss and pre-existing leucogranite, intruded by a second injection of leucogranite in close proximity to a mylonite band on the left side of Figure 3.13B.

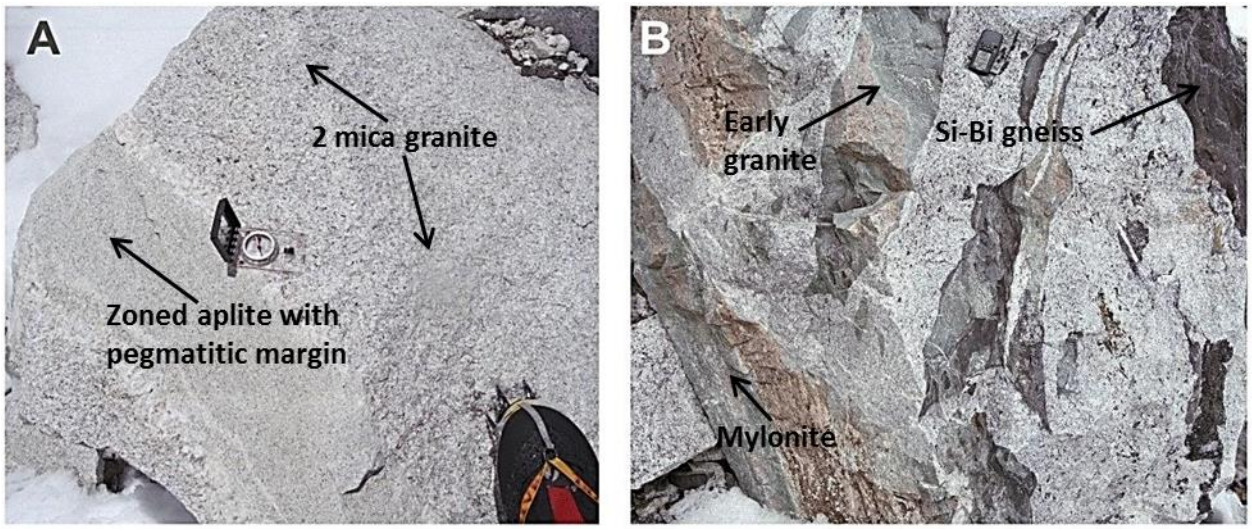


*Figure 3.13: (**A**) Fine-grained aplite dyke intruding two-mica granite. (**B**) Granite intruding sillimanite-biotite gneiss and an earlier generation of granite in moraine rock from Base Camp. Note the mylonitic zone seen near the bottom left of the photograph, indicating that granites have experienced shearing post-emplacement. "Fish-head" boudins can be seen in the sheared granite in B indicating continued deformation and thinning at the edges of the black amphibolite inclusions with the less viscous amphibolite elongated and leucosome melt forming between the inclusions. Photograph taken at GPS co-ordinates 28°0'6.58"N, 86°51'49.03"E.*

Between the dark sillimanite-biotite gneiss and sheeted sills found on Kala Pattar is a zone of intense shearing and deformation which may be the KT. Mylonite is present in most of the rocks found in the moraine at Base Camp. A sample from Camp II shows that mylonitic rock contains large amounts of plagioclase, quartz and biotite. Biotite has been slightly altered to chlorite, and minor amphibole is also found (Figure 3.14). The rock is fine-grained, with small (<0.2 mm) platy biotite and ribbon-like grains of quartz aligned to form a strong fabric. The very fine-grained nature of the rock is characteristic of mylonite, where intense deformation has led to grain size reduction.

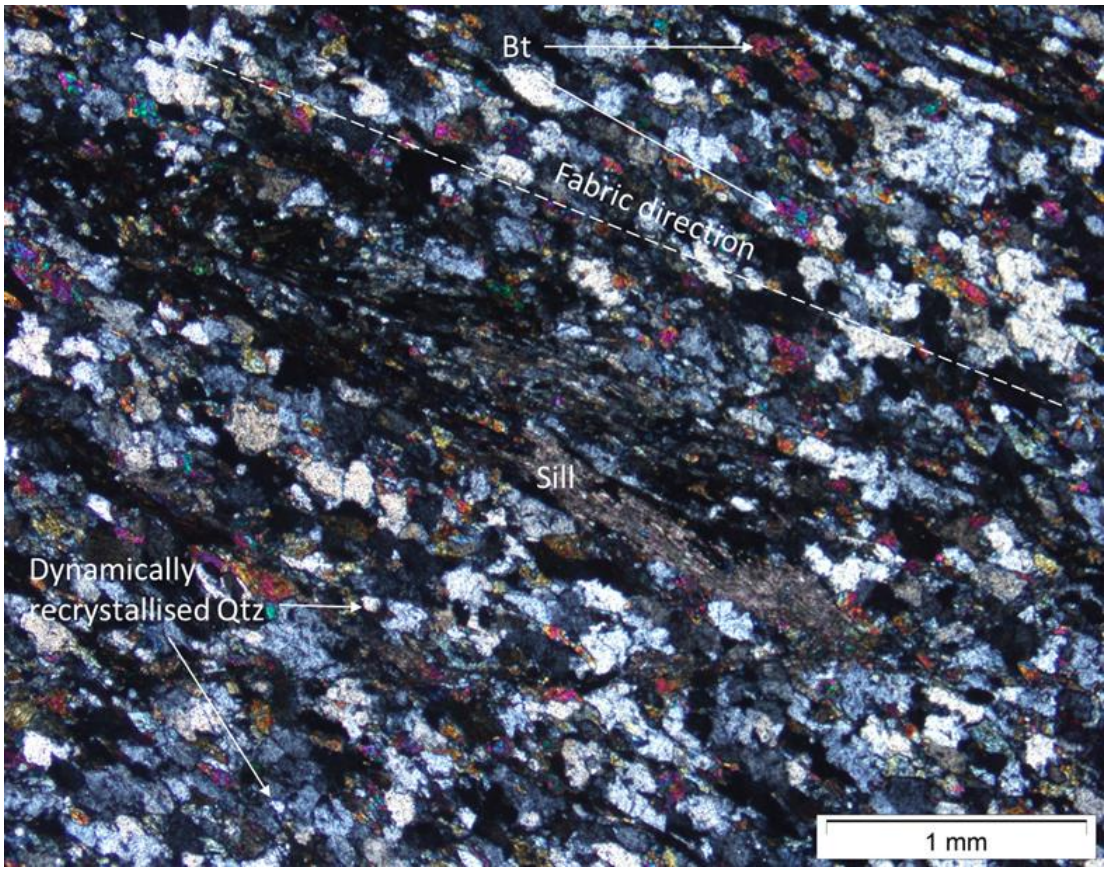


Figure 3.14: Photomicrograph (XPL) of a mylonite sample collected near Camp I. The rock is predominantly fine-grained quartz, biotite and plagioclase. The rock is very fine grained and platy biotite and quartz are aligned in a strong fabric. Intense deformation has led to a grain size reduction through dynamic recrystallization, a texture typical of mylonite. Sample collected at GPS co-ordinates 28°0'6.58"N, 86°51'49.03"E.

Leucogranite in places around Base Camp and in the Western Cwm is also commonly intensely sheared. The rock is very pale white and contains few mafic minerals (such as biotite). It is composed of quartz (~30%), K-feldspar (~30%) and plagioclase feldspar (~30%), with minor muscovite mica. The muscovite micas in this fine- to medium-grained rock are aligned to form fabric (Figure 3.15). Quartz is also elongate in places and aligned with the fabric, and shows evidence of shear strain. The deformation found in this granite is the result of its proximity to the Lhotse Detachment, which separates the underlying Greater Himalayan Sequence and Himalayan Leucogranites from the lower-grade Everest Series rocks (Map 4 and Figure 3.8).

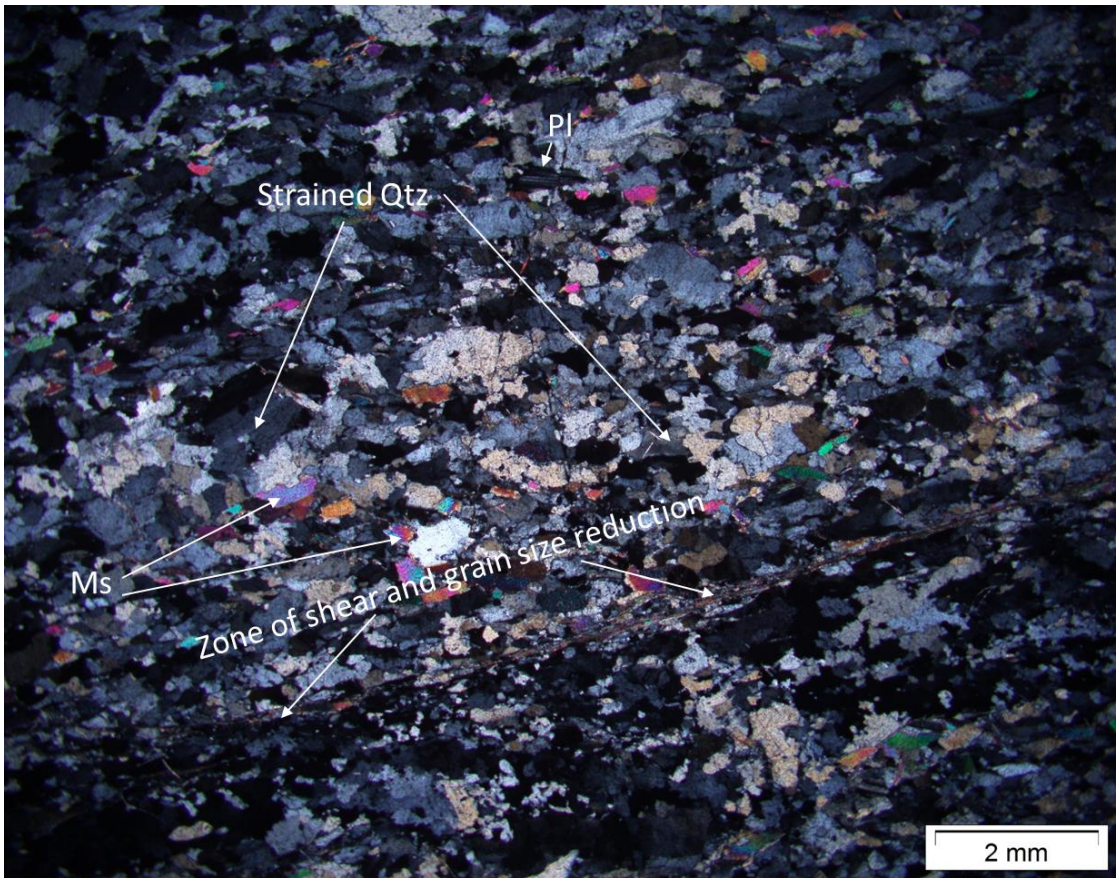


Figure 3.15 Photomicrograph (XPL) of strongly deformed protomylonite of leucogranitic origin collected from near Camp 2. The rock is very pale and has few mafic minerals. It is composed of quartz (Qtz), which is often strained, plagioclase (Pl), K-feldspar and lesser amounts of muscovite. Fine to medium grained muscovite mica grains are aligned to form a fabric, and quartz shows evidence of straining and grain size reduction. Note the zone of shear and intense grain size reduction cutting the sample. Sample collected at GPS co-ordinates 28°58'39.68"N, 86°53'58.89"E.

3.5 View from Base Camp and the Western Cwm

To the NW of Everest Base Camp, the striking feature is the Lingtren-Pumori ridge, which consists of leucogranite. Underlying this ridge is a thick sequence of dark sillimanite gneiss (Figure 3.16) with numerous sills of leucogranite (see Map4).

The geology of the Pumori-Lingtren ridge (as seen from base camp, looking west) is shown in Figure 3.16. Sillimanite-biotite gneiss with numerous leucogranite sills underlies the thick leucogranite pluton of Pumori and Lingtren, and dips gently to the north. The dip of the layering is sub-parallel to the dip of the major structures along which exhumation has taken place.

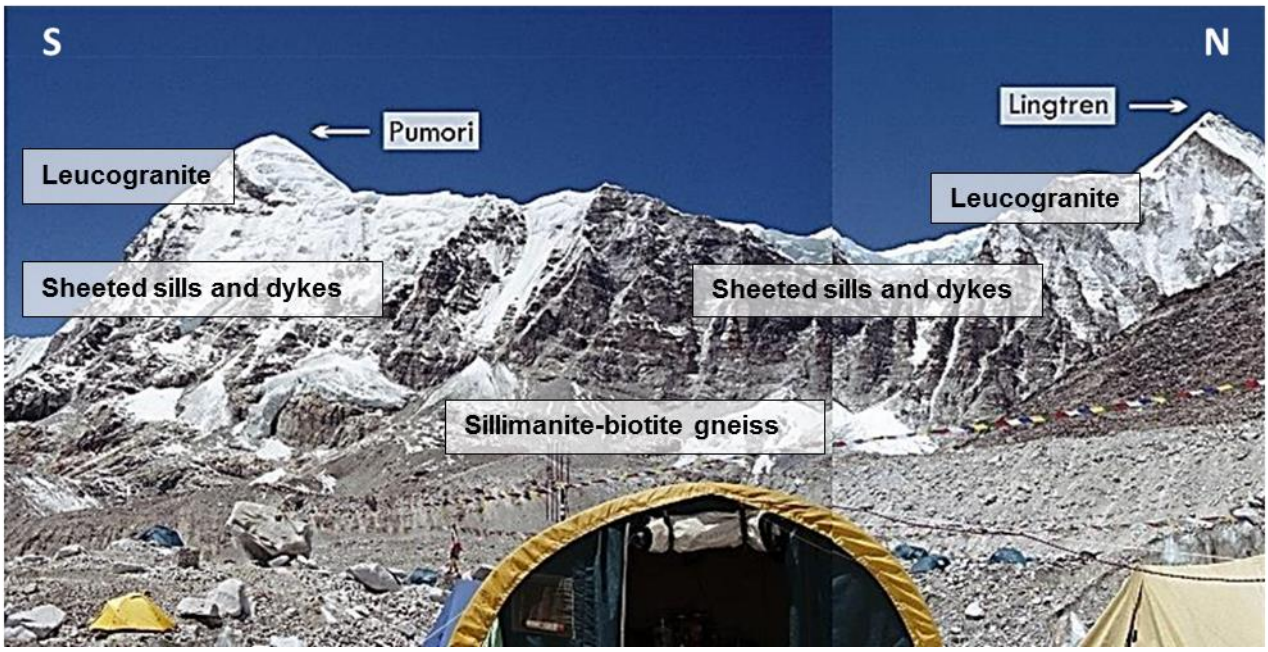


Figure 3.16: The east faces of Pumori and Lingtren above the Khumbu glacier showing exhumed leucogranite intruding sillimanite-biotite gneiss. Photograph taken from GPS co-ordinates 27°58'54"N, 86°49'48"E.

A closer look at the east face of Lingtren and Lingtren II, as seen from Base Camp, shows it is composed almost entirely of leucogranite (Figure 3.17), which contains xenoliths of sillimanite-biotite gneiss, and lies above biotite-sillimanite gneiss intruded by numerous sills of leucogranite.

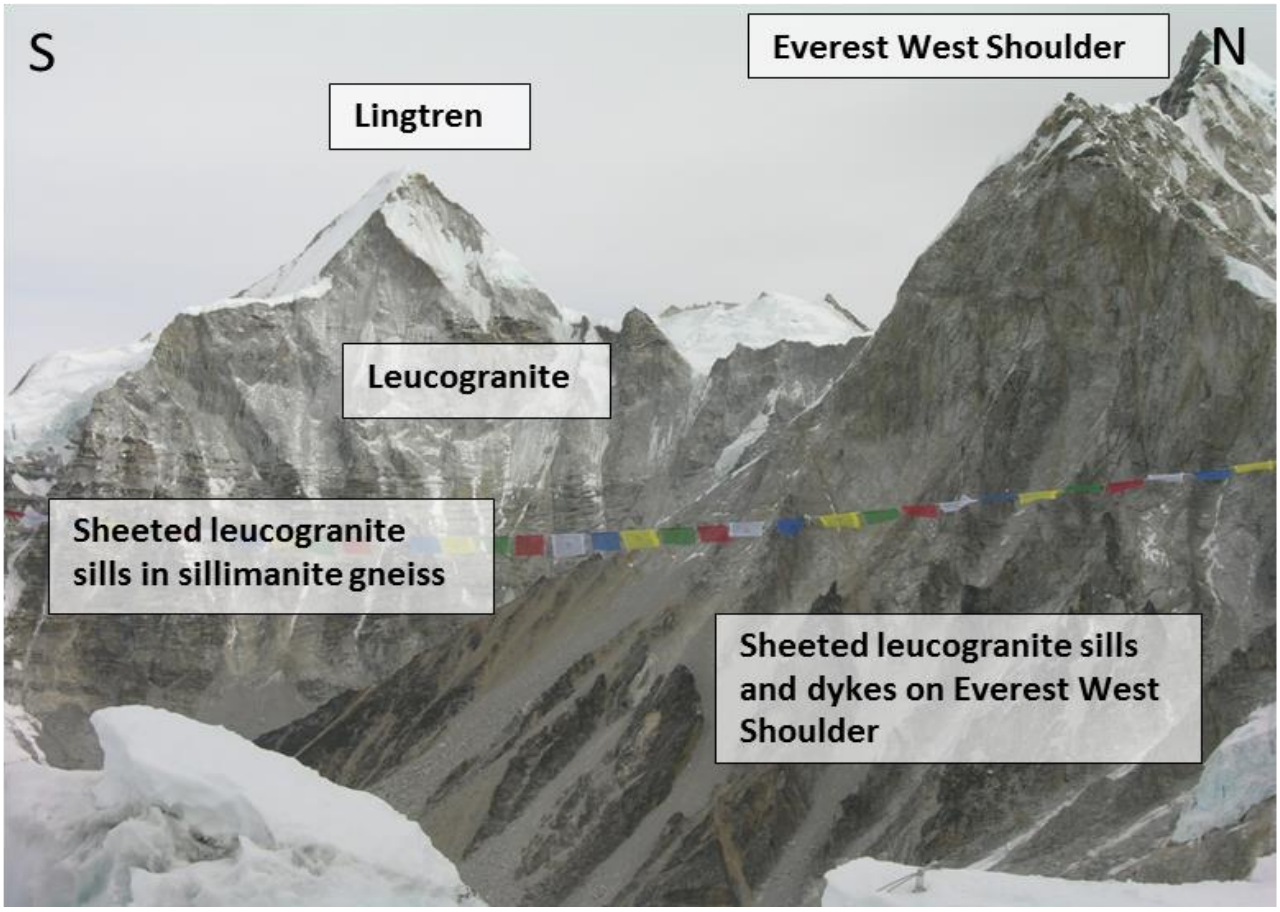


Figure 3.17: The east face of Lingtren viewed from Camp 1 (in the Khumbu Icefall) showing sheeted leucogranite sills in sillimanite-biotite gneiss below the leucogranite that forms the summit of Lingtren, and sheeted leucogranite sills and dykes on the West Shoulder of Everest. Photograph taken from GPS co-ordinates 28°0'6.58"N, 86°51'49.03"E.

The ridge is interpreted as an intrusion of leucogranite between the sillimanite-biotite gneiss and the Lhotse Detachment (Searle et al. 2003). Restoration of the Pumori Lingtren Everest profile (Figure 3.18) shows that melting of the leucogranite occurred at around 20km depth

(P=7 kb) and, depending on the dip of the LD samples taken from Kala Pattar show that these rocks have been displaced southwards for a distance of between 90 to 216km (Searle et al. 2003). The Pumori – Lingtren ridge is therefore the top part of a channel extruded between the STD (of which the LD and the QD for part of) and the MCT.

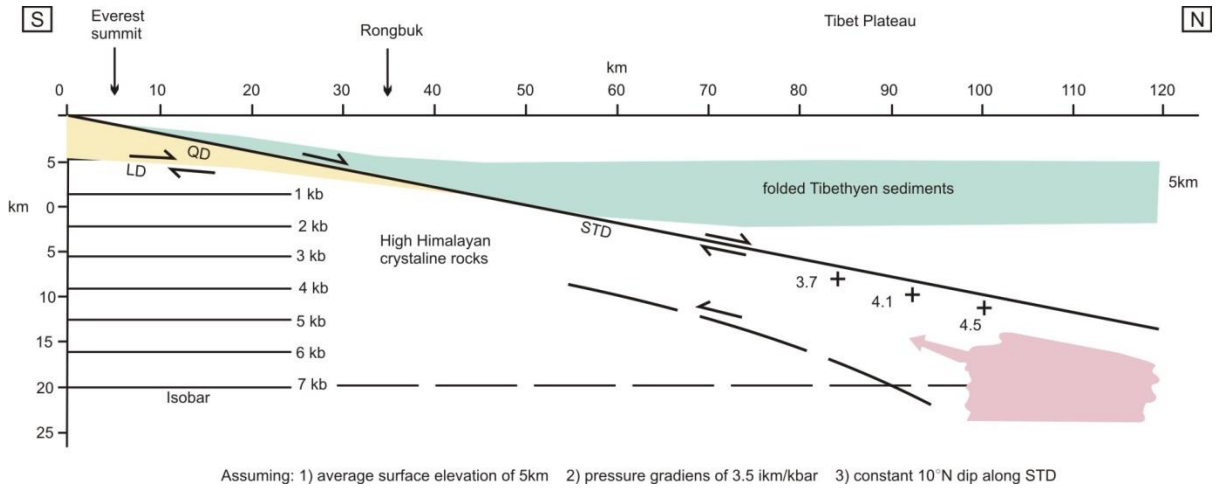


Figure 3.18: Restored Pumori – Everest profile before emplacement of the leucogranite. Crosses mark samples from Kala Pattar, 12km west of Everest (Map 4) which record pressures of 3.7, 4.1 and 4.5kb. at a true dip of 3° to 5°N measured on the N face of Everest, relative displacement is would be 180-216km (After Searle et al. 2003).

Partial melting (migmatisation) of the GHS took place between 25 and 22 Ma (Viskupic and Hodges (2001), and these melts segregated from the migmatites and ascended to the top of the GHS to form the leucogranites that we see on surface today. Higher Himalayan Leucogranites range in age from 20.5–21.3 Ma (Simpson et al. 2000) to as young as 16.8–16.5 Ma (Murphy and Harrison 1999) (Figure 3.19). The age differences between deformed and undeformed leucogranite sills and cross-cutting dykes constrains final stages of ductile shearing associated with sillimanite grade metamorphism at 17 Ma, whilst brittle faulting along the top of the South Tibetan Detachment shear zone must be younger than 16 Ma (Searle et al. 2003)

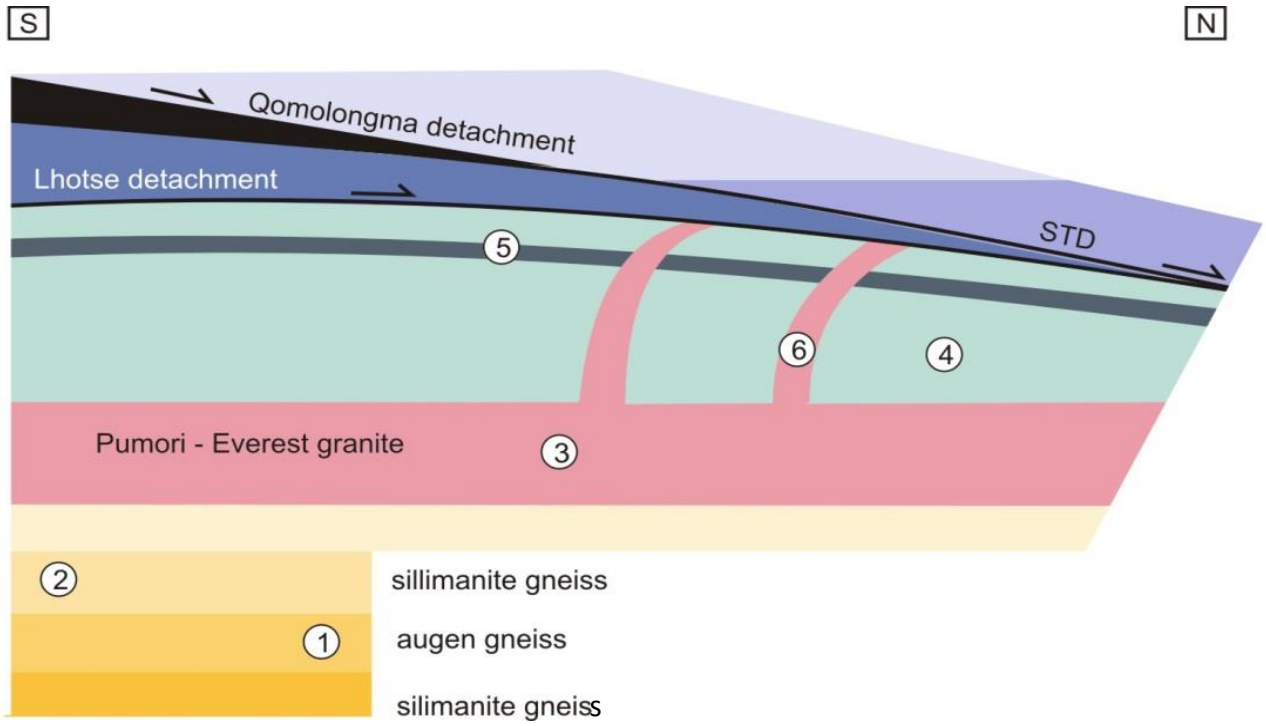


Figure 3.19: The age relationship between metamorphism (M_1 and M_2), the leucogranite of the Pumori-Lingtren-Everest ridge, the Rongbuk metamorphism, the deformed sills and dykes and ductile and brittle faulting on the STD (After Searle et al. 2003). 1 – Age of maximum pressure metamorphism (M1) 32.2 ± 0.4Ma (Simpson et al. 2000). 2 – Age of low pressure cordierite metamorphism (M2) 22.7 ± 0.2Ma (Simpson et al. 2000). 3 – Anatexis resulting in melts that formed leucogranites found on Everest 20.5–21.3 Ma (Simpson et al. 2000). 4 – Youngest metamorphism 17.9 ± 0.5 Ma (Simpson et al. 2000). 5 – Deformed leucogranite sills, 16.67–16.2 Ma (Hodges et al. 1998; Murphy and Harrison 1999). 6 - Undeformed cross-cutting dykes 16.8–16.5 Ma (Hodges et al. 1998; Murphy and Harrison 1999).

In the western Cwm, around 1000 m above Base Camp, a fold structure in the Lhotse-Nuptse ridge (Figure 3.20) supports the recumbent fold shown by Searle, (2007) on his map of the area. The fold is located in the Rongbuk formation immediately beneath the STD and has experienced P-T conditions of ~660 °C and ~4 kbar.

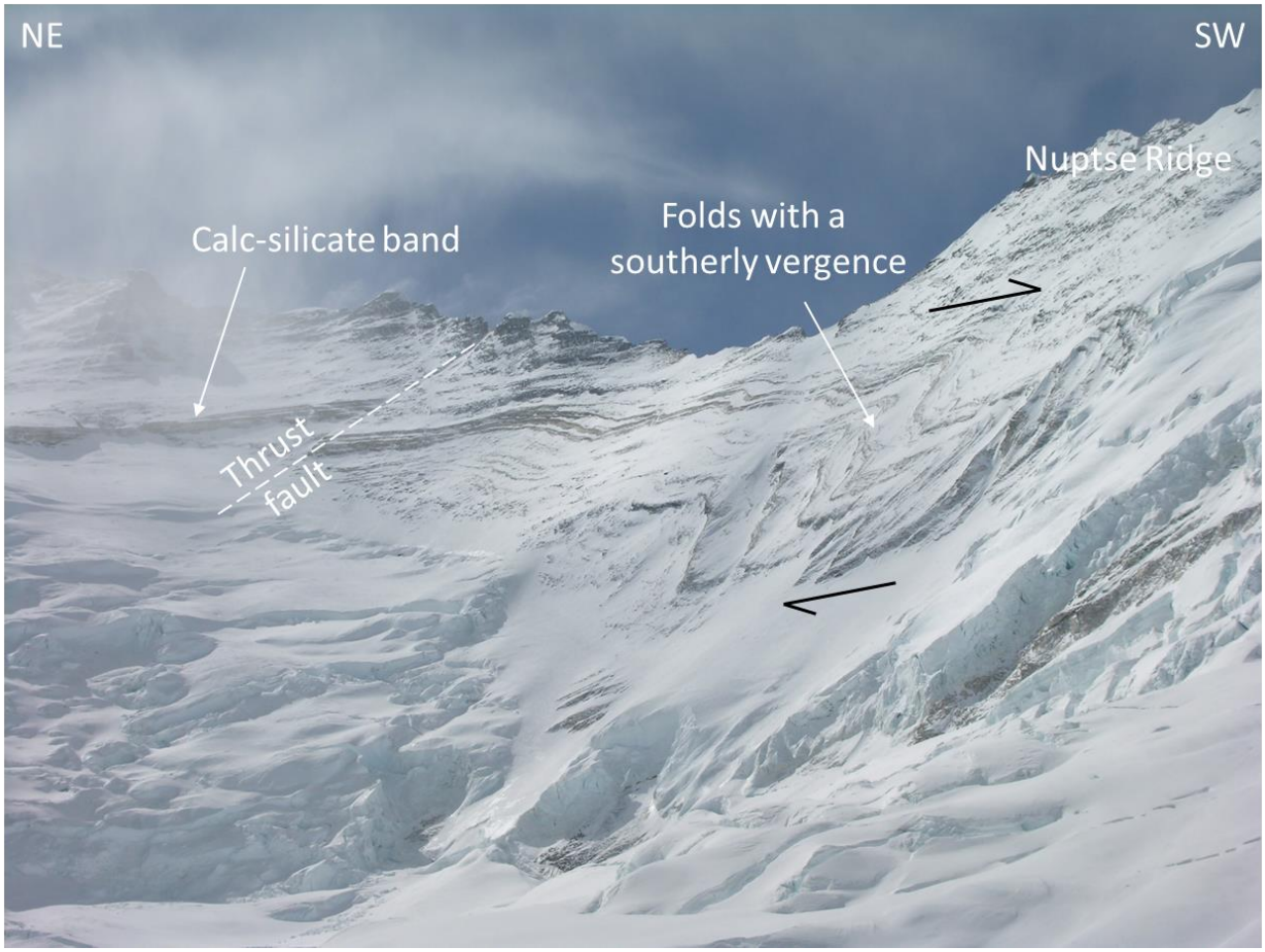


Figure 3.20: The Western Cwm fold structure as seen from Camp 2. The low angle of the northwards dipping metasediments and detachments are clearly visible. Note the thrust fault and folded calc-silicate bands with a south-westerly vergence, suggested to be related to the Lhotse Detachment (Searle, 1999). Photograph taken from GPS co-ordinates 28°0'42.75"N, 86°51'24.57"E looking northwest.

3.6 Glacial valleys/ erosion/ exhumation

Erosion is extreme in the Himalayas. At Base Camp, during April and May, 2006, a measurement of the time taken between erosional events was six seconds on average at night, and four seconds on average during the day. An erosional event was taken, by the author, as an audible or visual

movement of ice, snow or rocks in the form of serac collapse, avalanche, earth tremor, glacial movement of ice, moraine movement or rock fall. This illustrates the extreme rate of erosion and denudation that occurred. At the end of May that year, the Khumbu Icefall was severely depleted of ice as temperatures were relatively high with good weather through most of May. There was some running water beneath the ice at Base Camp, which increased in volume audibly over the month. Map 4, for example, shows 5 glaciers eroding the faces of Lingtren and Lingtren II and nine glaciers eroding the Everest-Lhotse-Nuptse massif (Figure 3.23 and Map 4). At altitudes such as those in the Everest area, glacial erosion is the most important form of erosion. Snowfalls occur mostly in the afternoons, adding frequently to glacial ice accumulation. Even though glaciers are retreating, they are still the main erosive force.

Earthquakes, such as the recent event of 25th April 2015, have a massive one-time impact with collapses of huge faces of rock and ice. The epicentre of the earthquake (28.15°N 84.7°E) has been estimated at 15 km depth, northwest of Kathmandu (Google Earth/DLR Earth Observation Center/Sentinel-1 satellite operated by ESA, Figure 3.21). In Base Camp, the 7.8 magnitude earthquake measured by the US Geological Survey (the China Earthquake Networks Centre reported the earthquake as 8.1) triggered a rock, ice and snow fall on the west face of the Nuptse massif which resulted in much of the Camp being devastated. There were 17 deaths, of which 7 were Sherpas with whom I had climbed on Ama Dablam. Movement most likely occurred on the Main Boundary Thrust or the Main Frontal Thrust as Kathmandu lies above both (Figures 2.2 and 3.21).

A second earthquake (magnitude 7.3) on the 12th May 2015, whose epicentre (27.84°N, 86.1°E) was virtually beneath Everest at a depth of 18.5 km, was reported as being the result of a thrust movement, probably again on the MCT (Wikipedia and USGS Earthquake Hazards Program http://earthquake.usgs.gov accessed June 2015). Despite the devastation, these earthquakes clearly illustrate the active exhumation of the GHS along the MCT. It is likely that there was also some sympathetic movement on the STD at the time of the earthquakes (http://earthobservatory.nasa.gov/IOTD/view.php?id=85871, accessed 30 April, 2016), but the depth of both epicentres points to thrust movement along the MCT.

Such high magnitude earthquakes are infrequent, with the previous big earthquake having occurred in 1934. However, there are continually, smaller earthquakes in this zone of active tectonics, including a number of earthquakes with magnitude >6 along the Himalayan mountain belt (Figure 3.22).

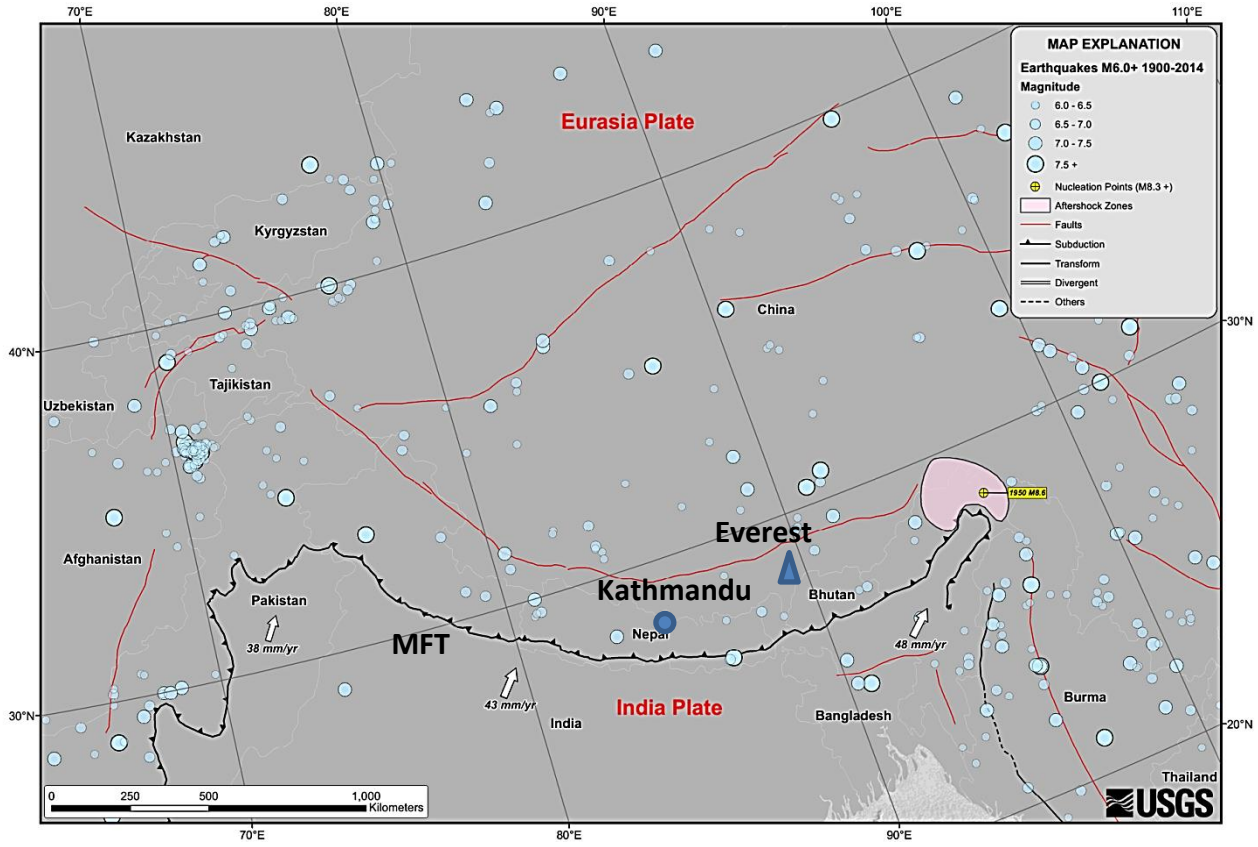
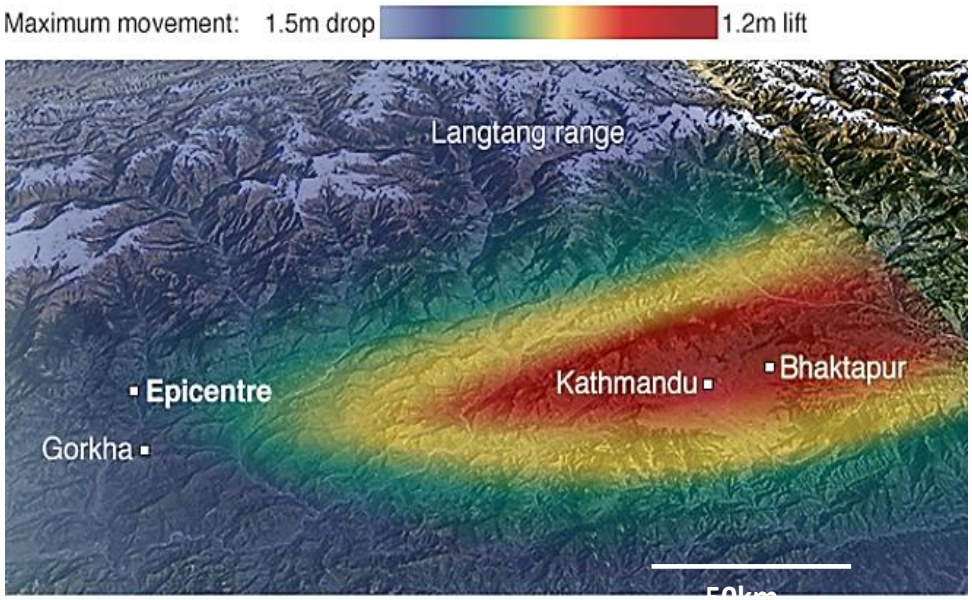


Figure 3.21: Earthquake epicentres and their magnitude recorded in the India-Eurasia area between 1900 and 2014. Note the greater number of earthquakes west of the Himalayas (in Uzbekistan, Tajikistan and Kyrgyzstan) and east of the Himalayas (in Burma), compared to the Himalayan Mountain chain (Pakistan, Nepal and Bhutan). (Source: http://earthquake.usgs.gov/earthquakes/tectonic/images/himalayatsum.pdf, accessed July 2014).

The total vertical movement indicated by the German Aerospace Centre (DLR), shown in Figure 3.22, is 2.7 m. The horizontal movement at an angle of 5° (the dip of the MCT) is approximately 30 m. If only the 1.2 m maximum lift is considered, then the horizontal movement at 5° dip is 13.7 m. Since the start of the collision of India and Asia, estimates of slip of greater than 400 km along the

Main Frontal Thrust alone (below the MCT), have been postulated by Coward and Butler (1985), Hauck et al. (1998) and Murphy and Yin (2003). The cumulative movement on all thrusts and detachments is likely to be significantly in excess of 400 km as some of this movement is translated into ductile strain. Extrusion of footwall gneisses and leucogranites is estimated at 200km southwards and brittle faulting in the QD which cuts all leucogranites in the footwall was post-16Ma (Searle et al. 2003). This suggests a lateral decadal slip/extrusion rate of 12.5cm (Searle et al.2003).



Source: Google Earth/ DLR earth Observation Centre/Sentinel-1 satellite operated by ESA

Figure 3.22: Map showing lift and drop of the 7.8 magnitude earthquake of 25th April, 2015 with epicentre west-north-west of Kathmandu. The epicentre was probably located on the MFT.

Although they have a major erosional impact, earthquakes are infrequent compared to the constant erosion of a glacier which constantly transports material to its snout. Erosion helps to increase the rate of extrusion of the mid-crustal wedge of rocks or channel by concentrated denudation (Figure 2.14) at the rangefront of the extruding crustal block (Figure 2.12). Should glaciers disappear completely from the Himalayas (taking the limit of probability, and given the current changes in global climate), then it is thought that the snow line would have to be well above 7000 m. Currently the snow line is at Pangboche ~4000 m, where trees begin to grow but should it move to above 7000m, water erosion may then become the main erosive force. This

statement would, however, need to be tested by researchers. A Google map view of the Everest Himalayas shows many sharp ridges and steep drop-offs from the ridges indicating U-shaped valleys (Figure 3.23). Erosion rates dictate the thickness of the Himalayan orogen. If erosion rates in the high mountains are too low, then the orogen thickens as the vertical extrusion of a channel of rock exceeds the rate at which it is eroded, and vice versa (Malavielle 2010, Bose and Mandal 2010) . If the extrusion rate as calculated from Searle et al (2003) is correct, then the vertical rate of movement at a dip angle of 10° is 2.17cm/decade. Hence the rate of erosion needs to match this to maintain the height of the mountains.

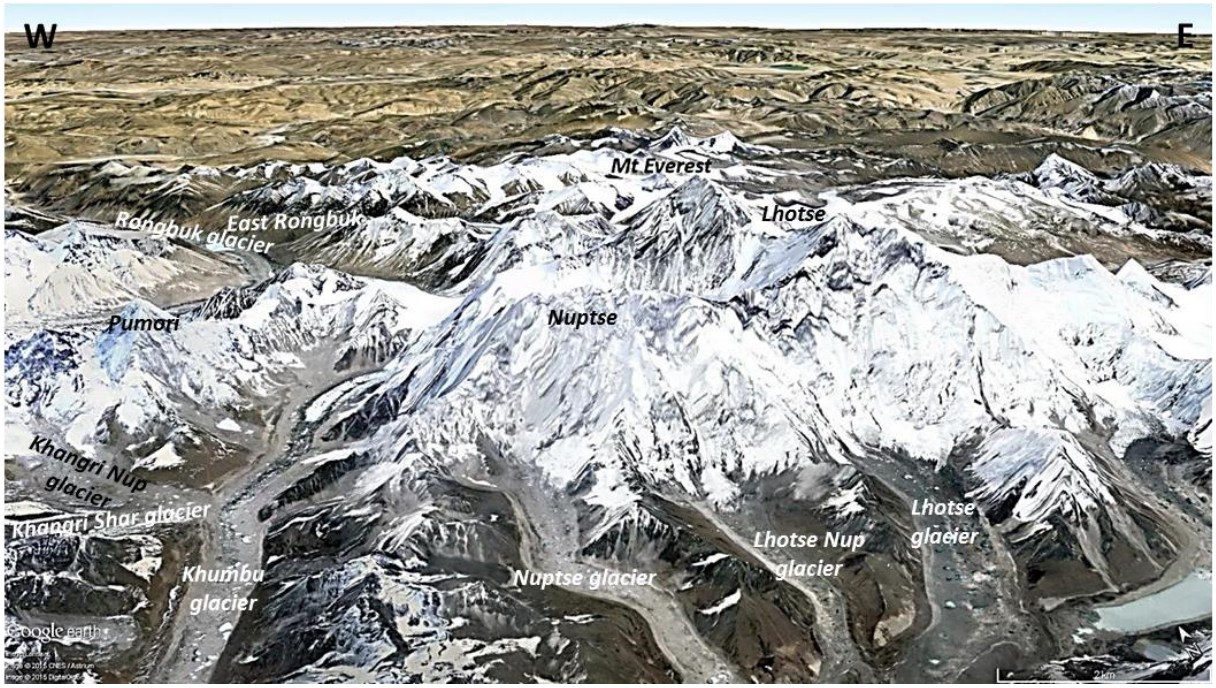


Figure 3.23: Oblique Google Map View of the Everest area from the south. Note the many U-shaped glacial valleys which are found in the Everest region. Glaciers are a powerful erosive force in the concentrated denudation of the high Himalayas (Egholm et al. 2009). In the Everest massif area, 8 major glaciers can be seen in this photograph. In the foreground from the left, the Khangri Nup, the Khangri Shar, the Khumbu, the Nuptse, the Lhotse Nup and the Lhotse glaciers can be seen. North of Everest from the left, the Rongbuk and the East Rongbuk glaciers can be seen. The east Rongbuk glacier is directly behind Everest and cannot be seen here.

3.7 Fossils of Everest Series/ age of sediments/ burial and exhumation/ early history of exploration/ Yellow Band

Noel Odell was the first geologist to examine, and describe, the rocks of the Yellow Band. He was part of the George Leigh Mallory expedition of 1924 and was able to make geological observations at altitudes never before reached by humankind. His notes and samples were however lost on a ship sailing from India. Nonetheless, he still managed to publish numerous observations (Odell, 1925, 1943, 1948, 1965).

The fossils of the Everest Series were first described by Gansser, 1964, from samples collected by the American expedition of 1963. They were received by Gansser courtesy of G.O. Dhyrenfurth (Gansser, 1964). Both samples contained crinoidal fragments with shell perforations (Figure 3.24A, B) whilst one showed stem segmentation (Figure 3.24B). Gansser mentions that, at the time, the age of the Everest limestones was thought to be Carboniferous to lower Permian. Fossils of the Everest Series rocks above the QD are now known to be Ordovician (500 Ma to 440 Ma). However, Gansser also found fossils in the Tibetan limestones, which he also dated as Permian and younger, which contained brachiopods, crinoids and ammonites (Figure 3.24C). There was also evidence of calcareous algae in the rocks he collected from Tibet. Although it seems that only crinoid particles were recovered from the Everest Series rocks on Everest itself, the other fossil evidence from Tibet and higher up in the Everest Series may therefore also be present in the rocks on Everest. There is very little Ordovician limestone present on Everest. It occurs near the top of the summit pyramid only. Below this, deformation related to movement on the QD, as well as greenschist metamorphism has obliterated any fossils that may have been present.

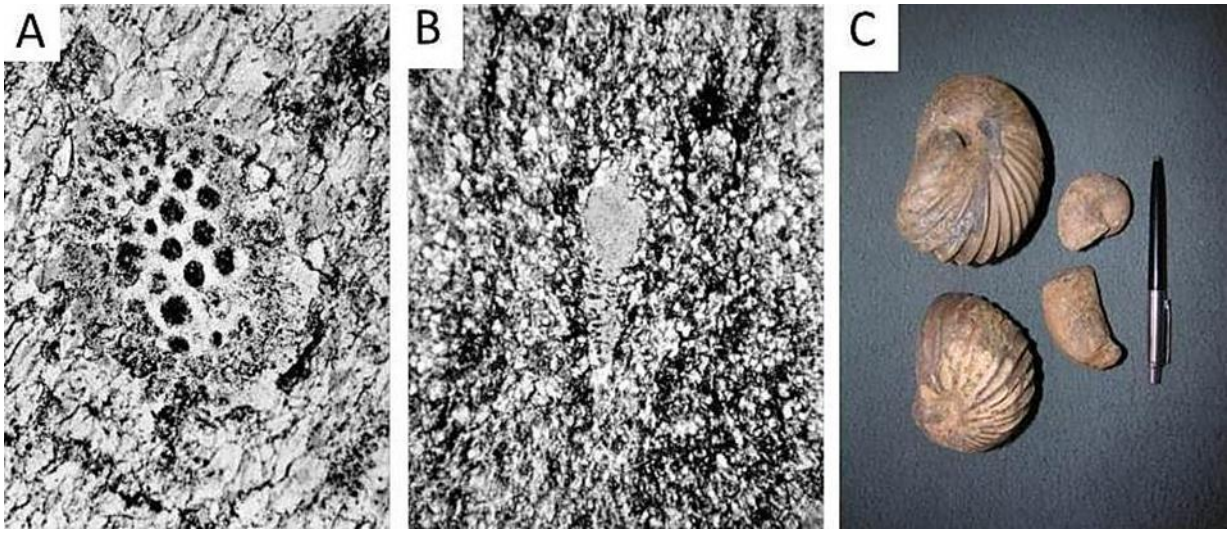


Figure 3.24: Fossils of the Everest Series: (A) - Crinoid plate with well-preserved perforations from the summit of Everest (enlarged 17x; Gansser, 1964). (B) - Stem fragment of crinoid in fine-grained limestone from the summit of Everest (enlarged 40x; Gansser, 1964). (C) - Ammonites (left) and a bi-valve mollusc (right) which are on display in Kathmandu at the offices of the Department of Mines and Geology of Nepal).

The Everest Series rocks above the QD are generally less altered than those below the QD, which were affected by movement along this detachment. Additionally, whilst in the leucogranite layer below, temperatures were around 700 °C (Searle, 2003) these dropped to 660 °C immediately beneath the LD, dropping further to 600 °C above the LD and further to 500-550 °C in the North Col formation (Carosi et al. 1999). This formation extends from the North Col (7000 m) to the top of the Yellow Band at 8600 m elevation. Jessup et al. (2008) state that the Everest Series schists record slightly higher metamorphic grades than Carosi et al. (1999) estimated, with temperatures of between 600 °C and 650 °C. Accepting the higher temperatures, pressure estimates, however, vary far more, ranging from 6.2 ± 0.7 kbar to 2.9 ± 0.6 kbar from below the LD to the QD (samples of glacial moraine examined by Jessup et al. 2008). This corresponds to burial depths of between 10 km and 20 km for these rocks. Burial and exhumation from these depths is likely to have deformed the original shapes of these fossils.

Nevertheless, there is significant evidence of fossils in the Everest rocks above the LD (Figure 3.25). Even below the LD, there are greenschist rocks which may be fossiliferous.

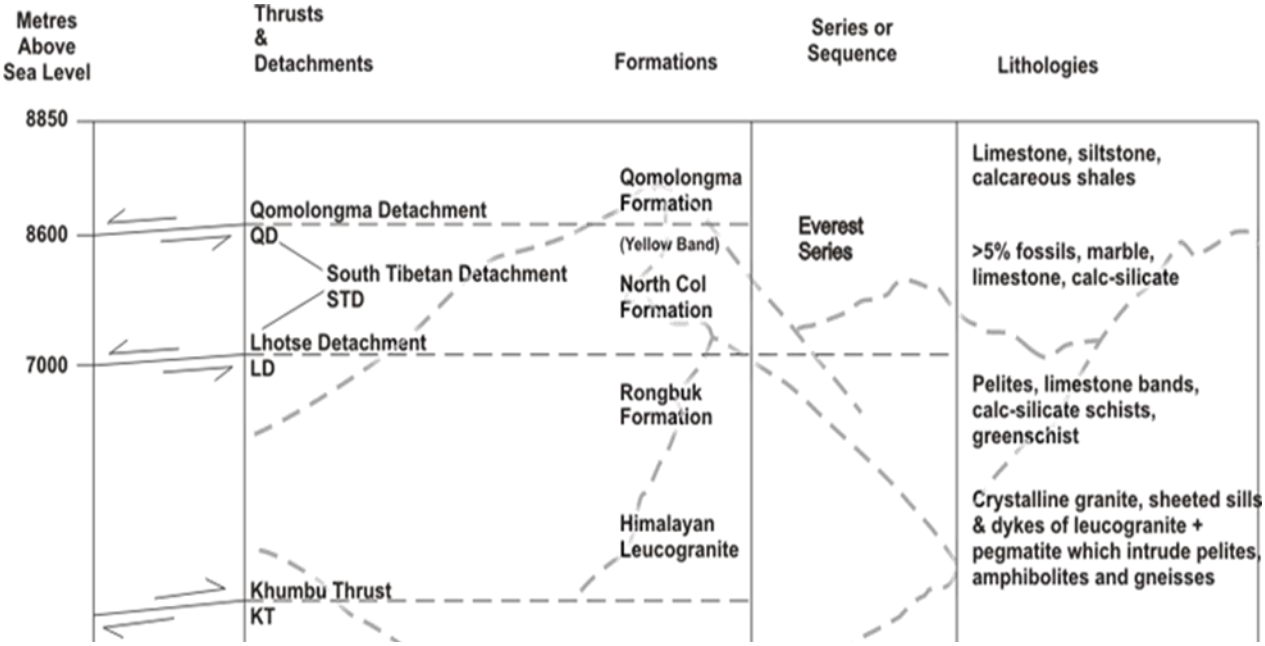


Figure 3.25: Stratigraphic column for Mt Everest and the Everest Series, showing the units where fossils are found.

Samples collected for the author by expedition Sherpas, from the Everest summit above the QD, the Hillary step and the South Summit below the QD, show evidence of pre-existing fossils. Stylolites and traces of carbon aligned along, and between, recrystallised grains of calcite are also recorded in all three samples (Figures 3.27, 3.28 and 3.29).

The samples were collected from between the South Summit to the summit of Everest along the route shown in Figure 3.26.

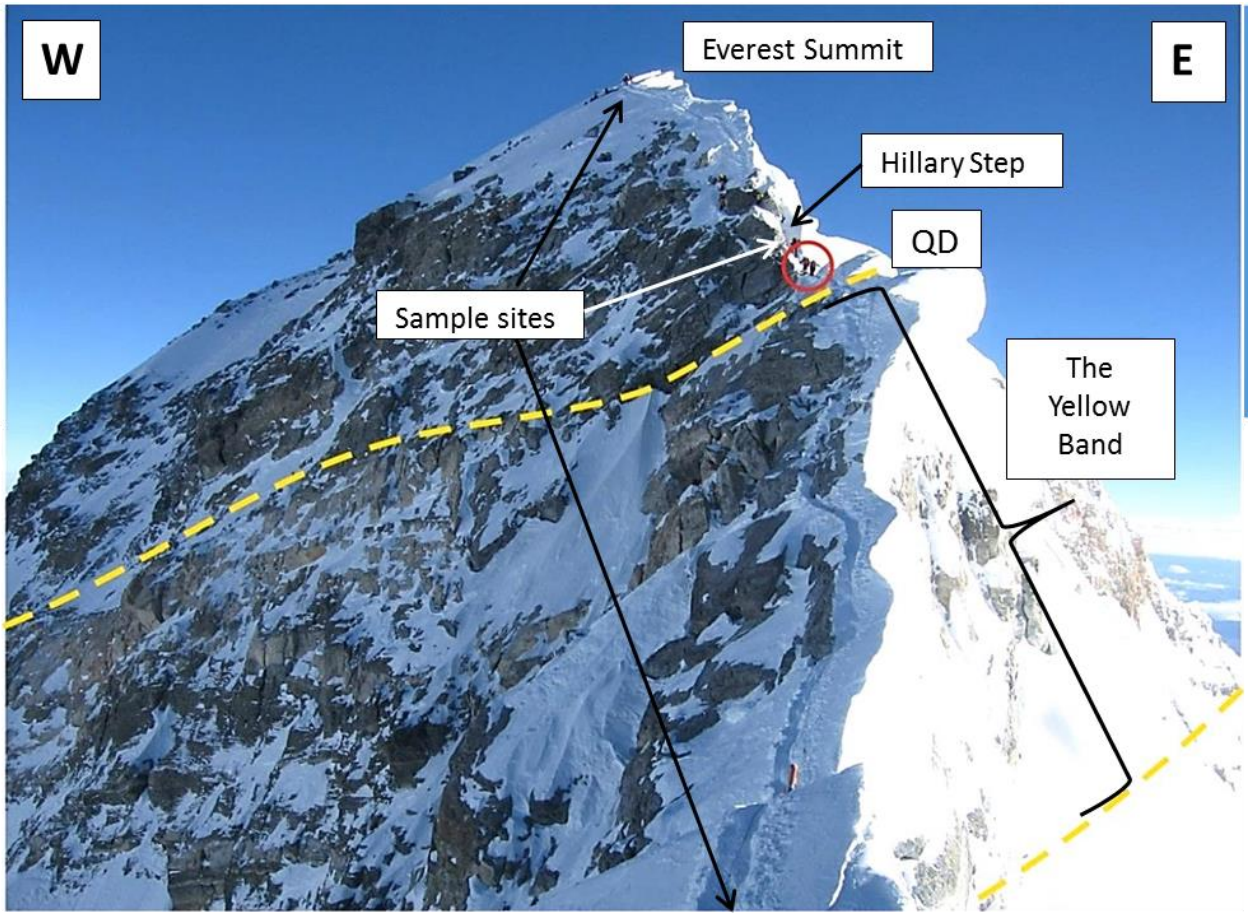


Figure 3.26: The Yellow Band as seen from the South Summit looking towards the Hillary Step, where two climbers are circled in red (Photograph: Sean Disney, 2006). Photograph taken from GPS co-ordinates 27°59'12.31"N, 86°55'26.76"E looking north-west towards the Everest summit. The outcrop near the summit shows the location of the summit samples taken shown in Figure 3.26.

The sample collected from the south summit (Figure 3.27) is a marble and is composed almost entirely of sparry calcite, with a number of large calcite single crystals showing twinning. Minor amounts of quartz and black carbonaceous material are found. Fossils can make up 5% by volume of the Yellow Band. Although the deformation and recrystallization in this sample may have destroyed fossil evidence, the wavy black carbonaceous material visible at the bottom of both photos could have originated from fossiliferous material. The rock is generally medium- to fine-grained (<0.3 mm) although some coarser calcite crystals are found. Numerous shears cut through

the sample and give the rock a strong fabric. Calcite grains form elongate lenses between the shear planes, and meandering veins of black carbonaceous (organic) material (stylolites) could represent remnants of fossils or fluid ingress related to shears or fractures.

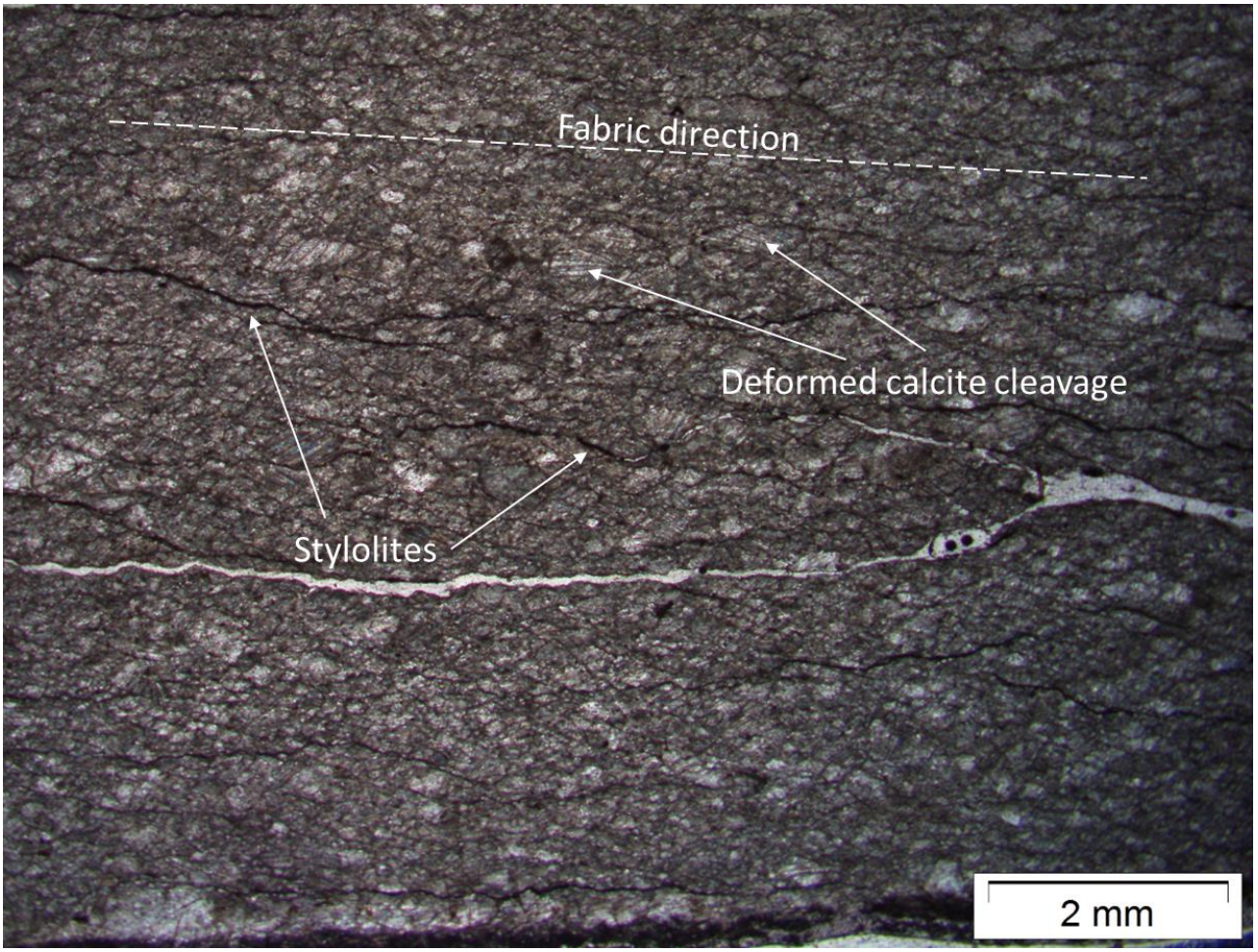


Figure 3.27: Photomicrograph (PPL) of a rock sample from South Summit, within the Yellow Band. The rock is a marble and is composed almost entirely of sparry calcite with a large number of crystals showing twinning. Black carbonaceous material is present as stylolites parallel to the fabric direction. These wavy, black carbonaceous layers may have originated from fossiliferous material on stylolite dissolution planes. The rock is medium to fine grained (<0.3 mm grains) with some coarser calcite crystals. Numerous shears cut through the sample. Calcite grains tend to form elongate lenses between the shear planes, and some calcite shows deformed cleavage bands. Sample collected at GPS co-ordinates 27°59'5.25"N, 86°55'31.17"E.

The sample collected from the Hillary Step (Figure 3.28) is composed of extremely fine-grained calcite with small carbonaceous grains and minor muscovite and epidote. The fine-grained, highly deformed nature of this sample suggests it comes from a fault zone (possibly a minor fault associated with the QD). As it is Ordovician limestone it should contain fossils, however these have also been deformed and the carbonaceous specs in the sample are all that remain of them. Sherpas have mentioned to the author that the South Col area (just above the LD) has many fossils contained in the slaty rocks. However, the author did not manage to locate such fossils.

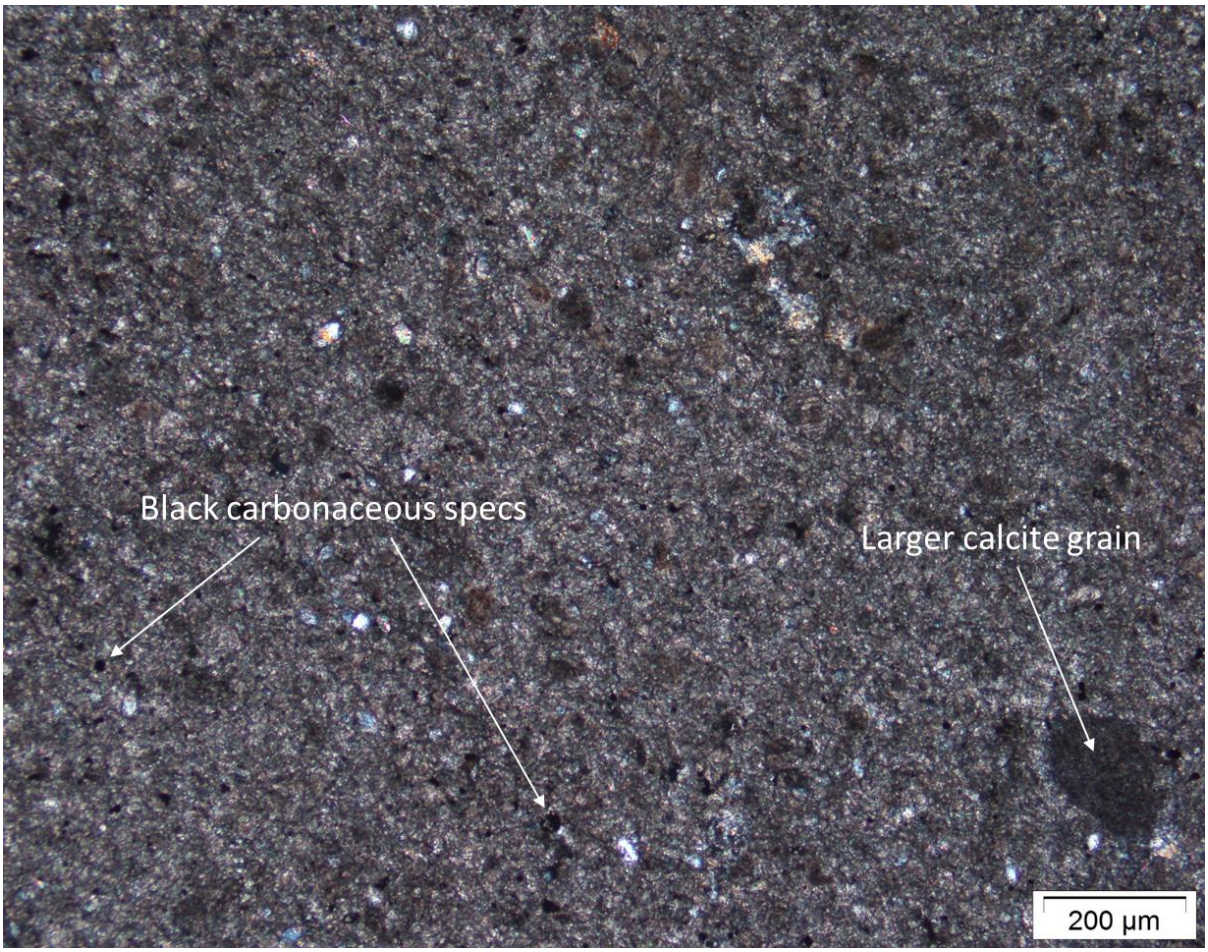


Figure 3.28: Photomicrograph (XPL) of rock sample RH17 from the Hillary Step (Figure 3.26). The rock is composed mostly of calcite with minor muscovite and, rarely, epidote. The sample is fine-grained although there are some coarser calcite grains present. Small carbon-rich (graphite) grains are visible. The fine-grained nature of this sample suggests it has experienced intense deformation. Sample collected at GPS co-ordinates 27°59'12.31"N, 86°55'26.76"E.

The sample taken from an outcrop 5 metres from the summit of Everest (this was possible because 2006 was an exceptionally warm and dry year) is composed almost entirely of calcite grains (Figure 3.29), with larger calcite grains forming a lens surrounded by extremely fine-grained calcite (an ultramylonite). Small amounts of mica are also found in addition to a number of opaque (black) grains. This opaque mineral, which forms cubic, hexagonal or polyhedral shapes, is the mineral pyrite. Some darker bands of organic-rich layers are also found. The extremely fine-grained nature of much of the sample is as a result of shearing and associated grain size reduction. This shearing has resulted in breccia zones. Further evidence for deformation is found, with folded carbonate layers and bent cleavage planes in some calcite crystals. The deformation appears to be more intense than that of the sample from the Hillary Step, implying that the very summit of Everest may be in a localised shear zone.

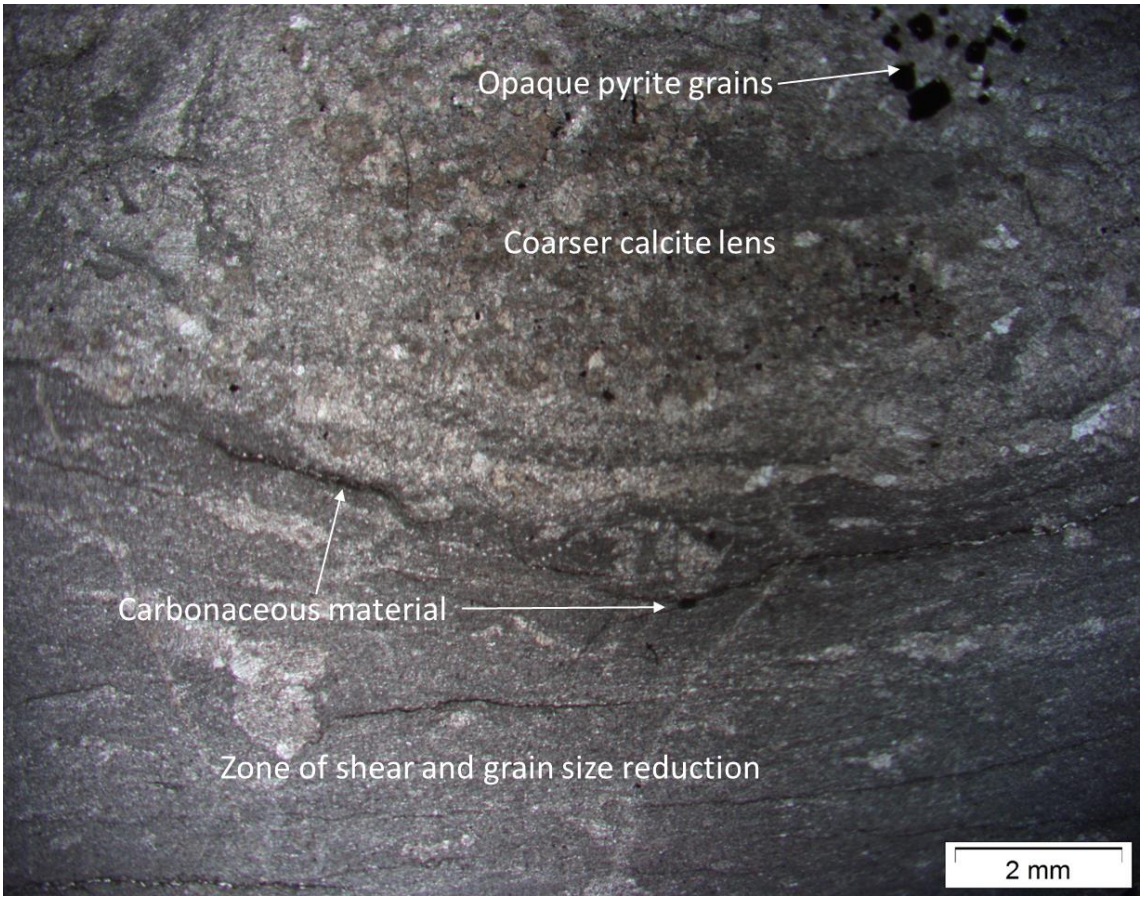


Figure 3.29: Photomicrograph of rock sample near the summit of Mount Everest. It is composed almost entirely of calcite grains. Small amounts of mica are also found, in addition to a number of opaque grains of pyrite and darker bands of organic-rich (carbonaceous) layers. The majority of the sample is fine grained due to shearing which has caused grain size reduction. This shearing has resulted in breccia zones with further evidence for deformation found in folded carbonate layers and bent cleavage planes in some of the calcite crystals. Sample collected at GPS co-ordinates 27°59'16.37"N, 86°55'30.23"E.

3.8 Top of Everest - lateral continuity of the Himalayan tectonic zones and the far-reaching effects of continental collision

The lateral continuity of the Himalayan and Tibetan tectonic belts, the trans-Himalayan batholith and the Indus Suture Zone, with an east-west strike length of around 3000 km extending into

Tibet, China, Burma, Bhutan, Pakistan, India and Afghanistan, are worthy of the status “geological wonder of the world” (Figures 1.4, 3.30 and 3.31). To illustrate this vast extent of the terranes, Debon and Le Fort, (1986), took samples from 492 localities over an area of 180,000 km² and analysed them petrologically, chemically, isotopically and mineralogically. The Transhimalayan belts were found to be continuous over the whole lateral extent with the exception of the Cenozoic granitoid belts which faded out near Nanga Parbat near Pakistan in the west.



Figure 3.30: Google earth image of the Tibetan Plateau showing its lateral extent of around 3000 km east-west and its north-south expanse of over 1500 km. The continental collision has resulted in a convex–to–south arc of the world’s loftiest orogenic system (Dhital, 2015) and has affected 7 countries.

The stratigraphic continuity along the Himalayan arc is also immense in its extent. The Siwaliks, the Lesser Himalayan Sequence, the higher Himalayan crystallines, the Tethys Himalaya and the Trans-Himalayan Batholiths can be traced along the whole 3000 km arc (Figures 3.30 and 3.31). Furthermore, north of the Himalayan Batholiths, the Tibetan Terranes from the Lhasa to the Kunlun terranes, as far as the North China Terrane (Figure 2.1) all show the enormous lateral extent, and the far-reaching effects, of the India-Asia collision that began roughly at 40 Ma.

Modelling of the collision of India and Asia by Royden et al. (1997), has illustrated far reaching effects through crustal flow. There is clear evidence for east-west extension within the Tibetan plateau with the model indicating the lower crust is so weak that it flows independently from upper crustal deformation and oozes out from under the middle of the Tibetan plateau towards its edges (Figure 1.2). The model suggests that the lateral extent of the lower crustal flow, implying molten material below the Himalayas, is of the order of 3000 km east-west.

Seismic data shows unusually weak zones in the crust below the Lhasa Terrane, the Qiangtang and the Songpan-Ganze Terranes (Klemperer, 2006). Cook and Royden (2008) showed widespread crustal flow beneath Tibet flowing from the centre of Tibet outwards in a westerly, a south-easterly and a north-easterly direction. The combination of a weak mid-crust and an active collision zone results in an orogenic belt of similar rock units extending for thousands of kilometres laterally.

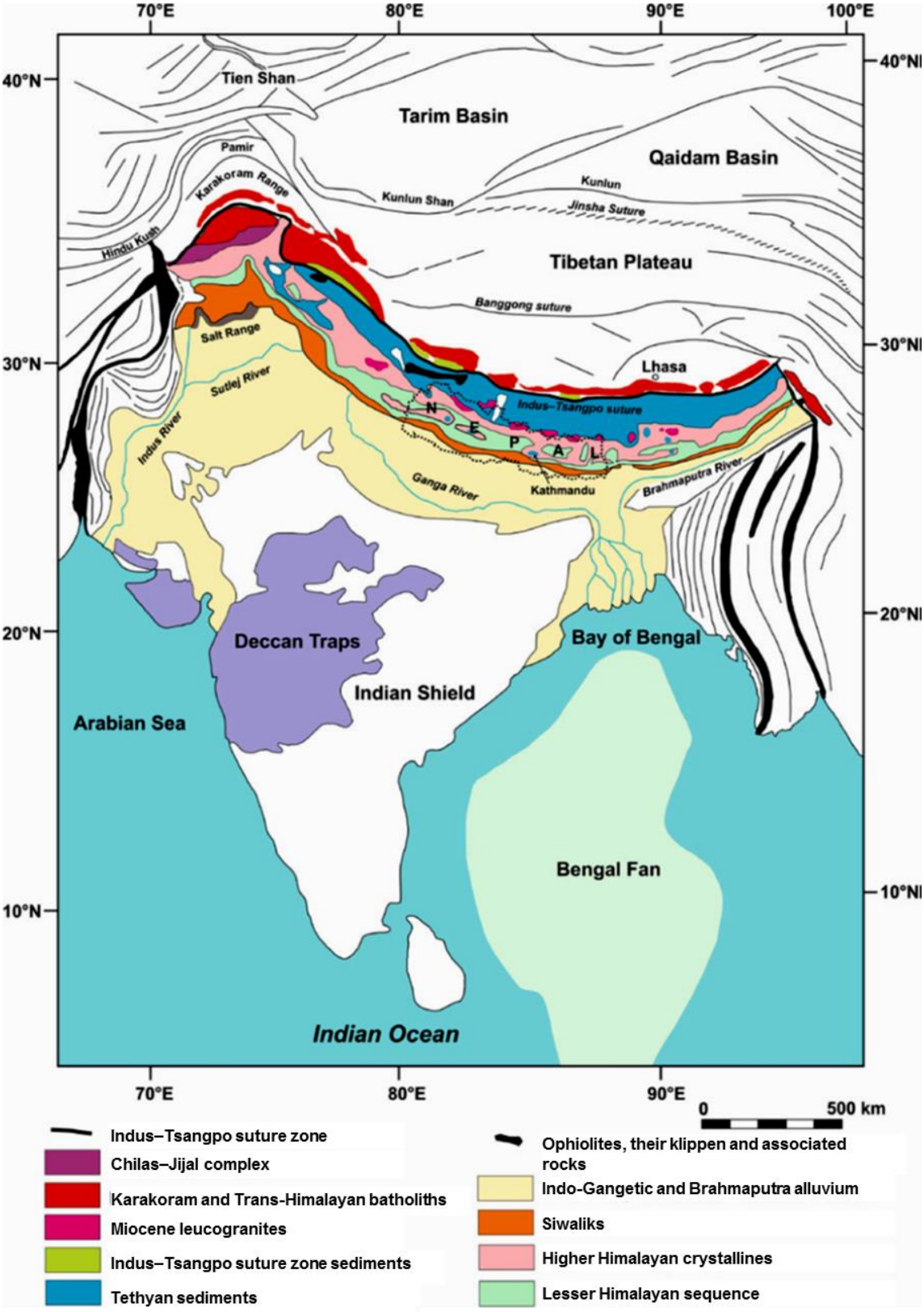


Figure 3.31: Simplified geological map of the Himalayas (from Dhital, 2015, modified from Stöcklin, 1980, Gansser, 1981, and Sorkhabi and Stump, 1993).

CHAPTER 4: DISCUSSION AND CONCLUSIONS

There has been a growing interest in channel flow theory throughout the geological community (Grasemann et al. 2006). Because the theory explains many of the features we see in the High and Crystalline Himalaya (in the area covered by this study), and may also explain features in the Lesser Himalaya, the Tibetan terranes and possibly the Siwaliks, its validity appears to be established within the geological community. Already, geologists are making the connection between channel flow and extrusional features in areas like Greece (Xypolias and Kokkalas, 2006) and Canada (Brown and Gibson, 2006). Other continent-continent collision zones, like the Usagaran/Pan African gneiss and migmatite belt which cross-cuts the African continent, may yet reveal channel flow mechanisms for their origin.

Channel flow appears to explain most of what was observed in the area between Lukla and Mount Everest. The observations made in Section 3 will now be tied back to the theory in Section 1 with this in mind.

4.1 Higher Himalayan Granite Gneiss, and the Namche migmatites

The granite gneiss of the Greater Himalayan Sequence (GHS), observed in the early part of the traverse from Lukla towards Everest, represents a granitic protolith that was subducted below the Asian continent during collision, and subsequently exhumed through crustal flow from below Tibet to its present position (Klemperer, 2006). The High Himalayan crystalline granite gneiss also shows numerous south-verging recumbent folds, often bound by abundant mylonite (implying faults) above and below the folds. The vergence of these folds (to the south) indicates that they are linked to channel flow type extrusion and exhumation with associated southwards thrusting. Much of the granite gneiss in the Lukla to Periche area, and even to Laboche, may have been brought to surface from below Tibet through exhumation resulting from high erosion rates in the Himalayas or through a channel flow mechanism. Grasemann et al. (2006) shows an unpublished sketch by D. Nelson, c. (1995); cf. fig. 6 of Wu et al. (1998) which depicts the “Higher Himalayan crystallines” (namely, the gneissic terrane of the GHS (Figure 3.31) and leucogranites, between the MCT and the STD, as being an integrated extruding slab.

The Namche migmatites are the product of deep burial and melting of muscovite and biotite-bearing rocks, at temperatures of up to 837 ± 59 °C and pressures of 6.7±1.0 kbar (Goscombe and Hand 2000 Searle et al. 2003), and segregation into leucosomes parallel to the S_1 fabric. Subsequent upwards migration and accumulation of this molten material just below the STD led to the formation of leucogranite plutons and their surrounding stockwork of sills and dykes. These plutons and their stockwork of sheeted sills were further deformed by simple shear along the edges of an extruding channel, resulting in the widespread generation of mylonite in these granites.

4.2 Sillimanite-biotite schist, the P-T-t-D path and the age relationship of the GHS to the Everest Series

The occurrence of sillimanite-biotite schist is widespread in an east-west direction along the Himalayan arc at the top of the GHS (or the Higher Himalayan crystallines, Figure 3.31) and is present along the route from Namche Bazaar to Everest Base Camp. Burial of the incoming Indian continent to depths of >45 km, decompression to granulite facies grade, and further decompression to amphibolite grade, led to the sequence of mineral growth as shown in Figure 4.1, below.

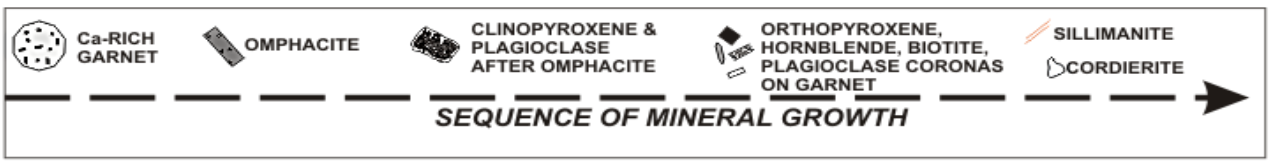


Figure 4.1: Sequence of growth of minerals of a subducted granulitic continental crust pertinent to the GHS.

The remnants of inclusions of granulitised eclogites are found locally in the Greater Himalayan Sequence, as lenses in the sillimanite-biotite schist from the GHS (Figure 2.8) show that burial to extreme depths occurred (Lombardo and Rolfo, 2000; Jessup et al. 2008). The rocks then followed an anti-clockwise P-T-D-t path (Figure 2.9) resulting in progressive decompression and eventual extrusion to surface. Temperatures in the GHS during migmatisation are estimated to be above

700 C, and although there is a zoning of temperatures across the GHS (Goscombe et al. 2006), temperatures remained roughly 837 ± 59 °C across about 50 km horizontal distance from the top of the MCT zone to the STD, with pressures varying between 4 and 8 kbar (Searle et al., 2003). Temperatures of up to have been recorded in the GHS (Goscombe and Hand 2000). In contrast, Everest Series rocks just above the STD experienced P-T conditions of between 600 °C and 650 °C with pressure estimates for these rocks ranging from 2.9 ± 0.6 kbar to 6.2 ± 0.7 kbar. These rocks record lower pressures than the GHS rocks which results in cordierite consuming staurolite, and the growth of andalusite over the S_2 fabric (Figure 2.6E). This cordierite and andalusite growth over the S_2 fabric shows that the rocks were being rapidly exhumed and this led to the final phase in their P-T-D-t history.

The Everest Series rocks are Ordovician, whilst the underlying leucogranites are Miocene (Dhital, 2015). These are separated by the STD, with the Everest series rocks having a top-to-north sense of movement, whilst the leucogranites and the GHS gneiss have a top-to-south movement. The GHS rocks are of Cambrian/Ordovician/Silurian age (Dhital, 2015). Hence the STD separates and juxtaposes high-grade metamorphic rocks with low-grade rocks that have similar protolith ages, but have experienced vastly different burial and exhumation histories.

4.3 Leucogranite, tourmaline-muscovite granite of Ama Dablam and the Khumbu thrust

The widespread and spectacular leucogranites of the Base Camp area are the product of the melting of the GHS sillimanite-biotite gneiss found near the Khumbu Thrust (KT) (Figures 2.6, 2.8 and 2.9). Numerous segregated leucosomes in migmatite, seen along the route from near Namche Bazaar (Figure 3.3) to Everest Base Camp, imply that there were substantial volumes of melt being generated in, and moving upwards through, the sillimanite-biotite schist. This upward intrusion was terminated by the Lhotse Detachment (the lower detachment of the STD bouquet of normal faults) as this was the start of the zone of the cold Everest Series rocks which led to the freezing of the leucogranite both in plutons as well as in the stockwork of sheeted sills and dykes surrounding the plutons.

The Khumbu Thrust (KT) itself is difficult to pin down as it is not a single narrow thrust, but a broad zone of deformation in the Base Camp area. The sillimanite-biotite schist around the fault is extremely slippery to the touch due to biotite flakes and is quite crumbly. This whole 1600 m thick zone of this particular schist may have taken up thrust movement across its vertical width, and may have thus facilitated exhumation of the overlying extruding leucogranite channel.

4.4 The View from Kala Pattar towards the Everest Series and South Tibetan Detachment

The geological processes described in Section 1, involving the extrusion/exhumation of a mid-crustal channel, reach their uppermost limit in features seen around Base Camp. The leucogranite massifs of Lingtren/Pumori, and the Nuptse granite, together with their stockwork of sheeted dykes and sills, are the result of a magma intrusion originating from accumulated leucosomes which were generated in the underlying migmatites. The numerous occurrences of mylonite and intensely sheared rocks are associated with the thrusts and detachments prevalent in the area. Sheared leucogranite occurrences indicate that there has been further movement after cooling and recrystallization of the leucogranite melt with continuing D_2 deformation even today (the recent earthquakes in the area on 25th April and 12th May 2015 may have had up to 30 m of relative movement in one event).

South-verging folds are clearly visibly on the face of Lhotse in the Western Cwm (Figure 3.20). Although their proximity to the LD suggest that they may be associated with the movement along the LD, their vergence is consistent with top-to-the-north movement the LD. A south–verging recumbent in leucogranites on the south face of Nuptse (Fig. 4.2) has been linked to thrusting on the KT (Searle 1999a). It may be that folds in the Rongbuk Formation are also related to movement on the KT, or these could be an earlier generation of folds related to crustal thickening north of the STD, but south of the Indus suture zone (Searle 1999a).

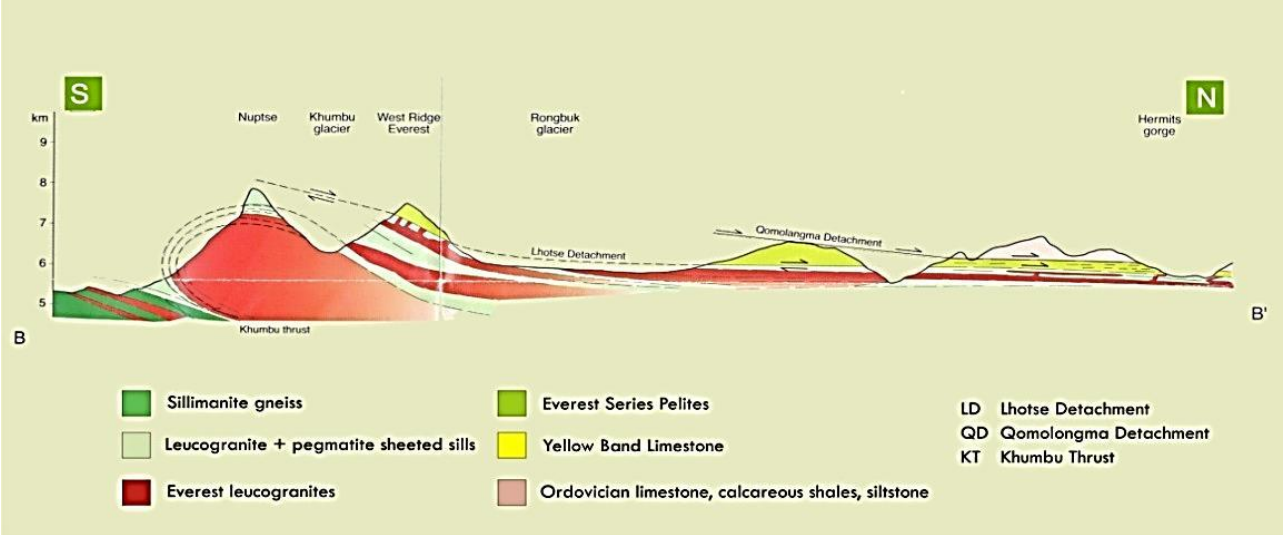


Figure 4.2: Cross section B-B' (Map 4) from Nuptse Northwards to Hermit's Gorge. According to Searle (2003), a large leucogranite outcrop is found on the south face of Nuptse. Folded yellow calc-silicate bands on the Lhotse face are separated from this leucogranite by the Lhotse Detachment. Searle shows the leucogranite as a recumbent fold. However, it may also be possible that there has been exhumation of leucogranite and extrusion southwards in a ductile channel between the Khumbu Thrust and the Lhotse Detachment.

4.5 Glacial valleys/erosion/ exhumation

The extremely rapid rate of erosion in the southern front of the Himalaya and the High Himalayas, through mainly glacial action as well as earthquakes, wind, avalanches and water action, leads to the formation of glacial U-shaped valleys and rapid denudation of the extruding crustal block (Figures 2.12 and 2.14) causes an increase in the rate of extrusion of the channel. Co-ordinated extrusion and erosion result in the geology that we see in the Himalaya today.

Evidence of active erosion is ubiquitous. An erosional event occurred every 6 seconds at Base Camp in April and May of 2006 (personal observation). The moraine-laden Khumbu glacier (Figure 3.16) transports 1 m to 5 m thick accumulations of moraine in places. Although glaciation

dominates the erosional processes at present, one could speculate that rivers could replace glaciers with continued global warming.

Between 1900 and 2014, numerous earthquakes have occurred in the Himalaya-Tibet region (Figure 4.3). The latest set of earthquakes in Nepal contributes to erosion, and, although a massive once-off effect results from such events, their frequency is separated by many years, in some instances, and their effect on erosion is therefore considerably less than glacial erosion.

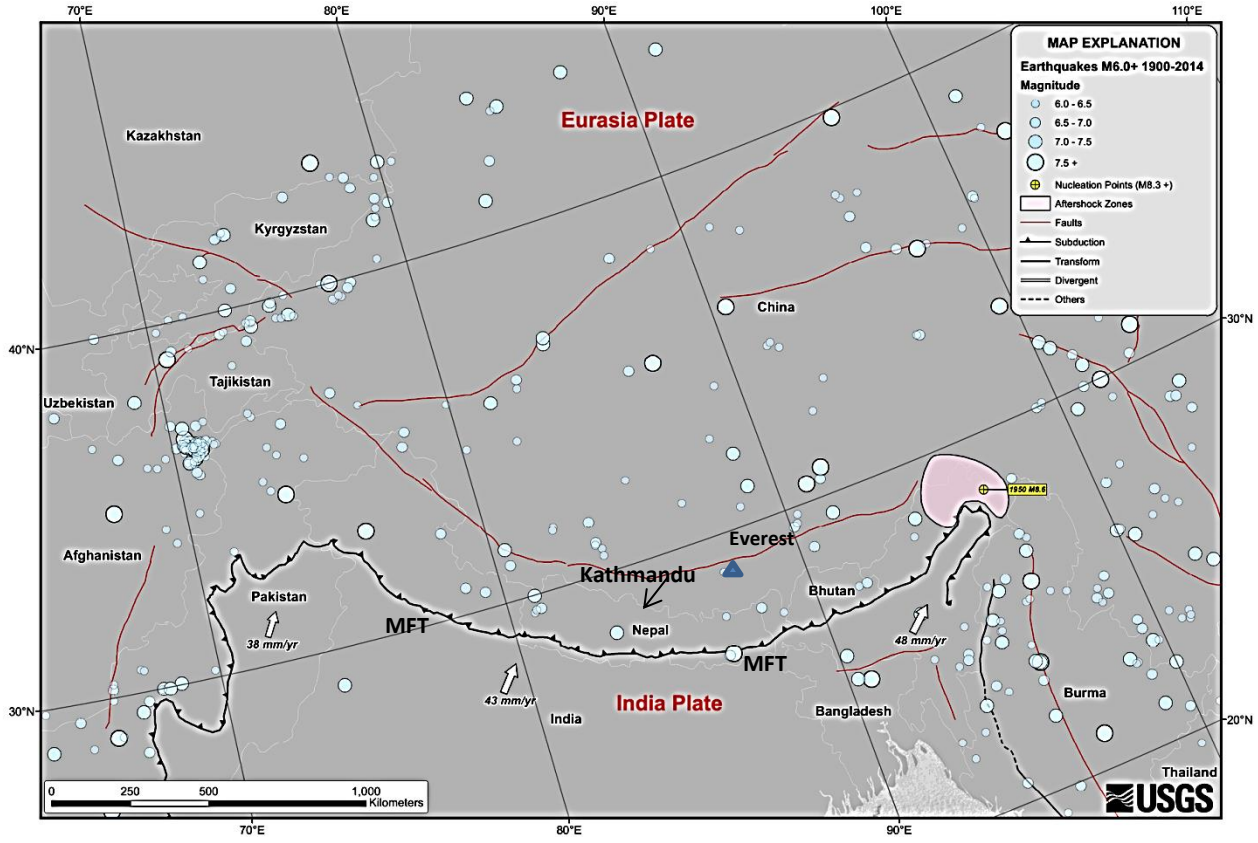


Figure 4.3: USGS map of earthquake epicentres since 1900.

(From: http://earthquake.usgs.gov/earthquakes/tectonic/images/himalaya_tsum.pdf)

Rapid exhumation is the result of this very rapid erosion, which in turn is an enabling factor for the channel flow of mid-crustal slabs. Erosion is thus an important component in the Himalayan orogenic belt.

4.6 Fossils of Everest Series/ age of sediments/ burial and exhumation/ early history of exploration/ Yellow Band

Even though the Everest Series and the Greater Himalayan Sequence are of similar age, they have experienced different histories of burial and exhumation. The early history of exploration in the Himalayas concentrated on fossils (Dhital, 2015). Noel Odell, in his expeditions to Everest in 1924 and 1938 when he reached the Yellow Band, came across fossils in this layer since it had experienced only low-grade metamorphism (Odell, 1965). Below the Yellow Band, detachments, shearing and progressively higher metamorphic grades would have destroyed some evidence.

The Ordovician fossils of the Everest Series have been buried to depths of up to 15 km and have therefore been altered and sometimes assimilated into the country limestone with only outlines or patterns remaining as evidence. Odell (1965), indicated that there were fossils high on the north side of Everest and in the Yellow Band of the North Col Formation. Gansser (1964), presented photomicrographs of fossils (Figure 3.24). The South Col is also reputed to be fossil rich; however, the author has not been able to locate reliable photographs or specimens of such fossils in the area studied.

4.7 Top of Everest / lateral continuity / tectonic zones / far-reaching effects (Tibet / China / Burma / Pakistan, etc.)

The summit of Mount Everest is a vantage point for observation of the east-west lateral continuity of the Himalaya mountain arc and the Tibetan geological terranes (Figures 1.4 and 2.1). Tectonic zones, too, have lateral continuity over thousands of kilometres and appear to have been

compressed in a north-south direction by the collision of India into Asia/Tibet. Far reaching effects of the collision, such as the ear-like structures on the outer edges of the Himalayan arc (Figures 1.2, 1.4, 3.30) , the mountainous terranes of the Karakoram and Pakistan/ Afghanistan, and on the eastern side, the mountains of Burma and China shown in Figure 4.4, are the result of this continental collision. The impact resulted in a 65 km thick crust beneath Tibet which, due to its thickness, has weakened (become plastic) and has begun to flow outwards towards the east. This is the zone of least resistance as the Pacific subduction zones offer less resistance than the Pakistani Asian continental crust, as suggested by the crustal flow model (Royden et al. 1997).

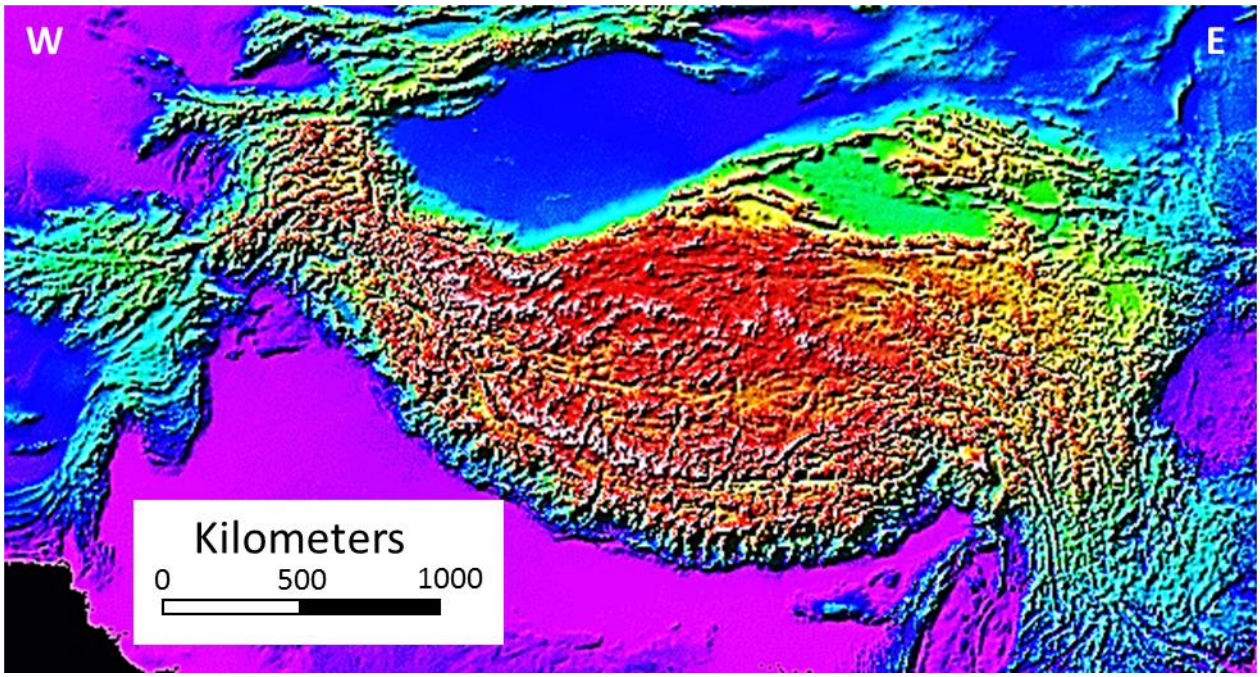


Figure 4.4: The Tibetan plateau is the largest plateau on Earth with an average elevation of 4880 m and a crustal thickness of 65 km. High elevations are shown in white (5000 m to 8850 m) red (4000 m to 5000 m) and low elevations in blue (1000 m to 2000 m) and purple (<1000 m). The Tibetan Plateau is bounded by the deserts of the Tarim and the Qaidam Basin to the north, and the Himalayan, Karakoram and Pamir mountain chains to the south and west (source: http://oak.ucc.nau.edu/wittke/tibet/plateau.html).

The Himalayan Mountains offer a unique insight into the processes involved in a continent-on-continent collision. Models such as the Channel Flow Theory, although fairly modern, have been recently developed by researchers to explain what we see in the field today (Beaumont et al. 2006; Brown and Gibson, 2006; Godin et al. 2006; Grujic, 2006; Hodges 2006; Jessup et al. 2006; Law et al. 2006; Scaillet and Searle, 2006; Searle et al. 2006). I believe this theory to be the crux of the geology of the GHS. This theory is being more widely accepted and is being extended to explain geological features in other parts of the world. However, the many other observations made in the area studied, such as the metamorphic minerals of the sillimanite-biotite schists, the deformed leucogranite, the thrusts with associated mylonite, the glaciers and the glacial valleys, the frequency of an erosional event, the QD and the LD of the STD, the MCT, and the KT all play a part in explaining the geology in this amazing part of the world.

References

Aitchison, J.C., Ali, J.R. and Davis, A.M. (2007). When and where did India and Asia collide? *Journal of Geophysical Research*, **112**, BO5423. http://dx.doi.org/10.1029/2009JB004706

Allegre, C.J., Courtillot, V., Tapponnier, P., Hirn, A., Mattauer, M., Coulon, C., Jaeger, J.J., Achache, J, Scharer, U., Marcoux, J., Burg, J.P., Girardeau, J., Armijo, R., Gariepy, C., Gopel, C., Tindong, L., Xuchang, X., Chenfa, C., Guanqin, L., Baoyu, L., Jiwen, T., Naiwen, W., Guoming, C., Tonglin, H., Xibin, W., Wanming, D., Huabin, S., Yougong, C., Ji, Z., Hongrong, Q., Peisheng, B, Songchan, W., Bixiang, W., Yaoxiu, Z., and Xu, R. (1984). Structure and evolution of the Himalaya–Tibet orogenic belt. *Nature*, **307**, 17-22.

Arkell, W.J. (1956). *Jurassic Geology of the World*. Oliver and Boyd, Edinburgh and London, 806 pp.

Alsdorf, D., Brown, L., Nelson, K.D.A., Makovsky, V., Klemperer, S. and Zhao, W. (1999). Crustal deformation of the Lhasa terrane from Project INDEPTH deep seismic reflection profiles. *Tectonics*, **17**, 501-519.

Beaumont, C., Jamieson, R.A., Nguyen, M.H. and Lee, B. (2001). Himalayan tectonics explained by extrusion of a low-viscosity crustal channel coupled to focused surface denudation. *Nature*, **414**, 738-742.

Beaumont, C., Jamieson, R.A., Nguyen, M.H. and Medvedev, S. (2004). Crustal channel flows: 1 Numerical models with applications to the tectonics of the Himalayan-Tibetan orogen. *Journal of Geophysical Research-Solid Earth*, **109**, B06406. DOI: 10.1029/2003JB002809

Beaumont, C., Jamieson, R.A. and Ellis, S. (2006). Crustal flow modes in large hot orogens. *In:* Law, R.D., Searle, M.P. and Godin, L. (Eds): Channel Flow, Ductile Extrusion and Exhumation in Continental Collision Zones. *Special Publications*, **268**, Geological Society, London, pp 91-145.

Bose, S. and Mandal, N. (2010). Interaction of Surface Erosion and Sequential Thrust Progression: Implication on Exhumation Processes. *Journal of the Geological Society of India*, **75**, 338-344.

Brown, R.L. and Gibson, H.D., (2006). An argument for channel flow in the southern Canadian cordillera and comparison with Himalayan tectonics. *Geological Society of London. Special Publication* **268**, 543-559.

Burchfiel, B.C. and Royden, L.H. (1985). North-south extension within the convergent Himalayan region. *Geology*, **13**, 679-682.

Burchfiel, B.C., Zhiliang, C., Hodges, K.V., Yuping, L., Royden, L., Changrong, D. and Jiene, X. (1992). The South Tibetan Detachment System, Himalayan Orogen: Extension contemporaneous with and parallel to shortening in a collision mountain belt. *Geological Society of America Special Papers*, **269**.

Burchfield, B.C., Chen, Z., Liu., Y., and Royden, L.H., (1995). Tectonics of the Longmen Shan and adjacent regions, Central China. *International Geology Review*, **37**, 661-735.

Burg, J. –P., and Podladchikov, Y. (2000). From buckling to asymmetric folding of the continental lithosphere: numerical modelling and application to the Himalayan syntaxes. In: Khan, M.A., Treloar, P.J., Searle, M.P., and Jan, M.Q., (eds) Tectonics of the Nanga Parbat Syntaxes and the Western Himalaya. *Geological Society, London, Special Publication* **170**, 219-236.

Burrard, S.G. and Hayden, H.H. (1907). A sketch of the geography and the geology of the Himalayan Mountains and Tibet. Pt.1, The High peaks of Asia. *Government of India Press, Calcutta*.

Burrard, S.G. and Heron, A.M. (1934). *Geography and geology on the Himalayan Mountains and Tibet*. Government of India, Manager of Publications, Delhi.

Butler, R.W.H., Wheeler, J., Treloar, P.J., and Jones, C. (2000). Geological structure of the southern part of the Nanga Parbat massif, Pakistan Himalayas, and its tectonic implications. In: Khan, M.A., Treloar, P.J., Searle, M.P., and Jan, M.Q., (eds) Tectonics of the Nanga Parbat Syntaxis and the Western Himalaya. *Geological Society, London, Special Publication* **170**, 123-136. S.G. and Heron, A.M. (1934). *Geography and geology on the Himalayan Mountains and Tibet*. Government of India, Manager of Publications, Delhi.

Carosi, R., Montomoli, C., Rubatto, D., Visona, D. (2006). Normal sense shear zones in the core of the Himalayan Crystallines (Bhutan Himalaya): evidence for extrusion? *Geological Society of London*. Special Publication **268**, 425-444.

Carosi, R., Lombardo, B., Musumeci, G., Pertusati, P.C., (1999). Geology of the Higher Himalayan Crystallines in Khumbu Himal (Eastern Nepal). *Journal of Asian Earth Sciences*, **17, 785-803.**

Clark, M.K. and Royden, L.H., (2000). Topographic ooze: Building the eastern margin of Tibet by lower crustal flow. *Geological Society of America*. **28**, no.8, 703-706.

Cook, K.L. and Royden, L.H. (2008). *Lower Crustal Flow and Strength Heterogeneities. Journal of Geophysical Research*. **94**, 2787-2838.

Copley, A., Avouac, J-P., Royer, J-Y. (2010). India-Asia collision and the Cenozoic slowdown of the Indian Plate: Implications for the forces driving plate motions. *Journal of Geophysical Research*. **115**, 1-14.

Cottle, J.M., Jessup, M.J., Newell, D.L., Horstwood, M.S.A., Noble, S.R., Parrish, R.R., Waters, D.J. and Searle, M.P. (2009*).* Geochronology of granulitised eclogite from the Ama Drime Massif: implications for the tectonic evolution of the South Tibetan Himalaya. *Tectonics*, **28**, TC1002, 25 pp.

Coward, M.P., Butler, R.W.H., Chambers, A.F. et al. (1988). Folding and imbrication of the Indian crust during Himalayan collision. *Philosophical transactions of the Royal Society*, **A326**, 89-116.

Coward, M.P. and Butler, (1985). Thrust tectonics and the deep structure of the Pakistan Himalaya. *Geology*, **13**, 417-420.

Crawford, A.R. (1974). The Indus Suture Line, the Himalaya, Tibet and Gondwana land. *Geol Mag*, 111 (5), 369-383.

Debon, F., Le Fort, P., Sheppard, S.M.F., Sonet, J., (1986). The Four Plutonic Belts of the Transhimalaya: a Chemical, Mineralogical, Isotopic, and Chronological Synthesis along a Tibet-Nepal Section*. Journal of Petrology*, **27**, Part 1, 219-250.

Department of Mines and Geology, Nepal. (2004). *Geological Map of Nepal*, S.M. Trading Centre. Maps of Nepal, New Baneswor, Kathmandu, Nepal. (Tel: 478-0304).

Dewey, J.F., Shackleton, R.M., Chengfa, C. and Yiyin, S. (1988). *The Tectonic Evolution of the Tibetan Plateau*, *Philosophical Transactions of the Royal Society of London*, **327**(1594), 379-413

Dézes, P. (1999). *Tectonic and metamorphic Evolution of the Central Himalayan Domain in Southeast Zanskar (Kashmir, India)*. PhD Thesis (unpublished), Institut de Mineralogie et Petrographie, Université de Lausanne.

Dhital, M.R. (2015). Geology of the Nepal Himalaya, Regional Perspective of the Classic Collided Orogen. *Regional Geology Reviews*, 499pp.

Doguzhaeva, L.A., Mapes R.H., Summesberger, H. and Mutvei, H. (2007). The Preservation of Body Tissues, Shell, and Mandibles in the Ceratitid Ammonoid Austrotrachyceras (Late Triassic), Austria. *In:* Landman, N.H., Davis, R.A. and Mapes, R.H. 2007. *Cephalopods Present and Past: New Insights and Fresh Perspectives*. Springer, Dordrecht. pp. 221–238.

England, P. and Molnar, P. (1990). Surface uplift, uplift of rocks, and exhumation of rocks. *Geology*, **18**, 1173-1177.

Ferrara, G., Lombardo, B., Tonarini, S. (1983). Rb/Sr geochronology of granites and gneisses from the Mount Everest region, Nepal Himalaya. *Geologisches Rundschau* **72,** 119–136

Gansser, A. (1964). The Geology of the Himalayas. *Wiley Interscience,* New York, 289pp.

Gansser, A. (1981). The geodynamic history of the Himalaya. In: Gupta, H.K,, Delany, F.M., (eds) Zagros Hindu Kush Himalaya. *American Geophysical Union, Geodynamics series*, **3**, 111–121

Geological Survey of India. (1879). A Manual of the Geology of India. pt. 1. Peninsular area, by H.B. Medlicott and W.T. Blanford (1879). pt. 2. Extra-peninsular area, by H.B. Medlicott and W. T. Blanford (n. d.). pt. 3. *Economic geology*, by V. Ball (1881). pt. 4. *Mineralogy* by F. R. Mallet (1887).

Godin, L., Grujic, D., Law, R.D. and Searle, M.P. (2006). Channel flow, ductile extrusion and exhumation in continental collision zones: an introduction. *Geological Society Special Publication 268. London*. , 1-23.

Godwin–Austen, H.H. (1864). Geological notes on part of the northwestern Himalayas. *Quarterly Journal Geological Society, London*. **20**, 383-387.

Goscombe, B., Gray, D. and Hand, M. (2006). Crustal architecture of the Himalayan metamorphic front in eastern Nepal. *Gondwana Research*, **10**, 232-255.

Grasemann, B., Edwards, M.A., and Wiesmayr, G., (2006). Kinematic dilatancy effects on orogenic extrusion. *Special Publications*, **268**, Geological Society, London, pp 183-199.

Grujic, D. (2006). Channel Flow and Continental collision tectonics: an overview. *In:* Law, R.D., Searle, M.P. and Godin, L. (Eds): Channel Flow, Ductile Extrusion and Exhumation in Continental Collision Zones. *Special Publications*, **268**, Geological Society, London, pp 25-37.

Grujic, D., Casey, M., Davidson, C., Hollister, L.S., Kündig, R., Pavlis, T., and Schmid, S. (1996). Ductile extrusion of the Higher Himalayan Crystalline in Bhutan: evidence from quartz microfabrics. *Tectonophysics*, **260**, 21-43.

Grujic, D., Hollister, L.S. and Parrish, R.R. (2002). Himalayan Metamorphic sequence as an orogenic channel: insight from Bhutan. *Earth and Planetary Science Letters*, **198**, 177-191.

Harris, L. B., Koyi, H. A. and Fossen, H. (2002). Mechanisms for folding of high-grade rocks in extensional tectonic settings. *Earth Science Reviews*, **59**, 163-210.

Harrison, T.M. (2006). Did the Himalayan Crystallines extrude partially molten from beneath the Tibetan Plateau? *Geological Society of London. Special Publication*, **268**, 237-254.

Harrison, T.M., Lovera, O.M., Grove, M. (1997). New insights into the origin of two contrasting Himalayan granite belts. *Geology*, **25, 899-902.**

Harrison, T.M., Grove, M., Lovera, O.M., Carlos, E. J. and Andrea, J.D. (1999). The origin of Himalayan anatexis and inverted metamorphism: Models and constraints. *Journal of Asian Earth Sciences*, **17**, 755-772.

Hatcher, R.D. and Merschat, A.J., (2006). The Appalachian Inner Piedmont: an exhumed strike-parallel tectonically forced orogenic channel. Geological Society of London. *Special Publication*, **268**, 517-541.

Hauck, M.L., Nelson, K.D., Brown, K.D., Zhao, W. and Ross, A.R. (1998). Crustal structure of the Himalayan orogen at ~90°east longitude from Project INDEPTH deep reflection profiles. *Tectonics*, **17(4)**, 481-500.

Heim, A. and Gansser, A. (1939). Central Himalaya. Geological observations of the Swiss expedition, 1939. *Denkschriften der Scheizzerrischen Naturforschenden Gesellschaft*, **73**, 1-245.

Heine, C., Meuller, R.D., Gaina, C., (2004). Reconstructing the Lost Eastern Tethys Ocean Basin: Convergence History of the SE Margin and Marine Gateways. *Continent-Ocean Interactions Within East Asian Marginal Seas Geolphysical Monograph Series* **149**, School of Geosciences, University of Sydney Institute of Marine Science., 37-54

Heron, A.M. (1922). Geological results of the Mount Everest expedition*, 1921*. *The Geological Survey of India*, 418-436

Hodges, K.V., Parrish, R.R., Housch, T.B., Lux, D.R., Burchfiel, B.C., Royden, L.H. and Chen, Z. (1992). Simultaneous Miocene extension and shortening in the Himalayan Orogen. *Science*. **258**, 1466-1479.

Hodges, K.V., Burchfiel B.C., Royden, L.H., Chen, Z. and Liu, Y. (1993). The metamorphic signature of contemporaneous extension and shortening in the central Himalayan orogen: data from the Nyalam transect, southern Tibet. *Journal of Metamorphic Geology*, **11(5)**, 721-737.

Hodges, K.V., Bowring, S.A., Davidek, K.L., Hawkins, D.P. and Krol, M.A. (1998). Evidence for rapid displacement on Himalayan normal faults and the importance of tectonic denudation of mountain ranges. *Geology*, **26**, 483-486.

Hodges, K.V. (2000). Tectonics of the Himalaya and southern Tibet from two perspectives. Geological Society of America Bulletin. **112**, 324-350.

Hodges, K.V. (2006). A synthesis of the channel flow-extrusion hypothesis as developed for the Himalayan-Tibetan orogenic system. *In:* Law, R.D., Searle, M.P. and Godin, L. (Eds): Channel Flow, Ductile Extrusion and Exhumation in Continental Collision Zones. *Special Publications*, **268**, Geological Society, London, pp 71-90.

Hubbard, M.S. (1988). Thermobarometry, 40Ar/39Ar geochronology and structure of the Main Central Thrust zone and Tibetan Slab, eastern Nepal Himalaya. *PhD thesis* (unpublished), Massachusetts Institute of Technology.

Hubbard, M.S. (1989). Thermobarometric constraints on the thermal history of the Main Central Thrust Zone and Tibetan Slab, Eastern Nepal Himalaya. *Journal of Metamorphic Geology*, **7**, 19-30.

Hunt, J. (1954). The Ascent of Everest. *The Companion Book Club*, by arrangement with Hodder and Stoughton, London.

Inger, S. and Harris, N.B.W., (2007). Techtonothermal evolution of the High Himalayan Crystalline Sequence, Langtan Valley, northern Nepal. *Journal of Metamorphic Geol*ogy, **10**, Issue 3, 439-452.

Jackson, J., McKenzie, D., Priestley, K., Emerson, B., (2008). New views on the structure and rheology of the lithosphere. *Journal of the Geological Society, London*, **165**, 453 – 465.

Jessup, M.J. (2007). Kinematic Evolution, Metamorphism and Exhumation of the Greater Himalayan Sequence, Mount Everest Massif, Tibet/Nepal. *PhD Thesis* (unpublished), Virginia Tech, Blacksburg, VA.

Jessup, M.J., Cottle, J.M., Searle, M.P., Law, R.D., Newell, D.L., Tracy, R.J. and Waters, D.J. (2008). P-T-t-D paths of Everest series schists, Nepal. *Journal of Metamorphic Geol*ogy, **26**, 717-739.

Jessup, M.J., Law, R.D., Searle, M.P. and Hubbard, M.S. (2006). Structural evolution and vorticity of flow during extrusion and exhumation of the Greater Himalayan Slab, Mount Everest Massif, Tibet/Nepal; implications for crustal-scale flow partitioning. *In:* Law, R.D., Searle, M.P. and Godin, L. (Eds): Channel Flow, Ductile Extrusion and Exhumation in Continental Collision Zones. *Special Publications*, **268**, Geological Society, London, pp 379- 413.

Jessup, M.J., Searle, M.P., Tracy, R., Law, R.D., Cottle, J.M. and Waters, D. (2005). Thermal-mechanical evolution of the upper section of the Greater Himalayan Slab, Everest Lhotse Massif, Nepal. *Geological Society of America Abstracts with Programs*, **37(7)**, 388.

Kellet, D.A., Grujic, D., Warren, C., Cottle, J., Jamieson, R. and Tenzin, T. (2010). Metamorphic history of a syn-convergent orogen-parallel detachment: the South Tibetan detachment system, Bhutan Himalaya. *Journal of Metamorphic Geology*, **28(8)**, 785–808.

Klemperer, S.L. (2006). Crustal Flow in Tibet: geophysical evidence for the physical state of the Tibetan lithosphere, and inferred patterns of active flow. *Geological Society, London, Special Publications*, **268**, 620pp

Koons, P.O., Zeitler, P.K., Chamberlain, C.P., Craw, D., and Meltzer, A.S. (2002). Mechanical links between erosion and metamorphism in Nanga Parbat, Pakistan Himalaya. *American Journal of Science*. **302**, 749-773.

Kosarev, G., Kind, R., Sobolev, S.V., Yuan, X., Hanka, W. and Oreshin, S. (1999). Seismic evidence for a detached Indian lithospheric mantle beneath Tibet. *Science*. **283**, 1306-1309.

Krakauer, J. (1997). Into Thin Air. *Villard Books, Random House*, New York.

Law, R.D, Searle, M.P. and Godin, L. (eds). (2006). Channel Flow, Ductile Extrusion and Exhumation in Continental Collision Zones. *Geological Society, London, Special Publications*, **268**, 620pp.

Lee, J., McClelland, W., Wang, Y., Blythe, A., McWilliams, M. (2006). Oligocene-Miocene middle crustal flow in Southern Tibet: geochronology of Mabja Dome. The Geological Society of London, Special Publication **268**, 445-469.

Leech, M. L., Singh, S., Jain, A.K., Klemperer, S.L. and Manickavasagam, R.M. (2005). The onset of India-Asia continental collision: Early, steep subduction required by the timing of UHP metamorphism in the western Himalaya, *Earth and Planetary Science Letters*, **234**, 83– 97.

Lehmann, U. (1981). The Ammonites: Their life and their world. *Cambridge University Press*, London, 246pp.

Le Fort, P. (1986). Metamorphism and magmatism during the Himalayan collision. eds Coward M.P. and Ries A.C. Collision Tectonics, *Geological Society of London. Special Publication 19*, 159-172.

Le Fort, P., Cuney, M., Deniel, C., France-Lanord, C., Sheppard, S.M.F., Upreti, B.N., Vidal, P., (1987). Crustal generation of the Himalayan leucogranites. Tectonophysics, **134,** 39-57.

Lombardo, B. and Rolfo, F. (2000). Two contrasting eclogite types in the Himalayas: Implications for the Himalayan orogeny, *Journal of Geodynamics*, **30**, 37–60.

Malavielle, J. (2010). Impact of Erosion, Sedimentation and structural heritage on the structure and kinematics of orogenic wedges: analogue models and case studies. *GSA Today*, **20**, 4-10.

Malavielle, J., Lu, C.Y., Chang, E., Konstantinovskaya, E., Bonnet, C., Mosar, J., Dominguez, S. and Graveleau, F. (2008). Impact of surface processes on the dynamics of orogenic wedges: analogue models and case studies. *GeoMod*, 238-242.

MacKenzie, W.S. and Guilford, C. (1980). Atlas of rock-forming minerals in thin section. Pearson, Prentice Hall, 98pp.

Means, W.D. (1989). Stretching Faults. *Geology*, **17**, 893-896.

Medlicott, H.B. (1864). On the geological structures and relations of the southern portion of the Himalayan ranges between the rivers Ganges and the Ravee. *Memoirs Geological Society of India*, **3**, 1-212.

Medlicott, H. B. (1875). Note on the Geology of Nepal. *Records of the Geological Survey of India*, **8**, 93–101.

Middlemiss, C.S. (1885). A fossiliferous series in the Lower Himalayas, Garhwal. *Records of the Geological Survey India*, **18**, 49-57.

Mojsisovics, E. von. (1900). Upper Triassic cephalopod faunae of the Himalayas. *Palaeontologica Indica*, 15:3 , Calcutta. 157pp.

Molnar, P. (1989). The Geologic Evolution of the Tibetan Plateau. *American Scientist*, 77, 350-360.

Molnar, P. and Tapponnier, P. (1975). Effects of a continental collision. *Science*, **189**, 419-426.

Murphy, M.A. and Harrison, T.M. (1999). Relationship between leucogranites and the Qomolongma Detachment in the Rongbuk Valley, South Tibet. *Geology*, **27**, 831-834.

Murphy, M.A., Yin, A., Harrison, T.M., Dürr, S.B., Chen, Z, Ryerson, F.J., Kidd, W.S.F., Wang, X and Zhou, X. (1997). Did the Indo-Asian collision alone create the Tibetan Plateau? *Geology*, **25**, 719-722.

Murphy, M.A. and Yin, A. (2003). Structural evolution and sequence of thrusting in the Tethyan fold-thrust belt and Indus-Yalu suture zone, southwest Tibet. *Geological Society of America Bulletin*, **115**, 21-34.

Myrow, P.M., Hughes, N.C., Searle, M.P., Fanning, C.M., Peng, S.C. and Parcha, S.K. (2009). Stratigraphic correlation of Cambrian Ordovician deposits along the Himalaya: Implications for the age and nature of rocks in the Mount Everest region. *Geological Society of America Bulletin*, **121**, 323-332.

Nocquet, J.M. and Calais, E. (2004). Geodetic measurements of Crustal Deformation in the Western Mediterranean and Europe. *Pure and Applied Geophysics*, **161**, 661-681.

Nelson, K.D., Zhao, W., Brown, L.D. Kuo, J., Che, J., Liu, X., Klemperer, S.L., Makovsky, Y., Meissner, R., Mechie, J., Kind, R., Wenzel, F., Ni, J., Nabelek, J., Leshou, C., Tan, H., Wei, W., Jones, A.G., Booker, J., Unsworth, M., Kidd, W.S.F., Hauck, M., Alsdorf, D., Ross, A., Cogan, M., Wu, C., Sandvol, E. and Edwards, M. (1996). Partially molten middle crust between southern Tibet; synthesis of Project INDEPTH results. *Science*, **274**, 1684-1688.

Odell, N.E. (1925). Observations on the rocks and glaciers of Mount Everest. *Geographical Journal*, **66**, 299-315.

Odell, N.E. (1943). The so-called "Axial Granite Core" of the Himalaya: its actual exposure in relation to its sedimentary cover. *Geology Magazine*, **80**, 148-154.

Odell, N.E. (1948). Geological and some other observations in the Mount Everest region. *In:* Tilman, H.W. (ed.) *Mount Everest 1938*. Cambridge University Press, 143–154.

Odell, N.E. (1965). The highest fossils in the world. *Geological Magazine*, **104**, 73-76.

Owens, T.J. and Zandt, G. (1997). Implications of crustal property variations for models of Tibetan plateau evolution. *Nature*, **387**, 37-43.

Park, R.G. (1988). *Geological structures and moving plates*. Blackie, London, 337 pp.

Parrish, R.R., Gough, S.J., Searle, M.P. and Waters, D.J. (2006). Plate velocity exhumation of ultrahigh-pressure eclogites in the Pakistan Himalaya, *Geology*, **34**, 989-992,

Pecher, A., and Le Fort, P. (1999). Late Miocene evolution of the Karakoram-Nanga Parbat contact zone (northern Pakistan). In: Macfarlane, A., Surkhabi, R.B., Quade, J. (eds) Himalaya and Tibet: Mountain Roots to Mountain Tops. *Geological Society of America Special Paper*, **328**, 145-158.

Peoples Republic of China, Ministry of Geology and Mineral Resources. (1993) Geological Map of Xizang (Tibet) Autonomous Region of the Peoples Republic of China. 1993. Peoples Republic of China, *Ministry of Geology and Mineral Resources Geological Memoirs*, Series 1 Number 31. Geological Publishing House, Beijing.

Pognante, U. and Benna, P. (1993). Metamorphic zonation, migmatisation and leucogranite along the Everest transect of eastern Nepal and Tibet: record of an exhumation history. *In:* Treloar, P.J. and Searle, M.P.(Eds) *Himalayan Tectonics*. Special Publications, **74**, Geological Society, London, 323-340.

Raymo, M.E., and Ruddiman, W.F., (1992). Tectonic forcing of the late Cenozoic Climate. *Nature*,**359**, 117 – 122.

Reed, F.R.C. (1908). Fossils from Nepal. *Geological Magazine*, **5**, 256-261.

Reichardt, H., Weinberg, R.F., Andersson, U.B., Fanning, C.M. (2010). Hybridization of granitic magmas in the source: the origin of the Karakoram Batholith, Ladakh, NW India. *Lithos*, **116**, 249-272.

Rowley, D.B. (1996). Age of initiation of collision between India and Asia. A review of stratigraphic data. *Earth and Planetary Science Letters*, **109**, 11-23.

Royden, L.H., Burchfiel, B.C., King, R.W., Wang, E., Shen, F., and Liu, Y., (1997). Surface deformation and lower crustal flow in eastern Tibet. *Science*, **276**, 788-790.

Sakai, S., Sawada, M., Takigami, Y., Orihashi, Y., Danhara, T., Iwano, H., Kuwahara, Y., Dong, Q., Cai, H. and Li, J. (2005). Geology of the summit limestone of Mount Qomolongma (Everest) and cooling History of the Yellow Band under the Qomolongma detachment. *The Island Arc*, **14**, 297-310.

Scaillet, B., France-Lanord, C., Le Fort, P., (1990). Badrinath-Gangotri plutons (Garhwal, India); Petrological and geochemical evidence for fractionation processes in a high Himalaya leucogranite. *J. Volcanol. Geotherm.* Res.**44**, 163-188.

Scaillet, B. and Searle, M. P. (2006). Mechanisms and timescales of felsic magma segregation, ascent and emplacement in the Himalaya. *In:* Law, R.D., Searle, M.P. and Godin, L. (Eds): *Channel Flow, Ductile Extrusion and Exhumation in Continental Collision Zones*. *Special Publication*, **268**, Geological Society, London, 293-308.

Searle, M.P. (1999a). Extensional and compressional faults in the Everest – Lhotse massif, Khumbu Himalaya, Nepal. *Journal of the Geological Society, London*, **156**, 227-240.

Searle, M.P. (1999b). Emplacement of Himalayan leucogranite by magma injection along giant sill complexes: examples from the Cho Oyu, Gyachung Kang and Everest leucogranite (Nepal Himalaya). *Journal of Asian Earth Sciences*, **17**, 73- 783.

Searle, M.P. (2007). Geological map of the Mount Everest Region Nepal - South Tibet Himalaya. Scale: 1:100,000. *Department of Earth Sciences*, Oxford University.

Searle, M.P., Windley, B.F., Coward, M.P. Cooper, D.J.W., Rex, A.J., Rex, D., Tingdong, L., Xuchang, X., Jan, M.Q., Thakur V.C. and Kumar, S. (1987). The closing of Tethys and the tectonics of the Himalaya. *Geological Society of America Bulletin*, **98**, 678-701.

Searle, M.P., Cooper, D.J.W. and Rex, A.J. (1988). Collision tectonics of the Ladakh-Zanskar Himalaya. *Philosophical Transactions of the Royal Society, London*. **A326**, 117-150.

Searle, M.P. and Rex, A.J. (1989). Thermal model for the Zanskar Himalaya. *Journal of Metamorphic Geology*, **7**, 127-134.

Searle, M.P., Metcalfe R.P., Rex A.J., Norry M.J. (1993). Field relations, petrogenesis and emplacement of the Bhagirathi leucogranite, Garhwal Himalaya eds Treloar P.J. and Searle M.P., Himalayan Tectonics, Geological Society of London, Special Publication **74**, 429-444

Searle, M.P., Parrish, R.R., Hodges, K.V., Hurford, A., Ayres, M.W. and Whitehouse, M.J. (1997). Shisha Pangma leucogranite, South Tibetan Himalaya; field relations, geochemistry, age, origin and emplacement. *Journal of Geology*, **105**, 295-317.

Searle, M.P., Simpson, R.L., Law, R.D., Waters, D.J. and Parrish, R.R. (2002). Quantifying displacement on the South Tibetan Detachment normal fault, Everest massif, and the timing of crustal thickening and uplift in the Himalaya and South Tibet. *Journal of Nepal Geological Society*, **26**, 1-6.

Searle, M.P., Simpson, R.L., Law, R.D., Parrish, R.R. and Waters, D.J. (2003). The structural geometry, metamorphic and magmatic evolution of the Everest Massif, High Himalaya of Nepal-South Tibet. *Journal of the Geological Society of London*, **160**, 345-366.

Searle, M.P., Law, R.D. and Jessup, M.J. (2006). Crustal structure, restoration and evolution of the Greater Himalaya in Nepal- South Tibet; implications for the channel flow and ductile extrusion of the middle crust. *In:* Law, R.D., Searle, M.P. and Godin, L. (Eds): *Channel Flow, Ductile Extrusion and Exhumation in Continental Collision Zones*. *Special Publication*, **268**, Geological Society, London, 620pp.

Seeber, L., and Pecher, A., (1998). Strain positioning along the Himalayan arc and the Naga Parbat antiform. *Geology*. **26**, 791-794.

Sharma, T. (1988). A study of the geology of the Mount Everest region, Nepal. Geological Survey of Nepal.

Simpson, R.L. (2002). Metamorphism, Melting and Extension at the Top of the High Himalaya Slab, Mount Everest Region, Nepal and Tibet. *DPhil. Thesis (unpublished), Oxford University*, Oxford.

Simpson, R.L., Parrish, R.R., Searle, M.P. and Walters, D.J. (2000). Two episodes of Monazite crystallisation during metamorphism and crustal melting in the Everest region of the Nepalese Himalayas. *Geology*, **28**, 403-406.

Sorkhabi, R.B., Stump, E., (1993). Rise of the Himalaya: a geochronologic approach. *GSA Today* 3(4):85–92

Stephenson, B.J., Searle, M.P. and Waters, D.J. (2001). Structure of the Main Central Thrust zone and extrusion of the High Himalayan crustal wedge, Kishtwar-Zanskar Himalaya. *Journal of Geological Society, London*. **158,** 637-652.

Stöcklin, J., (1980). Geology of Nepal and its regional frame. *Journal Geological Society*, London. **137,** 1–34

Stoliczka, F. (1866). Geological sections across the Himalayan mountains, from Wantu bridge on the Sutlej to Sungdo on the Indus, with an account of the formation in Spiti, accompanied by a revision of all known fossils from that district. *Memoirs of the Geological Society India*, **B,** 1-154.

Strachey, R. (1851). On the geology of part of the Himalaya Mountains and Tibet. *Quarterly Journal Geological Society, London*, **7**, 292-310.

Tapponnier, P. and Peltzer, G. (1998). Formation and evolution of strike-slip faults, rifts, and basins during the India-Asia Collision: An experimental approach. *Journal of Geophysical Research, Solid Earth*, **93**, Issue B12, 15085–15117.

Tapponnier, P., Peltzer, G. and Armijo, R. (1986). On the mechanics of the collision between India and Asia. *Geological Society, London*, Special Publications **19**, 113-157.

Tapponnier, P., Peltzer, G., Le Dain, A.Y., Armijo, R., Cobbold, P., (1982). Propagating extrusion tectonics in Asia: New insights from simple experiments with plasticine. *Geological Society, America*, v10, **12**, 611-616.

Tonarini, S., Lombardo, B., Ferrara, G. and Marcassar, P. (1994). Partial melting in the Namche Migmatic of Khumbu Himal (Nipal Himalaya). *Mineralogical et petrographica Acta,* **37**, 277-294.

US Geological Survey Website - http://pubs.usgs.gov/publications/text/himalaya.html

Van der Voo, R., Spakman, W. and Bijwaard H. (1999). Tethyan subducted slabs under India. *Earth and Planetary Science Letters*, **171**, 7-20.

Vielzuef, D. and Montel, J. (1994). Partial melting of metagreywackes Part I. Fluid-absent experiments and phase relationships. *Contributions to Mineralogy and Petrology*, **117**, 375-393.

Visona, D. and Lombardo, B. (2002). Two-mica leucogranites from the Everest-Makalu region (Nepal-Tibet). Himalayan leucogranite genesis by isobaric heating? *Lithos* **62**, 125-150.

Wager, L.R. (1934). A review of the geology and some new observations. *Everest* (ed Rutledge, H., 1933), Hodder and Stoughton, London, 312-337.

Wager, L.R. (1939). Injected granite sheets of the Rongbuk valley and the north face of Mount Everest. *In:* Wadia D.N, Commemorative volume. *India Mining, Geology and Metallurgy Institute*, 358-379.

Walker, J.D., Martin, M.W., Bowring, S.A., Searle, M.P., Waters, D.J. and Hodges, K.V. (1999). Metamorphism, melting and extension: Age constraints from the High Himalayan slab of Southeast Zanskar and Northwest Lahoul. *Journal of Geology*, **107**, 473-95.

Wegener, A. (1929). The Origin of Continents and Oceans, Translated from the 4th revised edition (Braunschweig, 1929) by John Biram. Dover, New York, 1967. 256 pp.

Waterhouse, J.B. (1996). The Anision amminoid succession of the Nepal Himalayas. *Journal of Nepal Geological Society*, **13**, 1-9.

Wegmann, C.E. (1935). The Zur Deutung der Migmatiten. (The meaning of migmatites.) *Geologische Rundschau*, **26**, 305-350.

Weinberg, R.F. and Searle, M.P. (1999). Volatile-assisted intrusion and autometasomatism of leucogranite in the Khumbu Himalaya, Nepal. *Journal of Geology*, **107**, 27-48.

Whitten, D.G.A. and Brooks, J.R.V. (1972). *The Penguin Dictionary of Geology.* Hazell Watson and Viney Ltd., Aylesbury, Bucks.

Wu, C., Nelson, K.D., Wortman, G., et al. (1998). Yadong cross structure and South Tibetan Detachment in the east central Himalaya (89° - 90° E). *Tectonics*, **17**, 28-45.

Xypolias, P., and Kokkalas, S. (2006). Heterogeneous ductile deformation along a mid-crustal extruding shear zone: an example from the External Hellenides (Greece). *The Geological Society of London.* Special Publication **268**, 497-516.

Yancey, T.E., Garvie, C. L. and Wicksten, M. (2010). The Middle Eocene Belosaepia ungula (Cephalopoda: Coleoida) from Texas: Structure, Ontogeny and Function. *Journal of Paleontology*, **84**, 267–287.

Yardley, B.W.D., (1989). An Introduction to Metamorphic Petrology. Harlow: Longman, New York: John Wiley, 248pp.

Yin, C.H.and Kuo, S.T. (1978). Stratigraphy of the Mount Jolmo Langma and its north slope. *Scientia Sinica*, **5**, 630-644

Yin, A., Kapp, P.A., Murphy, M.A., Manning, C.E., Harrison, T.M., Grove, M., Lin, D., Xi-Guang, D. and Cun-Ming, W. (1999). Significant late Neogene east-west extension in northern Tibet. *Geology,* **27,** 787-790.

Yin, A. and Harrison, T.M. (2000). Geologic Evolution of the Himalayan-Tibetan Orogen *Annual Review of Earth and Planetary Sciences* **28**, 211-280

Yuan, Wu Fu-, Wei-Qiang Ji, Chuan-Zhou Liu, Sun-Lin Chung, (2010). Detrital zircon U–Pb and Hf isotopic data from the Xigaze fore-arc basin: Constraints on Transhimalayan magmatic evolution in southern Tibet. *Chemical Geology 27, 13-25.*

Zeitler, P.K., Chamberlain, C.P. (1991). Petrogenetic and tectonic significance of young leucogranites from the northwestern Himalaya, Pakistan. *Tectonics* **10(4)**, 729–741

Zhao, W., Nelson, K.D., Che, J., Quo, J., Lu, D., Wu, C. and Liu, X. (1993). Deep seismic reflection evidence for continental underthrusting beneath southern Tibet, *Nature,* **366**, 557-559.

Zhang, Y. and Zheng J. (1994). Geologic Overview in Kokshili, Qinghai and Adjacent Areas. *Seismological Publishing House*, Beijing. 177 pp.